UNIVERSITEIT VAN PRETORIA
UNIVERSITY OF PRETORIA
YUNIBESITHI YA PRETORIA

UNIVERSITEIT VAN PRETORIA
UNIVERSITY OF PRETORIA
YUNIBESITHI YA PRETORIA

Identifying Instability in the Rock Mass Caused by Water Ingress into Abandoned Mines

by

DENVER JULIAN BIRCH

Submitted in partial fulfillment of the requirements for the degree

MAGISTER SCIENTIAE

in the Department of Physics

in the Faculty of Natural and Agricultural Sciences

University of Pretoria

Pretoria

November 19, 2013

© University of Pretoria

© University of Pretoria

UNIVERSITEIT VAN PRETORIA
UNIVERSITY OF PRETORIA
YUNIBESITHI YA PRETORIA

Declaration

I, ... declare that the dissertation, which I hereby submit for the degree Magister Scientiae at the University of Pretoria, is my own work and has not previously been submitted by me for a degree at this or any other tertiary institution.

Signature: .....

Date: .....

© University of Pretoria

UNIVERSITEIT VAN PRETORIA
UNIVERSITY OF PRETORIA
YUNIBESITHI YA PRETORIA

Identifying Instability in the Rock Mass Caused by Water Ingress into Abandoned Mines

By Denver Julian Birch

Supervisor: Prof. A. Kijko

Co-supervisor: Dr. A. Cichowicz

Abstract

The recent increase in seismic activity in the Central Rand Basin of South Africa was investigated using two different approaches. The closure of mines throughout the basin has left a large underground void behind that has rapidly filled with water, polluted by mine workings. There is concern over the possible triggering of a large earthquake beneath the city of Johannesburg. Questions surrounding the mechanism and nature of the seismicity still persist. Two approaches were selected to uncover early clues about the seismicity and possibly shed some light on future expectations.

The first approach was an analysis of the frequency-magnitude distribution (*b*-value) over time, while the second approach was an attempt at building a 3-dimensional geomechanical model to describe a possible driving force behind the seismicity. Results from a temporal *b*-value analysis show a strong correlation with a drop in the *b*-value and the onset of the largest events in the database. This is explained by the relationship between the *b*-value and physical properties of the rock mass. An overall decrease in the *b*-value was estimated since flooding started, indicating a shift towards a higher proportion of larger events.

The 3-dimensional geomechanical model provided a measure of the stresses and shear displacements that occur where geological discontinuities intersect the mine workings. This was compared to previous estimates of stress measurements in the mines and maximum possible magnitude estimations. The spatial distribution of recent, relocated seismicity was described in terms of the results from the model, which identified unstable geological features. The distribution of these features matched the seismic clusters that were observed, which provided some insight into the current tectonic setting of the Central Rand Basin.

© University of Pretoria

UNIVERSITEIT VAN PRETORIA
UNIVERSITY OF PRETORIA
YUNIBESITHI YA PRETORIA

Table of Contents

© University of Pretoria

UNIVERSITEIT VAN PRETORIA
UNIVERSITY OF PRETORIA
YUNIBESITHI YA PRETORIA

© University of Pretoria

UNIVERSITEIT VAN PRETORIA
UNIVERSITY OF PRETORIA
YUNIBESITHI YA PRETORIA

List of Figures

© University of Pretoria

UNIVERSITEIT VAN PRETORIA
UNIVERSITY OF PRETORIA
YUNIBESITHI YA PRETORIA

List of Tables

© University of Pretoria

UNIVERSITEIT VAN PRETORIA
UNIVERSITY OF PRETORIA
YUNIBESITHI YA PRETORIA

© University of Pretoria

UNIVERSITEIT VAN PRETORIA
UNIVERSITY OF PRETORIA
YUNIBESITHI YA PRETORIA

Chapter 1

1. Introduction

1.1. Problem Definition

The extensive mining and drying out of the rock mass that took place in the Central Rand Basin (CRB) since 1886 has forever changed the crustal stresses that govern seismic activity. In 2008, the last pumping station that controlled the rising water level in the mined out basin was shut down. This led to a great amount of public concern over various issues, one of them being the threat of a catastrophic seismic event underneath Johannesburg. Seismicity has always been closely linked to mining; yet, it has consistently been observed in the CRB without the presence of mining and is considered to be a cause of the water ingress.

Fluid-induced movement along a fracture/fault plane is caused by a decrease in the clamping force on the plane. Figure 1 is a schematic illustration of an experiment that identifies the forces involved in a typical normal faulting regime. A block of clay is compressed between two wooden planks, inducing a facture plane with trace AB, which represents a fault. The principle stresses σ_1, σ_2 and σ_3 are defined as $\sigma_1 >> \sigma_2 = \sigma_3$. Normal faulting will occur under this condition. The forces that exist on the fracture plane are the shear force σ_s and the normal force σ_n. The normal force is sometimes referred to as the clamping force as it determines the shear strength of the fracture plane i.e. the amount of resistance the plane has to shearing. Hydrostatic pore pressure at a point, P_p, is exerted in all directions equally and, thus, effectively reduces the magnitudes of the shear and normal stresses where stress is merely the force per unit area. If a fault plane is already stressed close to the point where failure occurs, even a slight increase in the pore pressure might induce displacement.

The alteration of minerals in the fault zone might also induce movement, since altered minerals have lower shear strength than minerals in unaltered rock. The water that enters mine workings is exposed to oxidised heavy metals. The polluted water may increase the rate of alteration. Measuring this effect was not undertaken in this study but should be taken into consideration for further studies.

© University of Pretoria

UNIVERSITEIT VAN PRETORIA
UNIVERSITY OF PRETORIA
YUNIBESITHI YA PRETORIA

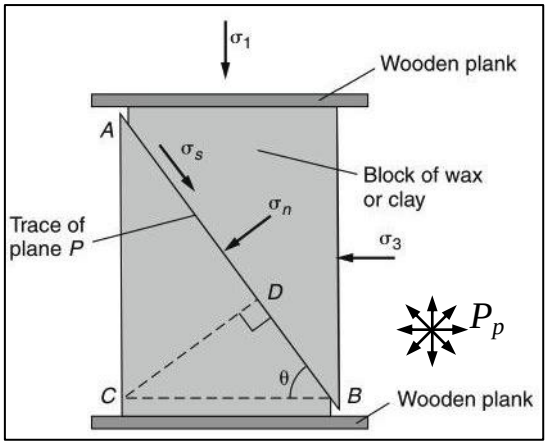

Figure 1 – Schematic illustration of an experiment where a block of clay is squeezed between two planks of wood creating a fracture plane with trace AB. The relationships between the principle stresses, σ_1 and σ_3 ($=\sigma_2$), and the shear (σ_s) and normal (σ_n) stresses are shown here. (Van Der Pluijm and Marshak, 2004).

Extensive studies have been conducted on reservoir impoundment being the cause of an increase in the level of seismicity of a region (Simpson, 1976). In such scenarios, the initial loading, when filling the reservoir, triggers an immediate increase in activity. Following this, delayed, cyclical changes to the seismic activity are observed and correlated with water level fluctuations, which control pore pressure (Bell and Nur, 1978; Roeloffs, 1988; Simpson, 1976). The case of the abandoned Central Rand Basin mines is unique. The mined out void dips underground at an angle of approximately 30 degrees to the south with the volume controlled by stoping height and amount of closure. It is also not a continuous void, whereas, a reservoir is a deep body of water on the surface. The increase in pore pressure is much higher than in reservoir-induced seismicity (gold mines are much deeper than reservoirs), with a maximum increase of approximately 35 MPa in the deepest part of the mines (based on an approximate depth of 3.5 km and pressure increase of 1 MPa per 100 m). These pressures are in the range of those produced in fluid-injection experiments (Healy *et al.*, 1968; Lightfoot and Goldbach, 1995) but the area involved is a lot larger in this case and the pore pressures are hydrostatic.

1.2. Objectives

The seismic activity currently being observed in the CRB has not yet been sufficiently characterized. Questions surrounding the mechanism and nature of the seismicity still persist. The Council for Geoscience operate a network of 12 seismograph stations spanning the CRB

© University of Pretoria

UNIVERSITEIT VAN PRETORIA
UNIVERSITY OF PRETORIA
YUNIBESITHI YA PRETORIA

that were commissioned in early 2010. The stations cover a rectangular area approximately 20 km from north to south and 50 km east to west. The objective is to combine structural information from the mines with a 3-dimensional geomechanical model and a recent distribution of seismic event epicentres to form an understanding of the driving force behind the seismicity. The nature of the seismicity will be described in a study of the frequency-magnitude distribution for recent and historic events that were recorded by the Council for Geoscience.

1.3. Research Methodology

An analysis of the frequency-magnitude distribution of the seismicity recorded by the Council for Geoscience was undertaken as an observational approach to characterize the nature of the seismicity. The frequency-magnitude relation, introduced by Gutenburg and Richter (1944; 1954) and referred to as the Gutenburg-Richter (G-R) relation, is often interpreted as an indicator of the physical state of the system. Comparisons with previous observations of the G-R relation were made.

To complement this characterization of the measured seismicity, a 3-dimensional model was constructed to reproduce the interactions between the crustal stress in the vicinity of the mine and structural features of the geology. The model-building software 3DEC (3-dimensional Distinct Element Code) was used to construct a geomechanical model of the geological discontinuities associated with the mining voids. The information available to this investigation includes a detailed structural geology map of the Central Rand Basin mines, stretching from Durban Roodepoort Deep in the west to East Rand Proprietary Mines (ERPM) in the east (Pretorius, circa 1970). The purpose of the model is to characterize the behaviour of these features when pore pressure increases as a result of the mines flooding. Clues derived from the model were correlated with observations made from an extensive data set of relocated seismicity recorded by a dense seismograph network of 12 strong ground motion sensors in the Central Rand Basin.

© University of Pretoria

UNIVERSITEIT VAN PRETORIA
UNIVERSITY OF PRETORIA
YUNIBESITHI YA PRETORIA

Chapter 2

2. Evaluation of the Frequency-Magnitude distribution

2.1. The Gutenberg-Richter Law

Seismicity in the Central Rand was originally a by-product of the deep gold mining that has taken place. Mining has since stopped but seismicity is still being recorded. The driving force behind the seismicity can no longer be attributed to the tabular mining, making this an unpredictable scenario. An investigation into the change in the physical characteristics of the seismicity was conducted on seismic data recorded in the Central Rand Basin by the Council for Geoscience. The area under investigation extends from Durban Roodepoort Deep Gold Mines in the west to the East Rand Proprietary Mines in the east.

The G-R relation describing the frequency-magnitude distribution of earthquakes is written as follows (Gutenburg and Richter, 1944):

$$\log_{10}[N(M)] = a - bM \tag{2.1}$$

where N is the number of events with magnitude M or larger. The parameters a and b are constants. a is a measure of the overall occurrence rate. When divided by the time window, this value becomes the seismic activity rate for the number of events of magnitude ≥ 0.

$$\log_{10}[N(0)] = a \tag{2.2}$$

The parameter b is defined by the ratio of small to large earthquakes. The b-value estimation is a widely used tool in seismic hazard studies (Gibowicz and Kijko, 1994). Inferences about the physical properties of the medium are often made based on this value. Scholz (1968) demonstrated a relation between the value of b and the stress conditions in rock in a laboratory. Many others (Enescu and Ito, 2003; Nuannin *et al.*, 2005; Tsukakoshi and Shimazaki, 2008) have attempted to use the b-value as a precursor, searching for a sudden decrease in b before the occurrence of a high-energy event.

Seismic monitoring in mines includes, among other things, a regular evaluation of the G-R relation to assess the potential for seismic activity. Mendecki *et al.* (1999) describe how to manipulate this relation to determine probabilistic recurrence times for seismic events

© University of Pretoria

UNIVERSITEIT VAN PRETORIA
UNIVERSITY OF PRETORIA
YUNIBESITHI YA PRETORIA

occurring in a given volume of rock. The *b*-value is also considered to be influenced by physical characteristics of the rock mass such as stiffness (ability of the rock mass to resist deformation), the level of stress (as demonstrated by Scholz (1968)) and heterogeneity of the rock mass. The physical characteristics of the rock mass derived from the *b*-value are discussed in Section 2.5. The following section will introduce the maximum-likelihood method for estimating the *b*-value.

© University of Pretoria

UNIVERSITEIT VAN PRETORIA
UNIVERSITY OF PRETORIA
YUNIBESITHI YA PRETORIA

2.2. The Maximum Likelihood Technique to Estimate *b*

Two approaches are commonly used to estimate the *b*-value and its associated error, the least squares and maximum likelihood techniques. The least squares approach does not have any statistical foundation (Bender, 1983) since it implicitly assumes a normal distribution of the data. The maximum likelihood method is considered to be a stronger approximation of the *b*-value (Marzochi and Sandri, 2003). The method was taken from a demonstration by Gibowicz and Kijko (1994) in a description of the procedure to evaluate *b* that was introduced by Aki (1965) and Utsu (1965).

The procedure of the *b*-value evaluation begins with the assumption that the magnitudes of the seismic events are considered to be independent, continuous random variables with an uncapped maximum. This allows us to write equation 2.1 in terms of the probability density, *f*(*M*), and cumulative distribution, *F*(*M*), functions of the magnitude, *M*, where *M* may assume any value above M_{min}.

$$f(M) = \begin{cases} 0 & M < M_{min} \\ \beta \exp[-\beta(M - M_{min})] & M \geq M_{min} \end{cases} \tag{2.3}$$

$$F(M) = \begin{cases} 0 & M < M_{min} \\ 1 - \exp[-\beta(M - M_{min})] & M \geq M_{min} \end{cases} \tag{2.4}$$

Where $\beta = b \ln(10)$ and M_{min} is the minimum allowable magnitude.

Since the magnitudes are independent, the joint probability density for a set of *N* magnitudes M_i (i = 1,…,*N*) is equal to the product of the individual probability densities $f(M_i)$. The joint probability density is proportional to the likelihood function $L(\cdot)$ and the value for which this likelihood function is maximised, called $\hat{\beta}$, is the maximum-likelihood estimate of β. The maximum-likelihood condition is:

$$L(\beta|M_1, \dots, M_N) = const \prod_{i=1}^{N} f(M_i|\beta) = max \tag{2.5}$$

The procedure for finding the maximum to the likelihood function is to find the value, in this case $\hat{\beta}$, which equates the first derivative of the log-likelihood to zero. The log of a product of two variables is simply the sum of the individual log of each variable. We now have the following condition:

© University of Pretoria

UNIVERSITEIT VAN PRETORIA
UNIVERSITY OF PRETORIA
YUNIBESITHI YA PRETORIA

$$\sum_{i=1}^{N} \frac{\partial}{\partial \beta} \ln f(M_i|\beta) = 0 \tag{2.6}$$

Taking the logarithm and calculating the derivative gives:

$$\frac{N}{\beta} - \left(\sum_{i=1}^{N} M_i - NM_{min}\right) = 0 \tag{2.7}$$

The value $\hat{\beta}$ is then the Aki-Utsu maximum-likelihood estimate of β for which the maximum likelihood function is maximised.

$$\hat{\beta} = \frac{1}{\bar{M} - M_{min}} \tag{2.8}$$

Where we have the sample mean magnitude $\bar{M} = \sum_{i=1}^{N} M_i / N$.

Written out explicitly, the estimate for *b* is (Aki, 1965 and Utsu, 1965):

$$b = \frac{1}{\ln 10 (\bar{M} - M_{min})} \tag{2.9}$$

A more explicit derivation can be found in Appendix A. The minimum magnitude is often referred to as the minimum magnitude of completeness or the threshold magnitude and is dependent on the detection capability of the seismograph network. It is assumed that all earthquakes above this magnitude were correctly measured.

2.2.1. Minimum magnitude of completeness

A crucial factor in any *b*-value estimation method is the determination of the threshold magnitude for a catalogue of events. Woessner and Wiemer (2005) describe various methods that can be employed when determining this parameter. Each method provides slightly different values for M_{min}, bringing with it its own set of strengths and weaknesses.

The methods include the entire-magnitude-range (EMR) method, maximum curvature (MAXC) method, the goodness-of-fit (GFT) method and the M_{min} by *b*-value stability (MBS) method. The EMR method attempts to fit the entire magnitude range of measured earthquakes using maximum likelihood estimates of probability functions that include parameters for the detection capabilities of the network. This is not a very straight forward technique and relies heavily on parameters that are not well understood. The MAXC method maximises the first derivative of the frequency-magnitude distribution, which usually assigns

© University of Pretoria

UNIVERSITEIT VAN PRETORIA
UNIVERSITY OF PRETORIA
YUNIBESITHI YA PRETORIA

M_{min} to the magnitude with the highest number of events. This is often an underestimation. The GFT method tests all possible choices for M_{min} systematically evaluating each one with a best-fit equation. A simple plot graphically illustrates the relative fit of each M_{min} allowing the user to verify a particular choice. The MBS method is based on the assumption that *b*-values increase for $M < M_{min}$, remain constant for $M \geq M_{min}$forming a plateau and increase again for $M \gg M_{min}$. $M_{min}$is then selected by setting some qualifying criterion based on the change in the *b*-value between successive magnitudes.

The GFT method was chosen for this study because of the straight forward approach of minimizing the misfit between the observed and predicted data without worrying about fitting the entire distribution (EMR), being biased towards the magnitude with the most events (MAXC) or constraining the behaviour of the *b*-value (MBS).

Goodness-of-Fit Test (GFT): Taken from Wiemer and Wyss (2000), the GFT method measures the fits of synthetic frequency-magnitude distributions, calculated from maximum likelihood estimates, with the observed distribution starting with the lowest M_{min}. The maximum likelihood estimates produce synthetic distributions for increasing values of M_{min}. The goodness-of-fit is defined by Wiemer and Wyss (2000) as "the absolute difference of the number of events in the magnitude bins between the observed and synthetic Gutenburg-Richter distribution". R, given as a percentage in equation 2.10 is the residual and B_i and S_i are the observed and predicted cumulative number of events in each magnitude bin, respectively.

$$R(a,b,M_i) = 100 - \left(\frac{\sum_{M_i}^{M_{max}} |B_i - S_i|}{\sum_i B_i} * 100\right) \qquad (2.10)$$

A qualifying criterion for R is set at either 95% or 90%. The smallest magnitude to meet this criterion is selected as M_{min}.

2.2.2. The effect of magnitude bins

The maximum likelihood estimate for *b* given by Aki (1965) and Utsu (1965) assumes a continuous distribution. In practice, seismic events when recorded instrumentally are measured up to one decimal point to account for uncertainties. The real frequency-magnitude distribution is, as a result, not continuous. The numbers of events are binned according to

© University of Pretoria

UNIVERSITEIT VAN PRETORIA
UNIVERSITY OF PRETORIA
YUNIBESITHI YA PRETORIA

their magnitudes, which has an effect on the parameters expressed in the Aki-Utsu maximum likelihood estimate (eq. 2.9).

Marzocchi and Sandri (2003) explain that $\bar{M}$ and M_{min} each introduce errors due to the differences in their values for continuous and binned distributions. Bender (1983) showed that $\bar{M}$ for real continuous magnitudes are not symmetrically distributed around the centre of the binned interval. It was also demonstrated that the error introduced here is negligible for bin intervals of 0.1. Utsu (1966) addressed the error in M_{min}, introduced through the use of binned magnitudes, and provided a modification of equation 2.9 to account for this. Equation 2.11 is the modified estimate of b.

$$b = \frac{1}{\ln 10\left(\bar{M} - (M_{min} - \Delta M/2)\right)} \tag{2.11}$$

Since each bin contains magnitudes ranging from $M_i - \Delta M/2 \leq M < M_i + \Delta M/2$, the real minimum magnitude within chosen minimum magnitude bin is in fact $M_{min} - \Delta M/2$.

2.2.3. Error estimation

The uncertainty in b, as estimated by Aki (1965), is given as:

$$\sigma_{b(Aki)} = \frac{b}{\ln(10)\sqrt{N}} \tag{2.12}$$

N is the number of earthquakes used in the b-value estimation. According to Gibowicz and Kijko (1994), this assumes that N is sufficiently large such that b is normally distributed about its mean value given by equation 2.9. A number of additional attempts were made at constraining the variation in b. Gibowicz and Kijko also highlight approximations by Zhang and Song (1981) and Shi and Bolt (1982), a method that was also highly regarded by Marzocchi and Sandri (2003). The equation given by Zhang and Song (1981) is:

$$\sigma_{b(ZS)} = \frac{bN}{(N-1)(N-2)^{1/2}} \tag{2.13}$$

A considerable contribution was made by Shi and Bolt (1982). Their estimation of the standard deviation is considered reliable in periods of a slowly changing b-value with large samples (N=100). Thus, it is well suited when searching for temporal or spatial changes in b

© University of Pretoria

UNIVERSITEIT VAN PRETORIA
UNIVERSITY OF PRETORIA
YUNIBESITHI YA PRETORIA

using sample windows of 100 or more earthquakes wherein b is assumed to be constant. Their equation is:

$$\sigma_{b(SB)} = 2.30b^2\sqrt{\frac{\sum_{i=1}^{N}(M_i-\bar{M})^2}{N(N-1)}} \quad (2.14)$$

To appreciate these approximations and the difference selecting a particular one would make to our interpretation, we tested them on a sample of data from our catalogue for different numbers of events.

Table 1 – Comparison of standard deviation approximations for b from different authors

N	$\sigma_{b(Aki)}$ **Aki (1965)**	$\sigma_{b(ZS)}$ **Zhang and Song (1981)**	$\sigma_{b(SB)}$ **Shi and Bolt (1982)**
260	0.07	0.03	0.02
198	0.08	0.04	0.02
160	0.10	0.04	0.03
125	0.12	0.05	0.04
94	0.14	0.06	0.05
60	0.15	0.07	0.05
49	0.19	0.08	0.07

The results from the comparison in Table 1 show that significant improvements have been made on the estimation of the standard deviation of b given by Aki (1965). The standard deviations calculated using the Zhang and Song (1981) and Shi and Bolt (1982) equations are comparable and much smaller than those of Aki (1965). $\sigma_{b(SB)}$ not only performed better in the comparison, it is also considered suitable to cases where the b-value changes over time (Gibowicz and Kijko, 1994; Marzocchi and Sandri, 2003). This serves our purpose in this investigation, which is why equation 2.14 was chosen for implementation in the b-value estimation.

© University of Pretoria

UNIVERSITEIT VAN PRETORIA
UNIVERSITY OF PRETORIA
YUNIBESITHI YA PRETORIA

2.3. A MATLAB Code to Calculate the *b*-Value

The data processing software used at the Council for Geoscience during the period under analysis was SEISAN Earthquake Analysis Software. Information about a particular seismic event is contained in a text file called an S-file. A script was written in MATLAB (Appendix B) to extract event information from the s-files for all the events occurring within the time window and located in the CRB. MATLAB was further used to automate the procedure for our *b*-value estimation. An option to analyse the temporal variation of the *b*-value was also included. Writing a program to process the data in MATLAB as opposed to using freely-available and widely-used software packages such as ZMAP gave full control over all the methods that were used and their implementation. Valuable skills in using MATLAB and a deeper understanding of the methods were also achieved.

The program starts by reading information about all of the events from a text file. One can choose to perform a temporal study of the *b*-value, where a given number of events stepped through time are used to calculate a *b*-value, thereby identifying any temporal changes. Or one can perform a single *b*-value estimation on a particular set of data. The user is able to select M_{min} in three ways; as the magnitude with the highest number of events, a user defined M_{min} based on an inspection of the magnitude distribution or M_{min} as determined by the GFT method (Wiemer and Wyss, 2000). From here, the maximum likelihood procedure for estimating the *b*-value is performed.

The purpose of this exercise was to determine if there have been any significant changes in the characteristics of the seismicity that can be attributed to the flooding of the abandoned mines and then to explain those changes. For this purpose, we computed the *b*-value for seismicity before and after the last pump stopped pumping. The procedure for estimating the *b*-value in this study involved the use of equation 2.11, the Aki (1965) and Utsu (1965) maximum likelihood solution with the Utsu (1966) correction. The estimation of the standard deviation was computed by equation 2.14 from Shi and Bolt (1982) and the minimum magnitude of completeness was chosen by the GFT method of Wiemer and Wyss (2000) or where the minimum qualifying criterion of at least a 90% fit could not be satisfied, it was user defined based on an inspection of the frequency-magnitude and GFT distributions.

© University of Pretoria

UNIVERSITEIT VAN PRETORIA
UNIVERSITY OF PRETORIA
YUNIBESITHI YA PRETORIA

2.4. The Seismic Catalogue

Data was extracted for the time period starting from October 1996 up to the end of October 2012. The data was collected by two different networks during this time: the broad national network, which monitors the entire country, thus, having a lower detection threshold, and a local network constructed specifically for the Central Rand Basin in 2010. Both are described below.

2.4.1. The South African National Seismograph Network

The National network reached a maximum of 27 seismograph stations around the country in 1997, which were predominantly vertical-component short-period sensors. The network was modernized through a government grant in 2003 with the purchase of three-component extended short-period and broadband sensors. The development of this network is presented in detail by Saunders *et al.* (2008). Only one station was placed in the CRB at the time. This was at East Rand Proprietary Mine (ERPM) in mid-2006. The next closest station was in Silverton, Pretoria.

The numbers and quality of events improved considerably from 2006 onwards due to improved equipment and processing procedures. Prior to this, data is sparse, especially for events smaller than M_L 2.5. This was confirmed by plotting the number of events recorded bi-monthly over time for different magnitudes. With the final closure of deep mining and pumping operations in the Central Rand Basin in 2008, interest in the seismic risk due to flooding-induced seismicity prompted the establishment of a localized network to monitor activity. This was only completed by 2010.

© University of Pretoria

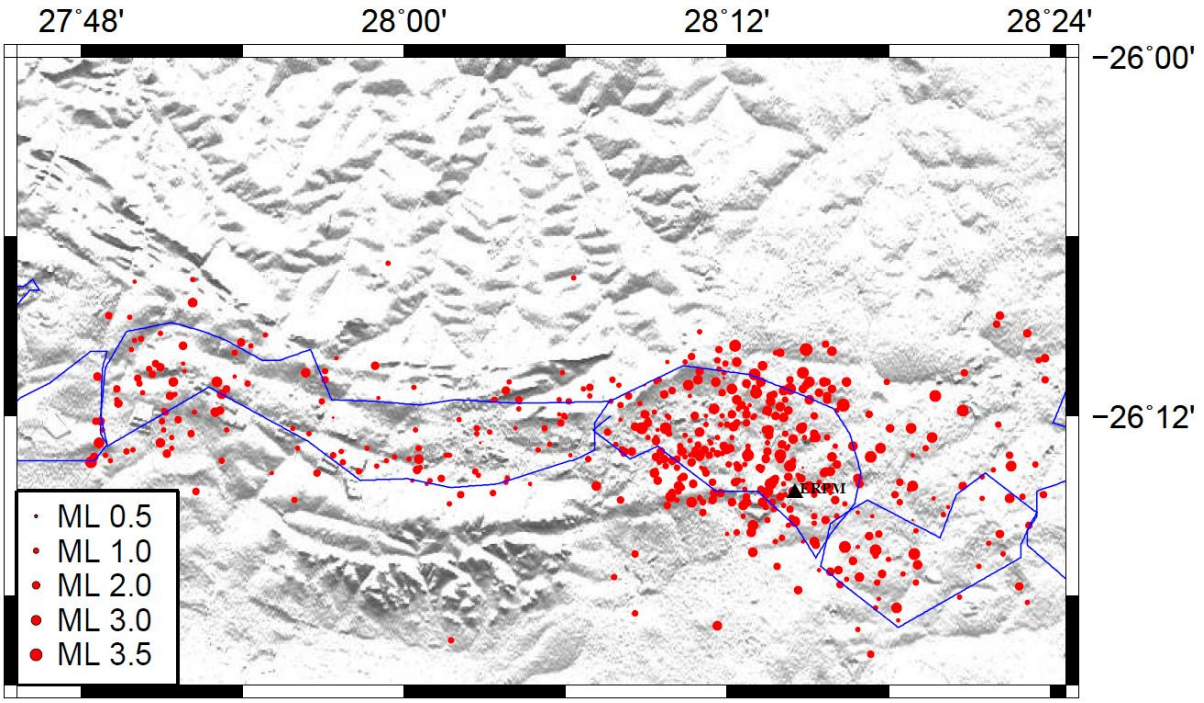

Figure 2 – Seismicity (red dots) recorded by the South African National Seismograph Network in the Central Rand Basin mining areas (boundaries defined by the blue lines) between 1996 and November 2008.

Figure 2 shows the distribution of seismicity in the Central Rand Basin as recorded by the national network up to November 2008. There is a large scatter and very few small magnitude events. Magnitudes range from M_L 0.8 to M_L 4.1. A total of 516 events are plotted here.

2.4.2. The Strategic Water Management Project Network

A network of 12 seismograph stations has been in operation in the Central Rand Basin since March 2010, providing valuable seismic data. The network has a wide longitudinal coverage (~50 km) as opposed to latitudinal (~15 km) due to the shape of the basin. This has an adverse effect on the latitudinal constraint of seismic event locations. Current longitude and latitude location errors are in the range of 500 m. Almost all of the events that have been recorded to date fall within mine boundaries, suggesting that the presence of the abandoned mine void and associated induced stresses is still the main driving force behind the observed seismicity. Accurate depth determination would answer this question with certainty. Although 12 stations over such a small area seems dense, depth determination without the use

© University of Pretoria

UNIVERSITEIT VAN PRETORIA
UNIVERSITY OF PRETORIA
YUNIBESITHI YA PRETORIA

of additional phase identification requires that the nearest station be a distance away from the epicentre that is similar to the depth of the event. Due to the shallow nature of the seismicity (mining extends 3.5 km deep) this rarely happens for the larger events that are observed.

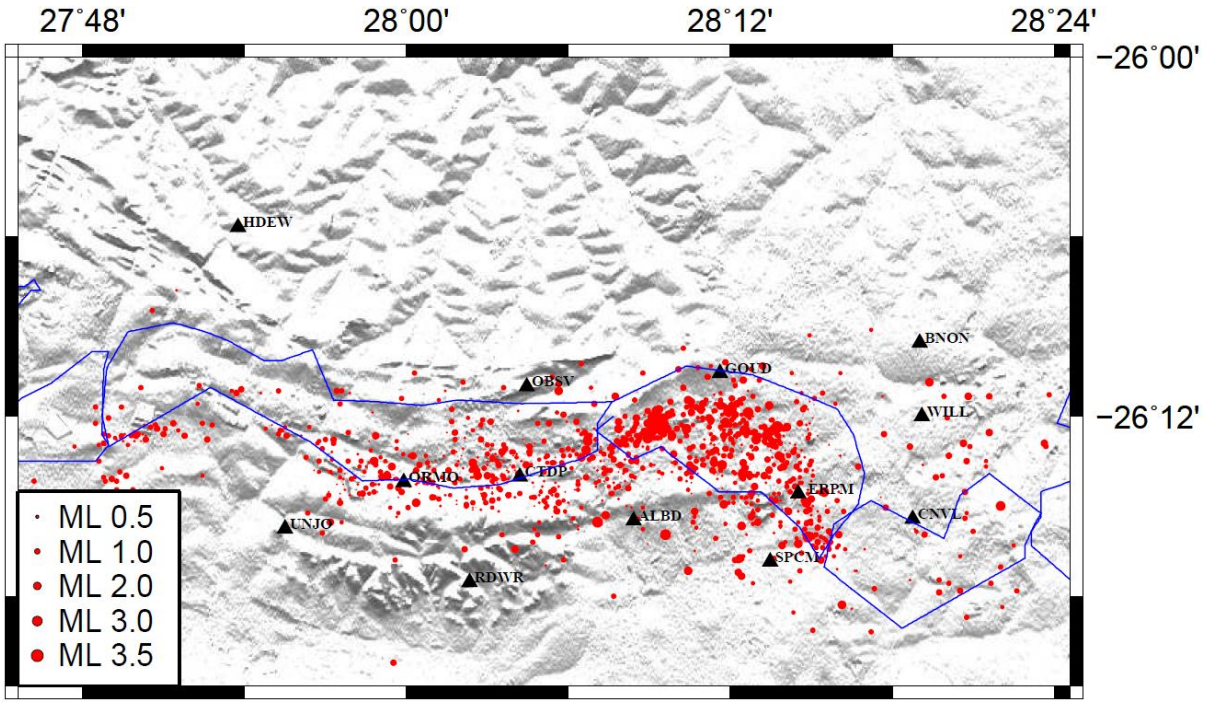

Figure 3 – Seismicity recorded by the South African National Seismograph Network and the newly established SWMP Network in the Central Rand Basin between November 2008 and October 2012.

Figure 3 shows a reduced scatter, more clustering concentrated within the mine boundaries and a higher proportion of small magnitude events. Magnitudes range from M_L 0.2 to M_L 3.5. A total of 1197 are plotted here with 215 recorded before March 2010 and 982 recorded with the SWMP network between March 2010 and October 2012. The impact of the denser SWMP network on the measured seismicity is clearly evidenced by the dramatic increase in the number of events that were recorded. Accuracy has also improved as denser clusters of seismicity can be seen.

© University of Pretoria

UNIVERSITEIT VAN PRETORIA
UNIVERSITY OF PRETORIA
YUNIBESITHI YA PRETORIA

2.5. A Physical Interpretation of the *b*-Value

The *b*-value is often found to be close to one in studies of natural earthquakes in different areas around the globe (Wolf *et al.*, 1997; Frolich and Davis, 1993). This implies a type of self-similarity under the G-R law for natural seismicity, which is theoretically explored by Kanamori and Anderson (1975). A temporal change in the value of *b* should then have implications on the system responsible for producing the earthquakes.

A basic physical interpretation of a certain value of *b* can be made once it is understood that *b* represents the ratio of small to large events. The magnitude of a seismic event is dependent on the amount of energy that is released. A system which can store a large amount of energy i.e. accumulate a large amount of stress, has the ability to generate larger earthquakes than a system which stores less. Goertz-Allmann and Wiemer (2013) demonstrate this effect through geomechanical modelling of seismicity induced through pore-pressure perturbations within a geothermal reservoir. They show that at the points where the pore-pressure perturbations are the highest, the stress states responsible for triggering seismic events become less, leading to higher numbers of lower energy (smaller) events and a higher *b*-value.

Scholz (1968) successfully demonstrated a strong dependence of the *b*-value on stress during the deformation of rock in laboratory experiments. Rock samples were stressed in uniaxial compression and it was found that not only did the frequency-magnitude distribution obey the Gutenberg-Richter relation, but that a higher uniaxial compressive stress resulted in a lower *b*-value. Dependence on rock type and confining pressure were also tested but were not found to be significant. Others have demonstrated dependencies on material heterogeneity (Mogi, 1962) and even the thermal gradient of the crust (Warren and Latham, 1970; Farrell *et al.*, 2009). Nowadays it is widely accepted that a deviation in *b* carries a certain degree of significance. Continuous monitoring of the *b*-value has a place in routine seismic monitoring in mines (Gibowicz and Kijko, 1994) where stiffness, stress and rock mass heterogeneity are important.

The stiffness is defined as the ability of the rock to resist deformation (Mendecki *et al.*, 1999). A higher *b*-value indicates a stiffer rock mass since an increased resistance to large deformation would result in a higher proportion of small magnitude events. An increase in rock mass heterogeneity also corresponds with a higher *b*-value since uniformity would

© University of Pretoria

UNIVERSITEIT VAN PRETORIA
UNIVERSITY OF PRETORIA
YUNIBESITHI YA PRETORIA

encourage larger ruptures to occur, thereby, lowering the *b*-value. It follows that the *b*-value, in cases of induced seismicity, whether it is fluid- or mining induced, can vary considerably, i.e. $0.5 < b < 1.5$ (McGarr, 1976; Mendecki *et al.*, 1999; Nuannin *et al.*, 2005; Farrell *et al.*, 2009; Goertz-Allmann and Wiemer, 2013) depending on the state of the system concerned.

It is clear then, that the *b*-value is indicative of the current state for a given section of the earth's crust and due to its apparent simplicity is a very attractive method for tracking changes in a seismogenic region. Temporal changes in the *b*-value are often used to search for precursory phenomena associated with large earthquakes (Gibowicz, 1973; Enescu and Ito, 2003; Nuannin *et al.*, 2005; Tsukakoshi and Shimazaki, 2008).

© University of Pretoria

UNIVERSITEIT VAN PRETORIA
UNIVERSITY OF PRETORIA
YUNIBESITHI YA PRETORIA

2.6. Results and Discussion

The *b*-value was calculated for the period before pumping at ERPM was stopped, between January 1996 up to the end of October 2008, and then for a period afterwards, from November 2008 up to 31 October 2012. ERPM was the deepest mine and the last to close in the CRB. When it closed, rapid flooding commenced. The closure of the mine also meant that mining activities stopped, thus, marking the end of so-called mining-induced seismicity.

Figures 4 and 5 show results of the *b*-value and GFT estimations, respectively, for a period of time prior to the closing of the pump station at ERPM.

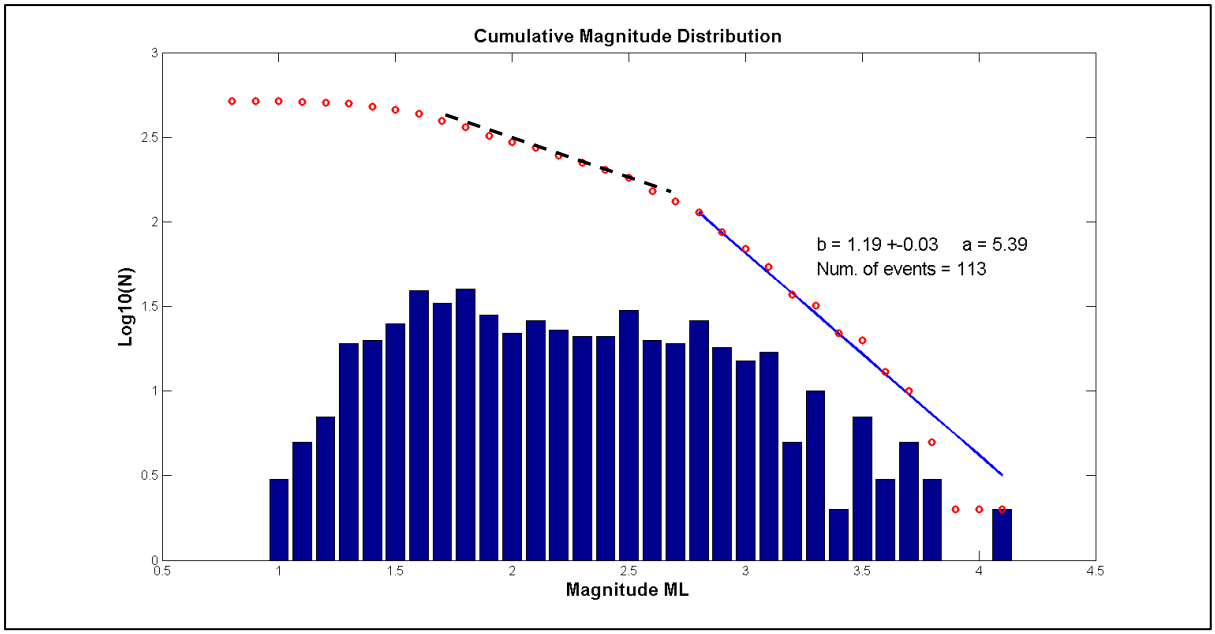

Figure 4 – b-value estimation for the Central Rand Basin in the period 1996 to 2008 before the closure of the pumps at ERPM.

The data in Figure 4 was recorded on the sparse national network, which was in operation at the time. There are two apparent slopes in the cumulative frequency-magnitude distribution (red circles), which is a common feature of mining-induced earthquakes related to two different mechanisms (Kijko *et al.*, 1987; Gibowicz and Kijko, 1994; Richardson and Jordan, 2002; Saunders *et al.*, 2010). The first mechanism, marked by the black dashed line is described as the fracturing of fresh rock associated with blasting activities and usually occurs

© University of Pretoria

close to the mining advance. The second slope is associated with larger magnitude events dominated by frictional sliding in pre-existing shear zones such as faults or dykes. These are usually a delayed response to blasting activities and are ascribed to the removal of rock underground occurring throughout the mining region. Evidence of these two types of mechanisms is given by Richardson and Jordan (2002) as well as Saunders *et al.* (2010) as observed in South African deep gold mines. Another plausible explanation is that there is a lack of events at smaller magnitudes due to the detection capabilities, which improved after the mines in the CRB had all closed.

Whatever the reason for these two slopes, the *b*-value was calculated for the second slope (blue solid line) because the catalogue is more complete at higher magnitudes. The *b*-value was 1.19 ± 0.03 for this period.

The GFT plot in Figure 5 shows that the optimum fit is reached where M_{min}= 2.8, although for all other magnitudes a very poor fit is obtained. The GFT% should become more stable at higher magnitudes but in this case it shows an erratic pattern due to incomplete data at higher magnitudes. This is because not enough data was present to fill in the gaps. As mentioned in Section 2.4.1, recording capabilities were fairly limited during this time.

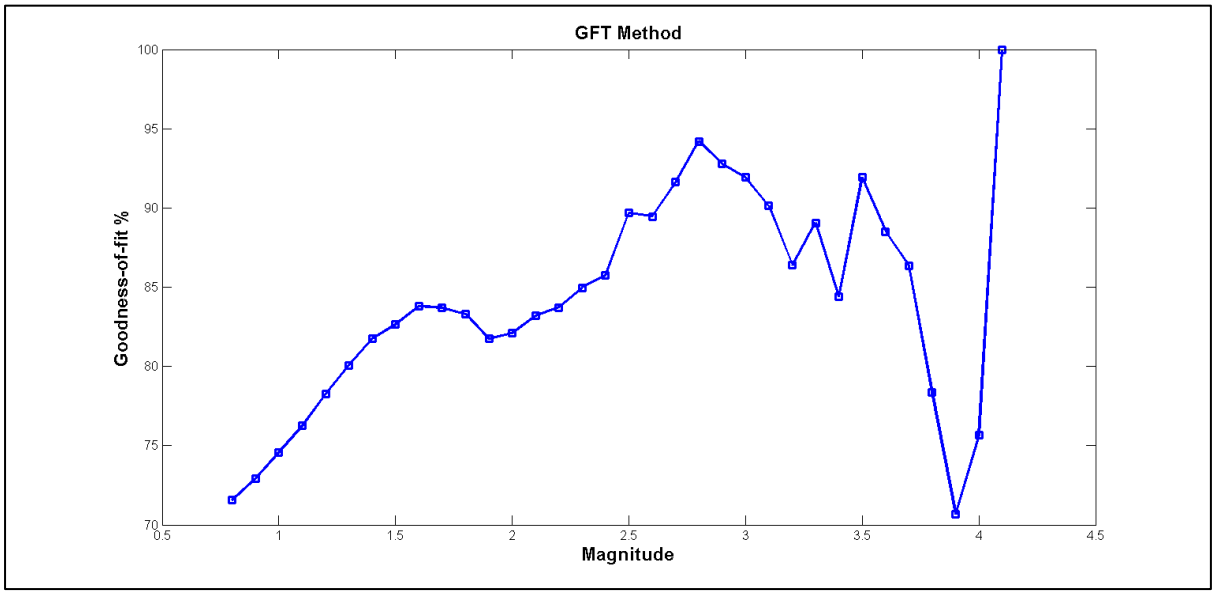

Figure 5 – Goodness-of-fit plot for the minimum magnitude of completeness estimation. A level of 95% could not be reached, thus, 94.21% reached at M_L 2.8, was used.

© University of Pretoria

UNIVERSITEIT VAN PRETORIA
UNIVERSITY OF PRETORIA
YUNIBESITHI YA PRETORIA

The dataset for the period after the closure of the pumping stations at ERPM extends from November 2008 to the end of October 2012. The *b*-value and GFT estimations are presented in Figures 6 and 7, respectively.

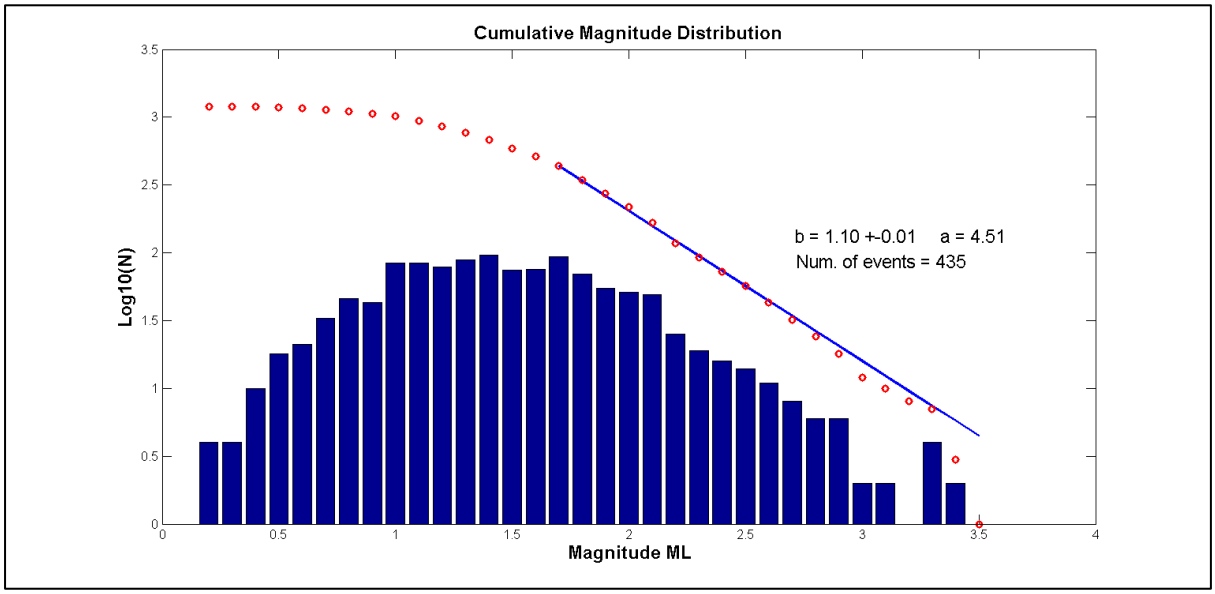

Figure 6 - b-value estimation for the Central Rand Basin in the period of November 2008 to October 2012 after the closure of the pumps at ERPM.

The bi-modal distribution seen in Figure 4 is not present in Figure 6 as would be expected with the closure of the mines. The database is clearly a lot more complete with a much lower minimum magnitude of completeness, M_{min}= 1.7. This is evidence of the improvement in detection capabilities and seismograph network coverage that took place during this period. The *b*-value for this period is 1.10 ± 0.01, suggesting a migration towards a more "natural-seismicity-like" system where stress reaches higher levels before it is released. Yet $b > 1$, which may indicate that characteristics associated with induced seismicity, still exist. Factors such as the high heterogeneity of the mined out rock and a lower stiffness may still be playing a role. Pore-pressure perturbations as a result of the flooding will also contribute to a higher *b*-value.

Figure 7 plots the results of the GFT estimations for the different magnitudes of completeness and clearly identifies M_{min}= 1.7 as the lowest magnitude with the best possible fit. The

© University of Pretoria

UNIVERSITEIT VAN PRETORIA
UNIVERSITY OF PRETORIA
YUNIBESITHI YA PRETORIA

GFT% is stable above 95% at magnitudes > 1.7 before dropping off as expected. This is indicative of a much more complete dataset.

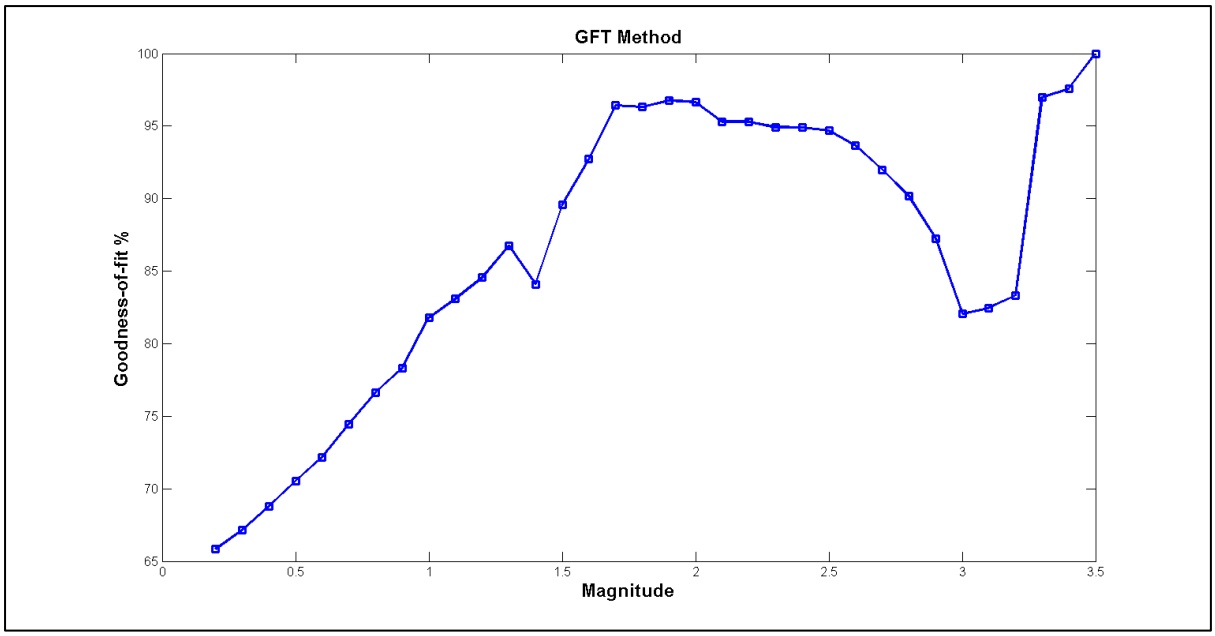

Figure 7 - Goodness-of-fit plot for the minimum magnitude of completeness estimation. A level of 95% was reached at M_L 1.7.

Results from the study of the temporal change in the *b*-value are presented in Figure 8 together with a histogram of the number of events recorded every two months. Improvements in the detection capability of the National Seismograph Network as well as improvements due to the establishment of the SWMP Network can clearly be seen. The *b*-values and corresponding standard deviations were estimated for every 100 events occurring in time. The value of 100 events was chosen to be enough for statistically defensible *b*-values so that the standard deviations did not obscure possible deviations and not so much that the deviations were smoothed out by windows that were too large.

The GFT method was once again used, where possible and standard deviations were estimated with equation 2.14 from Shi and Bolt (1982). Markers for the closure of the last pumping station in the CRB (red line) and rolling out of the local SWMP Network (green line) are plotted. The blue lines mark the points in time when the largest earthquakes occurred, $M_L \geq 3.3$.

© University of Pretoria

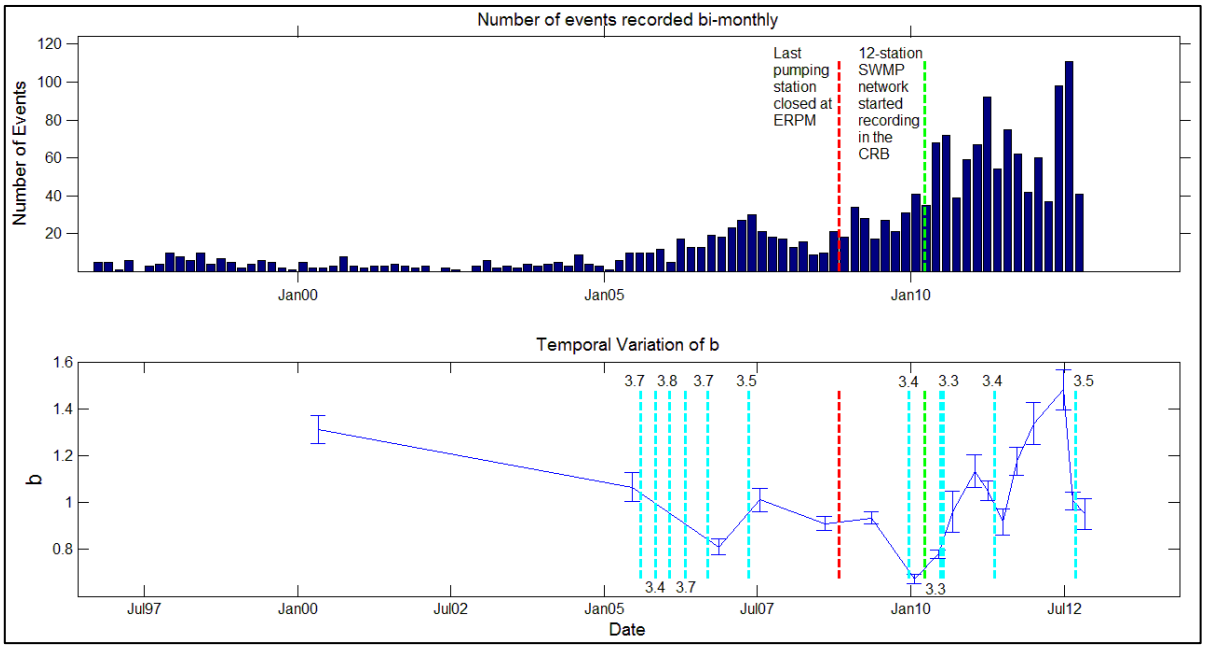

Figure 8 – Number of events recorded bi-monthly (top) and the b-value with error bars for every 100 events in time (bottom). The blue lines mark the occurrence of the largest earthquakes, ML ≥ 3.3.

In the short period under analysis there appears to periods of decreasing *b*-value followed by the onset of a large seismic event, in this case $M_L \geq 3.3$. This is similar to discoveries by Nuannin *et al.* (2005) and Tsukakoshi and Shimazaki (2008) for their respective scenarios. The *b*-value ranges between 0.7 and 1.5. The maximum magnitude does not appear to change much. Not a lot can be said about the period from 1996 to 2006 because of the sparse dataset. Only two *b*-value estimations could be made in this time window because of the poor detection capabilities in the CRB of the national network at the time. The period after the local SWMP network was commissioned boasts sufficient data but is relatively short.

It would be speculative to confirm, but one cannot ignore the possibility of a much larger event taking place ($M_L \geq 5$) considering that the rock mass is still seismically active 5 years after mining has stopped and that a lower *b*-value indicates a higher proportion of large magnitude events occurring. Another assessment at a later stage could be significant.

© University of Pretoria

UNIVERSITEIT VAN PRETORIA
UNIVERSITY OF PRETORIA
YUNIBESITHI YA PRETORIA

Chapter 3

3. A 3-Dimensional Distinct Element Model – Static Solution

The modelling software that was used is called 3DEC, a 3-dimensional distinct element code, part of the discrete element family of methods. It uses deformable contacts and an explicit, time-domain solution of Newton's equations of motion (Itasca Consulting Group, Inc., 2007). The model we created is an isotropic, elastic model. The program divides the blocks, which have been cut to form the mine void/faults/dykes, into zones with deformable contacts. The system is given boundary conditions and pre-mining in-situ stresses. The equations of motion are then solved for each contact as it is allowed to step through time.

The 3DEC model provided static solutions. Figure 9 is a schematic illustrating the extreme changes in the pore pressure along a fault intersecting the mined reef. The water table is lowered to the bottom of the lowermost stope during mining. Flooding then returns it to its original level, while also filling the mine void.

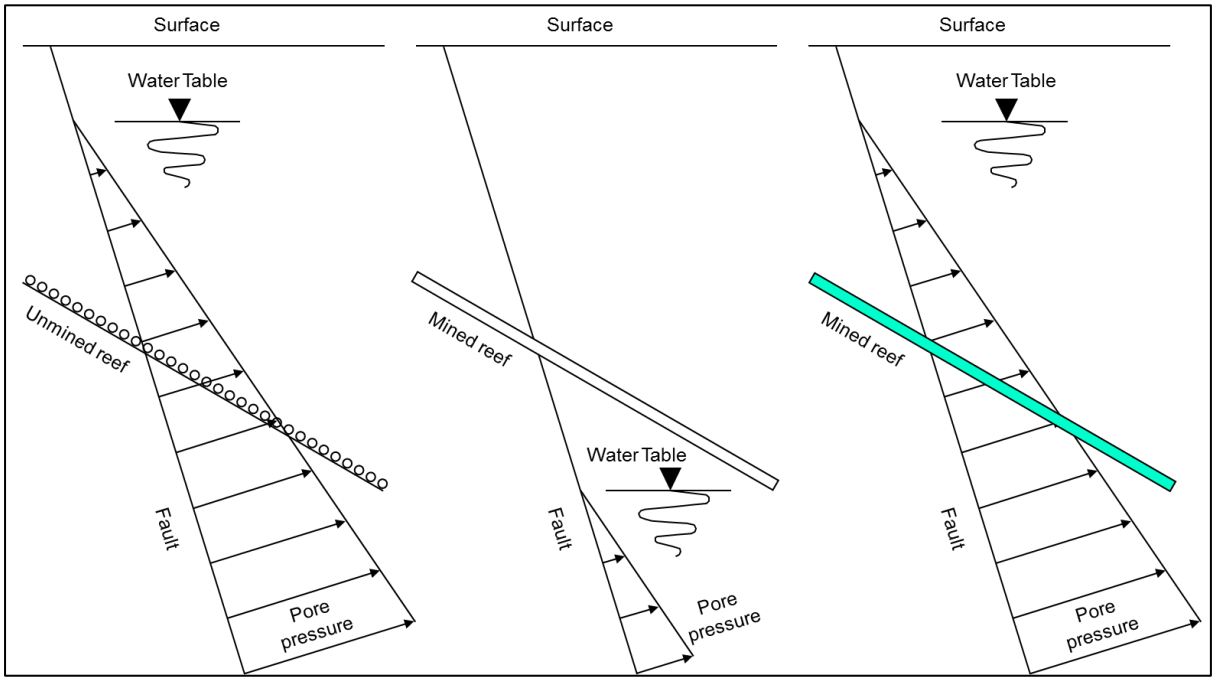

Figure 9 – Large scale changes in pore pressure as a result of mining.

© University of Pretoria

UNIVERSITEIT VAN PRETORIA
UNIVERSITY OF PRETORIA
YUNIBESITHI YA PRETORIA

The process of defining zones of seismic potential is a first step towards the mitigation of the seismic risk, since knowledge of high risk areas could lead to better city planning and readiness of emergency services. An attempt was made at finding the largest possible shear displacement in search for a measure of the largest possible earthquake. A plot of relocated seismic events that were recorded between 25 March 2010 and 30 June 2012 was used for comparison with the results.

© University of Pretoria

UNIVERSITEIT VAN PRETORIA
UNIVERSITY OF PRETORIA
YUNIBESITHI YA PRETORIA

3.1. Description of the Central Rand Goldfields

The Central Rand Basin forms the northernmost goldfield in the Witwatersrand Basin. It stretches 50 km from west to east along the outcrops of the Main Reef Leader, the Main Reef, and the South Reef, which formed the most important gold-bearing ore bodies in this region. Mining took place from surface to 3500 m below surface along much of the extent of the Central Rand Basin, commencing in 1886 after discovery of the goldfield and finally coming to an end in 2009 with the final closure of East Rand Proprietary Mines (ERPM).

Mining activities allow for rare insight into the crustal state especially when depths reach 3.5 km as in the case of ERPM. Mining followed the reef in a tabular fashion, which dipped to the south at roughly 30°. Over a century of mining, which started in 1886, has left behind a vacant slot in the earth's crust extending from the surface down to a maximum depth of 3500 m, and extending some 50 km from east to west.

The hypothesis for this study is that this particular geometry and left-lateral wrenching caused by a northeast/southwest basin-wide compression will cause structures of a certain orientation to be more prone to movement than others. Identifying these structures is important to understanding the risk that flooding might pose. The model interpretation was confined to an analysis of the steady-state solution. Any observations noted in the 3DEC model relied heavily on the initial stress conditions; therefore, care had to be taken in selecting these. A pre-mining stress state for the area under investigation was derived through an analysis of the Southern African Stress Measurement Database (Stacey and Wesseloo, 1998a; Handley, 2012).

© University of Pretoria

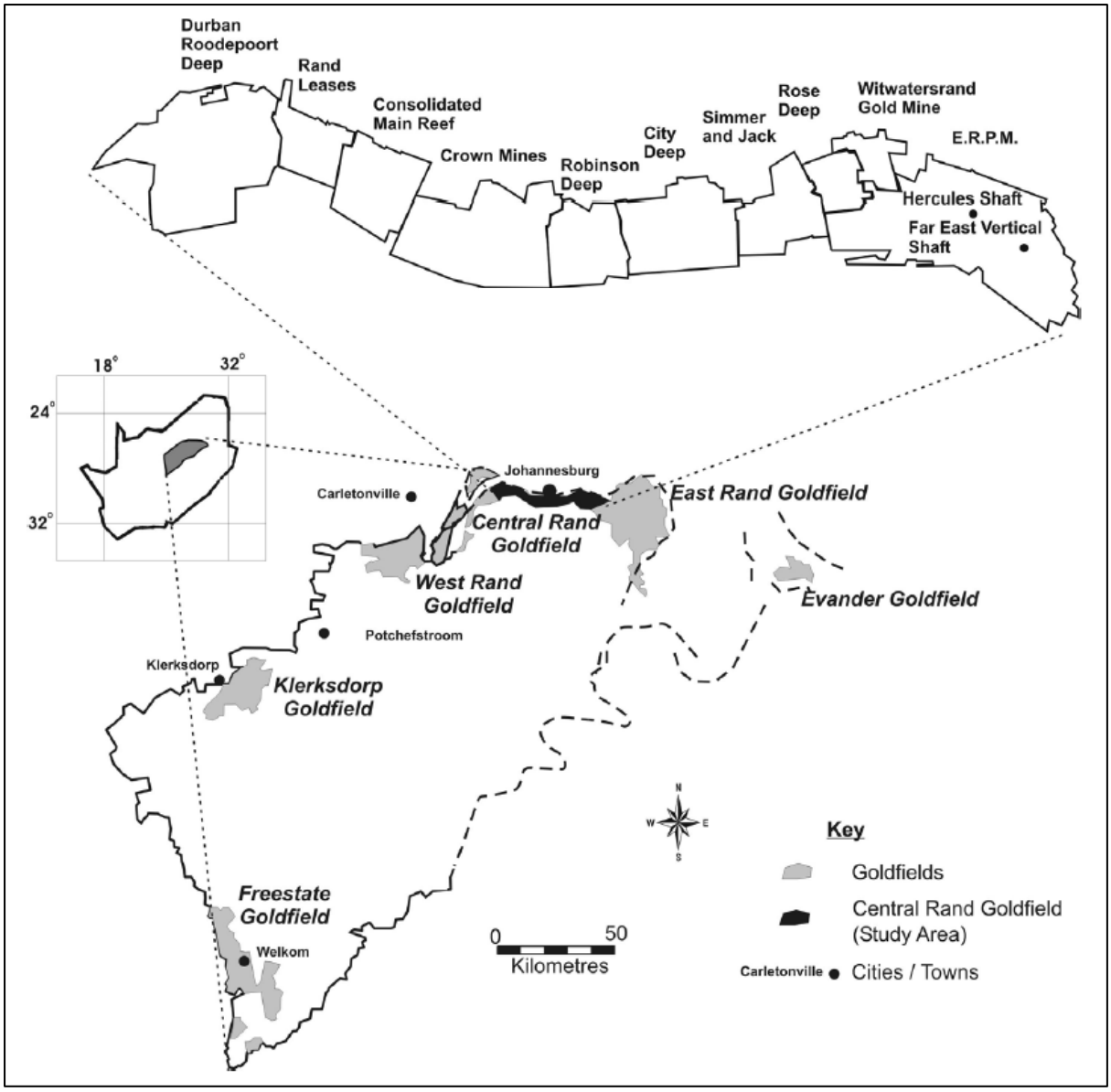

Figure 10 – Locality map of the Witwatersrand Basin, showing the location of the Central Rand and other goldfields of South Africa (modified by Stewart et al., 2004, after Schweitzer and Johnson, 1997). Also indicated are the mine boundaries of the Central Rand Goldfield.

© University of Pretoria

UNIVERSITEIT VAN PRETORIA
UNIVERSITY OF PRETORIA
YUNIBESITHI YA PRETORIA

3.2. Structural Setting

A detailed structural geology map based on underground observations is an example of important information that can be extracted while mining is taking place (Figure 11). The map shows all the dykes and faults together with their dislocation ages and some characteristics (normal, wrench, thrust etc.) overlain onto the reef contours.

In assessing this map, all the structures could be grouped into four distinct orientations. These orientations were later modelled to ascertain each ones propensity to slip. According to these orientations, labelled 1 to 4, the map can be divided into two parts. From DRD in the West up to Robinson Deep, orientations 1 and 4 appear to dominate and from City Deep to ERPM in the East orientations 2 and 3 occur most frequently (Figure 12). The dip direction of the mining also changes as it follows the folded reef, varying between approximately 140° to 220°.

© University of Pretoria

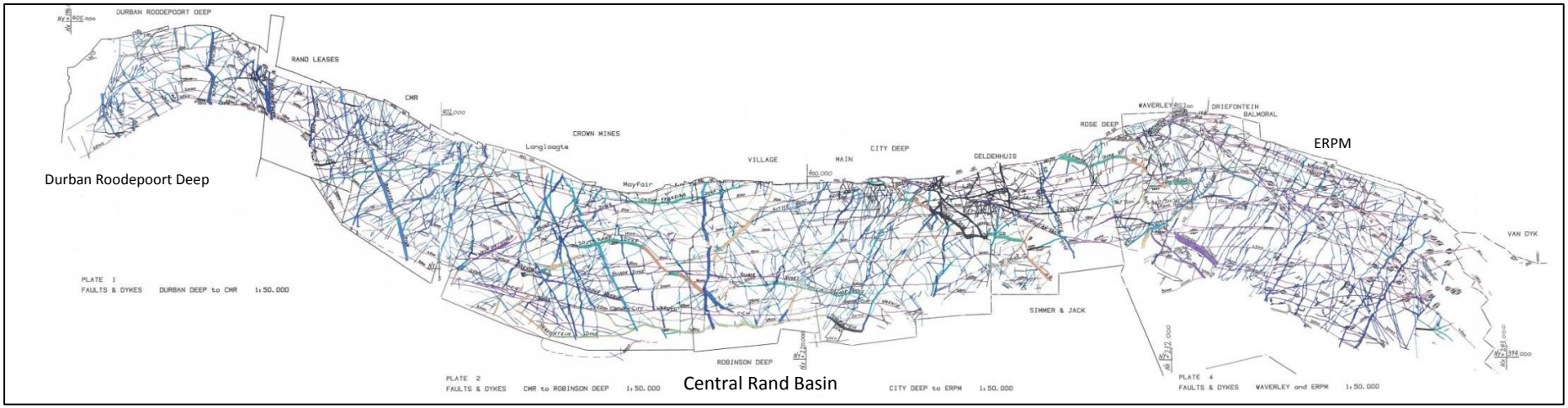

Figure 11 – Structural geology mapped underground in the mines (Pretorius, circa 1970).

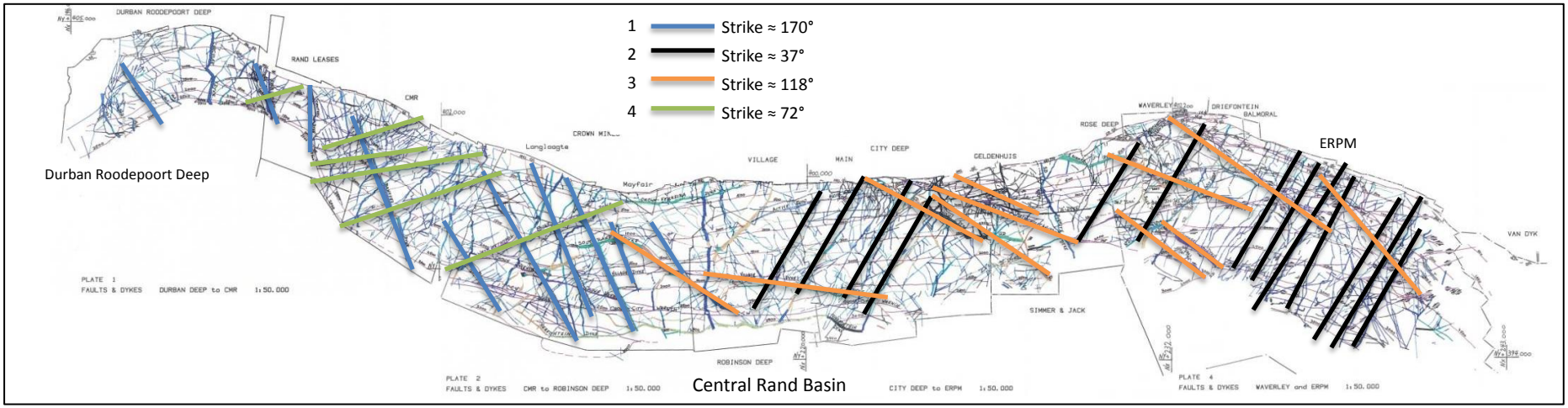

Figure 12 – Grouping dykes and faults according to approximate orientation.

© University of Pretoria

UNIVERSITEIT VAN PRETORIA
UNIVERSITY OF PRETORIA
YUNIBESITHI YA PRETORIA

3.2.1. Regional tectonics

Stewart *et al.* (2004) proposed a structural model for the Central Rand Goldfield which agrees well with findings of previous investigators. In this paper, the authors explain that the Witwatersrand Basin underwent northeast/southwest compression and throughout Central Rand Group times, the Rietfontein and West Rand faults (Figure 13) controlled sediment distribution. Regional synclines and anticlines formed in response to this basin-wide tectonic compression. Left-lateral wrenching associated with the Rietfontein fault later resulted in local folds being superimposed on the regional folds. The Rietfontein fault outlines the shape of the Central Rand Goldfield, changing from northwest/southeast in the west to northeast/southwest in the east. This might explain the bi-modal distribution of structure orientations across the basin. It is also probable that the eastern section of the Rietfontein fault experienced more left-lateral strike-slip under northeast/southwest compression, which would explain why left-lateral wrenching was only observed underground at ERPM (see Figures 11 and 12).

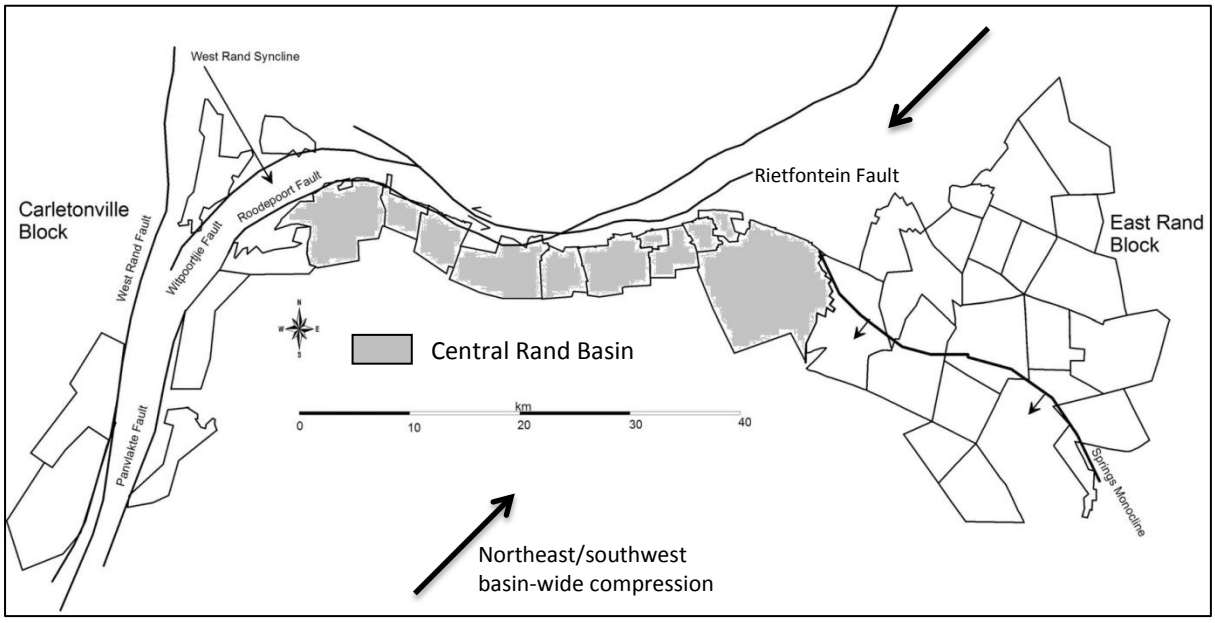

Figure 13 – Rietfontein fault with respect to the Central Rand Goldfields. (After Stewart et al., 2004)

© University of Pretoria

UNIVERSITEIT VAN PRETORIA
UNIVERSITY OF PRETORIA
YUNIBESITHI YA PRETORIA

3.2.2. Water ingress

The majority of the mines had closed by 1980, consequently ceasing their pumping operations. DRD in the west and ERPM in the east were the last to close in 2001 and late 2008 respectively. Since pumping stopped at ERPM, the water level has risen at approximately 0.3 m/day (Lixiang Lin, personal communication, 2010) according to measurements taken across the basin. In 2010 the water had reached essentially the same level across the basin, with ERPM being the last to fill up. Currently, the water level is at less than 400 m below the surface with the entire basin linked and filling up as one.

Goldbach (2010) completed a study based on data collected at ERPM. The study provides an extensive overview of examples of fluid related seismicity and evidence that the observed seismicity in ERPM was fluid-induced. It was observed that the seismicity was mainly located in the reef and migrated up-dip with a substantial increase in the event rate over an 18 month period. This trend followed the rising water level very closely. There was a 14 month delay before the onset of this period of rapid seismicity. It appeared that the delay was to allow sufficient build-up of pore pressures, which induced the seismic events. One particular reference addresses the hydromechanical interactions in a fault zone showing changes in fluid pressure, stress, and slip along the principal shear zone that depend on the heterogeneity of the fault (Cappa, 2009).

Many studies on the effects of reservoir impoundment on the level of seismicity in an area can be found (Athavale, 1975; Hsieh, 1981; Brandt, 2004). Studies that model the effects of high pressure fluid injection also offer some insight (Johnston, 2006). Seasonal changes have been linked to changes in reservoir induced seismicity as well (Saar and Manga, 2003).

© University of Pretoria

UNIVERSITEIT VAN PRETORIA
UNIVERSITY OF PRETORIA
YUNIBESITHI YA PRETORIA

3.3. Model Construction

Three models with a simplified mined out void were built. Each model contained the same four discontinuities dipping vertically and intersecting the void and each other. The only difference between the three was the orientation of the 30°-dipping void which varied in dip-direction from 142° (DRD) to 180° (City Deep) to 218° (ERPM).

The modelling procedure involved 4 stages:

1. The block was cut; creating the contacts for the mine void and geological discontinuities, and then zoned into distinct elements. The edge lengths were 50 m. Faults were represented by planar contacts.
2. Velocity boundary conditions, in-situ stress and stress gradients, gravitational constant, joint properties for the faults and rock properties for the rock mass were initialized. Automatic damping was assigned. The model was then allowed to step through time until a stopping criterion was reached indicating that the model reached equilibrium. This criterion was defined as the r-type average $\leq 1x10^{-5}$. R-type is defined as the average unbalanced mechanical force magnitude divided by the average applied mechanical force magnitude. The result of stage 2 represents an un-mined rock mass.
3. The mine excavation is then formed through the removal of material in a region defined during stage 1. This throws the model into an unbalanced state and it is again allowed to settle by stepping through iterations until the stopping criterion was reached. Shear displacements and stresses created through the removal of the rock mass are recorded and plotted.
4. All displacement values are reset without altering any deformation that has taken place in the model up to this point. A water table is established by defining a plane below which pore pressures at each grid point are defined. The pore pressure gradient was given by the direction of the gravity vector and the density of the water was defined as 1000 kg/m3. The model was once again allowed to settle after which results were extracted.

© University of Pretoria

UNIVERSITEIT VAN PRETORIA
UNIVERSITY OF PRETORIA
YUNIBESITHI YA PRETORIA

3.3.1. A pre-mining stress model

Because of the expense and difficulty of making stress measurements in rock, data are rare. Therefore, the pre-mining stress in the Earth's Crust is still poorly understood and poorly known. From 1963 to 1998, a period of 35 years, only 526 measurements have been made of the pre-mining stress state (also known as the virgin stress, or primitive stress) in Southern Africa. These were collected into a database by Stacey and Wesseloo (1998). Of the 526 measurements, 305 reported the full stress tensor, which includes the magnitudes of the nine components with reference to a pre-defined co-ordinate system. The remaining 221 produced partial results that were not used to estimate a pre-mining stress state for the 3DEC model.

Of the 305 complete stress measurements, 250 are consistent (see Handley, 2012), and these are used to determine a pre-mining stress model for ERPM, situated on the eastern edge of the Central Rand Basin. Only one measurement contained in this dataset was made at ERPM itself by Pallister (1969), and the result produces a vertical stress component that is some 40% less than the expected vertical stress due to the overburden weight. This result is shown in Figure 14 in relation to the least-squares best fit lines for the 250 stress measurements.

© University of Pretoria

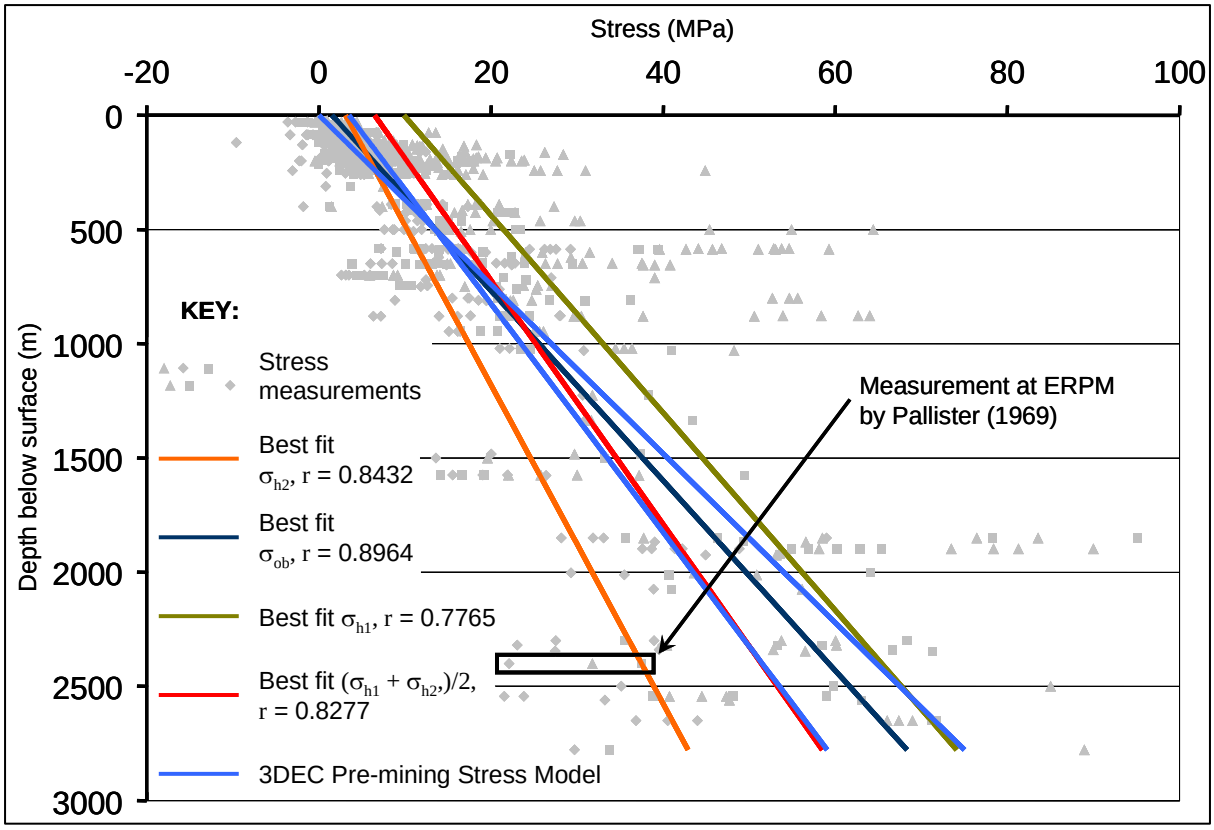

Figure 14 – Best fit pre-mining stress lines versus depth with stress measurement data in the background (Handley, 2012).

The grey symbols in Figure 14 represent the three principle stress components; maximum horizontal (σ_{h1}, tri-angle), minimum horizontal (σ_{h2}, diamond) and vertical (σ_{ob}, square). The least squares best fits were plotted for all three as well as for the average horizontal stress and then compared to the 3DEC pre-mining stress model. The 3DEC pre-mining stress model is plotted by the two light blue lines, one for the vertical stress and only for the horizontal stresses since they were assumed to be equal. The horizontal stresses are non-zero at the surface and equal with the vertical stress at a depth of 500 m. The vertical stress is simply equal to the overburden with an average assumed material density of 2,700 kg/m3.

The vertical stress has been shown to be fairly predictable, being close to the weight of the overburden (McGarr, Spottiswoode and Gay, 1975; McGarr and Gay, 1978; Gay, 1979). The maximum principal stress is horizontal above a depth of 500 m and vertical below that. This crossover is identified and discussed by McGarr and Gay (1978). Although the aforementioned authors have defined two different horizontal stresses, they are equal here for

© University of Pretoria

UNIVERSITEIT VAN PRETORIA
UNIVERSITY OF PRETORIA
YUNIBESITHI YA PRETORIA

two reasons: firstly, there is too little measured data (only one measurement in the region; Pallister, 1969); and secondly, to avoid directional bias in the geomechanical model.

The high r-values for the best fits can be attributed to the large concentration of measurements at shallow depths where the results are more consistent than at greater depths. The red (average horizontal stress best fit) and dark blue (vertical stress best fit) agree fairly well with the two light blue lines of the 3DEC pre-mining stress model.

Hoek and Brown (1980) report a world-wide trend with depth in the ratio of the horizontal stresses to the vertical stresses (known as the k-ratio), which appears in Figure 15. The k-ratio versus depth for the stress measurement dataset appears in the background of the plot (grey data points), which also contains the k-ratio for the 3DEC pre-mining stress model (light blue line).

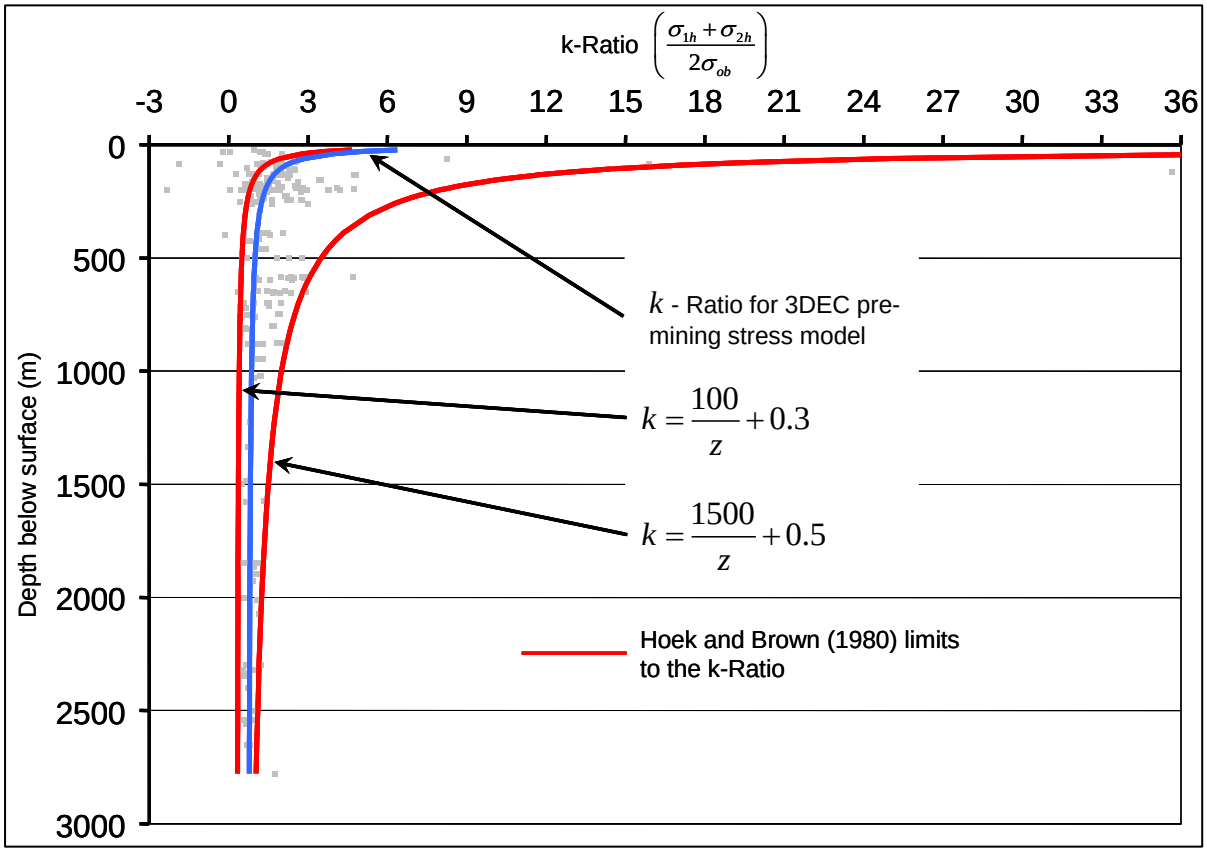

Figure 15 – Plot of k-Ratio variation with depth together with the Hoek and Brown (1980) limits and the 3DEC model (adapted from Handley, 2012).

© University of Pretoria

UNIVERSITEIT VAN PRETORIA
UNIVERSITY OF PRETORIA
YUNIBESITHI YA PRETORIA

Appropriate stress conditions are crucial to any model attempting to simulate processes in the earth's crust realistically. The selected pre-mining stress state was based on the work by Handley (2012), represented in Figures 14 and 15, which proposes a crustal stress model for Southern Africa based on a collection of stress measurement data collected by Stacey and Wesseloo (1998a). The 3DEC pre-mining stress model was defined as follows, where z is depth in metres:

Vertical stress (MPa): $\sigma_v = 0.027z$

Horizontal stress (MPa): $\sigma_{H1} = \sigma_{H2} = 3.5 + 0.02z$

The use of equal horizontal stresses is justified but it does present a possible oversight. A bias towards a particular stress orientation would influence the length of rupture, i.e. seismic event magnitude, and the definition of which areas are the most susceptible to large events.

3.3.2. Boundary conditions

The boundary conditions that were used are standard practice in this type of modelling (Itasca Consulting Group, Inc., 2007). Zero-velocity conditions were imposed on the sides and bottom of the model, preventing the block from moving downwards under the influence of gravity, while the top surface was constrained by the stress boundary condition defined in Section 3.3.1.

The use of zero-velocity boundary conditions is crucial in that it prevents the model from moving at a constant velocity when material is added or removed. This would not be a true representation of the earth's crust, yet adding zero-velocity boundaries is not a real-world representation either. This introduces boundary effects, which have to be considered. To account for this, a larger block was defined than was analysed. The dimensions of the full model were 2000 m x 2000 m x 1200 m while an inner zone of size 1400 m x 1400 m x 1200 m was viewed under analysis. The inner zone had edge lengths of 50 m while the less important "buffer zone" was assigned edge lengths of 100 m to speed up computation.

A key feature of the model is the creation of a void that represents a simplified mining excavation. When material is removed/excavated in the model, null blocks are created and all stresses are removed from these elements. As a result, stress-free surfaces are created on the boundary of an excavation.

© University of Pretoria

UNIVERSITEIT VAN PRETORIA
UNIVERSITY OF PRETORIA
YUNIBESITHI YA PRETORIA

3.3.3. Material properties

The rock mass in the deep gold mines of the Witwatersrand Basin tends to be strong and brittle (McGarr and Gay, 1978; Gay, 1979) consisting largely of Precambrian quartzites. Mechanical rock properties that were used in the model were taken from many studies that were conducted in the deep gold mines of South Africa while mining was still taking place (McGarr, Spottiswoode and Gay, 1975; McGarr and Gay, 1978; Gay, 1979). Table 2 defines estimations of the mechanical properties of Witwatersrand quartzite used in the model and Table 3, those for a typical fault.

Table 2 – Mechanical properties of the rock mass.

	Density (kg/m³)	**Bulk Modulus (GPa)**	**Shear Modulus (GPa)**
Witwatersrand Quartzite	2700	39.8	37.7

Table 3 – Mechanical properties of the fault.

Normal stiffness (N/m)	**Shear stiffness (N/m)**	**Cohesion (kPa)**	**Tensile strength (kPa)**	**Friction Angle (degrees)**
2×10^{10}	2×10^{10}	50	5	30

3DEC treats the rock mass as impermeable and pore pressure is only exerted along the contacts hydrostatically, throughout the model. This means that all faults are treated as 100% porous and the rocks as 0% permeable. The Witwatersrand quartzite has a very low permeability and the fracture system accounts for a high porosity (Goldbach, 2010), which suits the assumptions in the model.

© University of Pretoria

UNIVERSITEIT VAN PRETORIA
UNIVERSITY OF PRETORIA
YUNIBESITHI YA PRETORIA

3.4. Results and Discussion

The models behaved very regularly producing shear stresses and displacements very similar in magnitude to those observed underground by McGarr and others (McGarr, Spottiswoode and Gay, 1975; McGarr and Gay, 1978; Gay, 1979). McGarr *et al.* (1979) described observations of stress in seismogenic regions near a tabular mine excavation at ERPM. They noted that the typical shear stress in this region is approximately 70 MPa and that stress drops for mine tremors are similar to those for natural earthquakes, which range from 0.1 to 10 MPa. The maximum shear stress created along the discontinuities by the simple mining excavation (Stage 3 in the model construction described in Section 3.3) was approximately 60 MPa (see Figure 18) and the stress drop, which occurred as a result of adding the water table, was 8.5 MPa. This lent some credibility to the use of the pre-mining stress and boundary conditions. Figure 16 is an image of the model, showing the four discontinuities and mine void.

© University of Pretoria

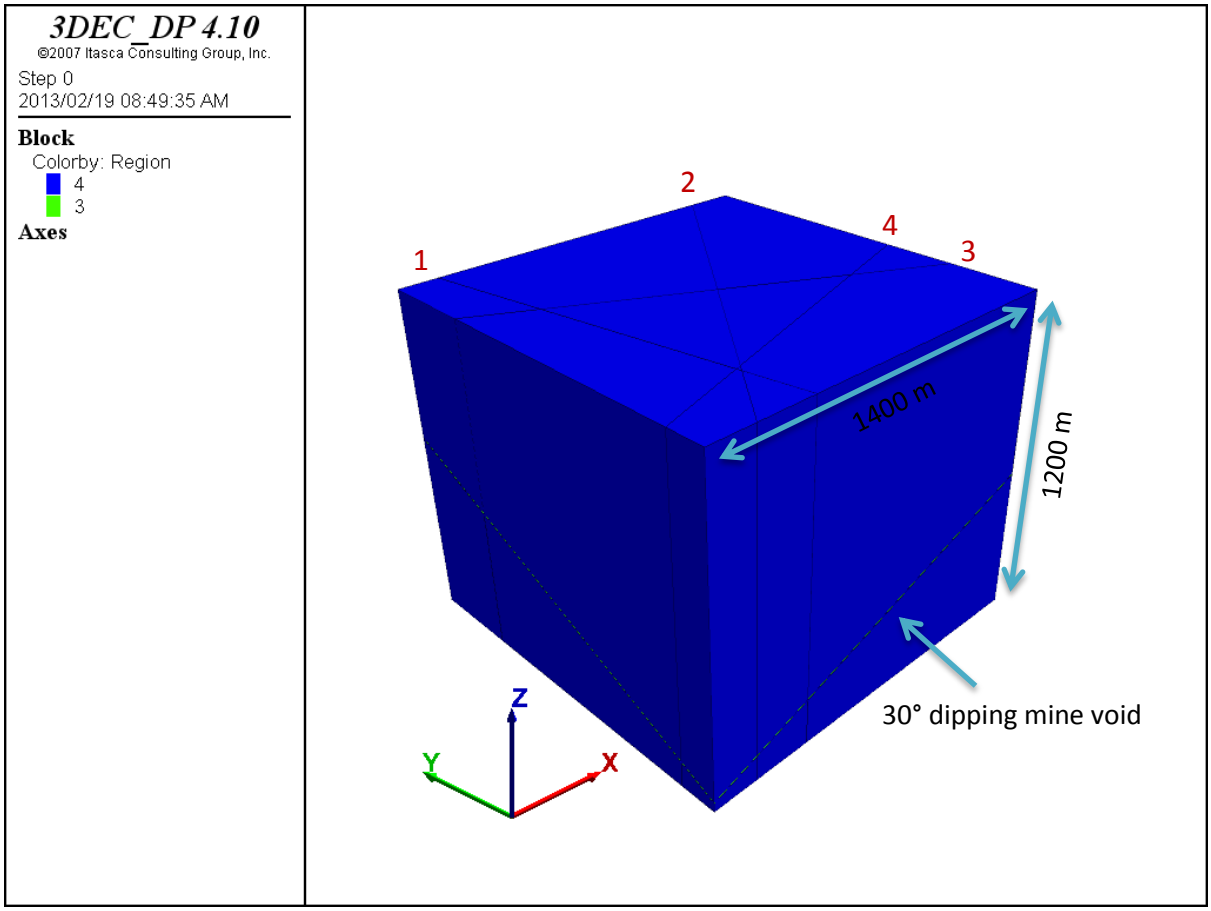

Figure 16 – 3DEC block model showing the vertically dipping faults orientated in the four directions and intersecting the mine void.

The excavation of material to form the simple mine void created highly stressed zones and some shear displacement near the void. This simulated the effect of a very simple, worst case mining geometry causing stress on the geological features. Figures 17 and 18 show the joint shear displacement and shear stress magnitude contours on the geological features in the model.

© University of Pretoria

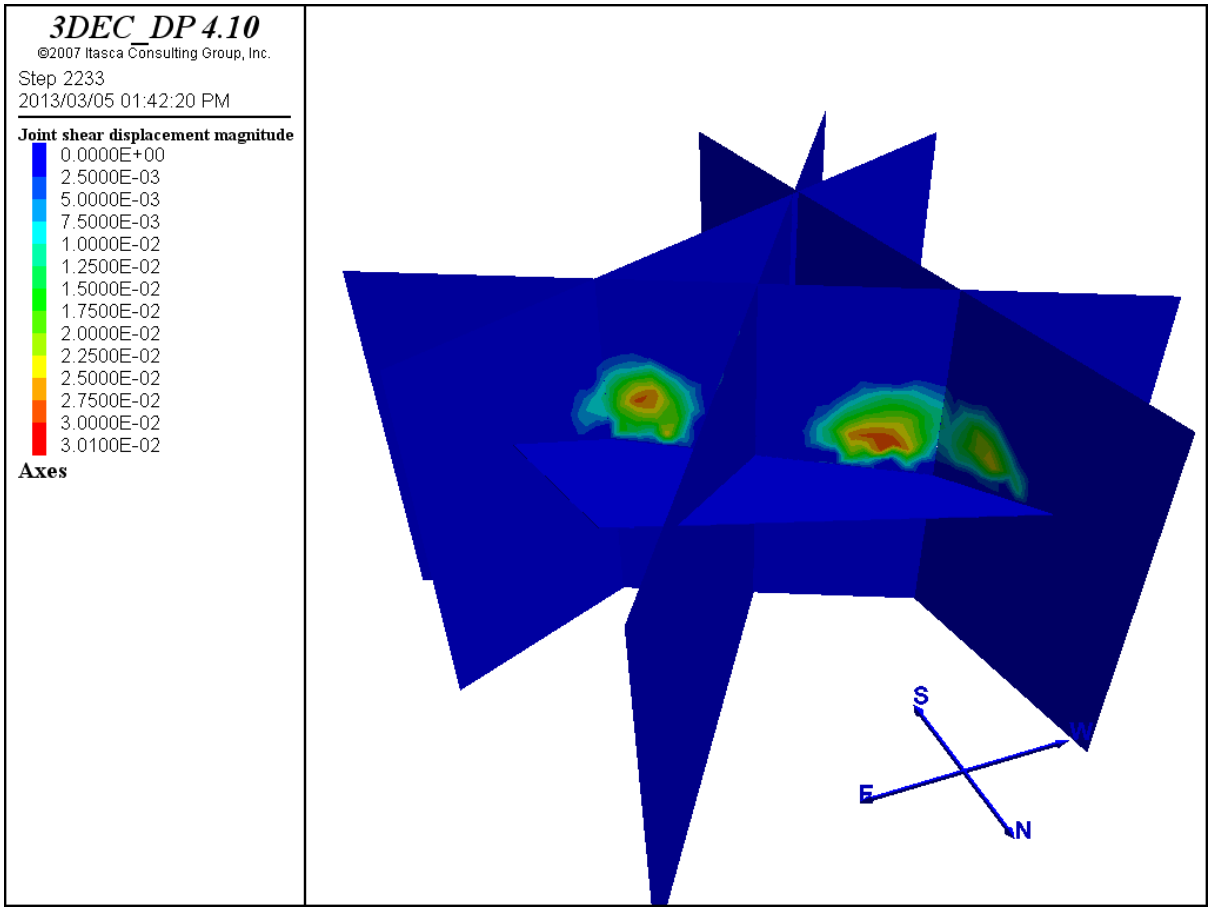

Figure 17 – Joint shear displacement magnitude contours that were induced by the formation of the simple void (Stage 3 in the model construction).

© University of Pretoria

UNIVERSITEIT VAN PRETORIA
UNIVERSITY OF PRETORIA
YUNIBESITHI YA PRETORIA

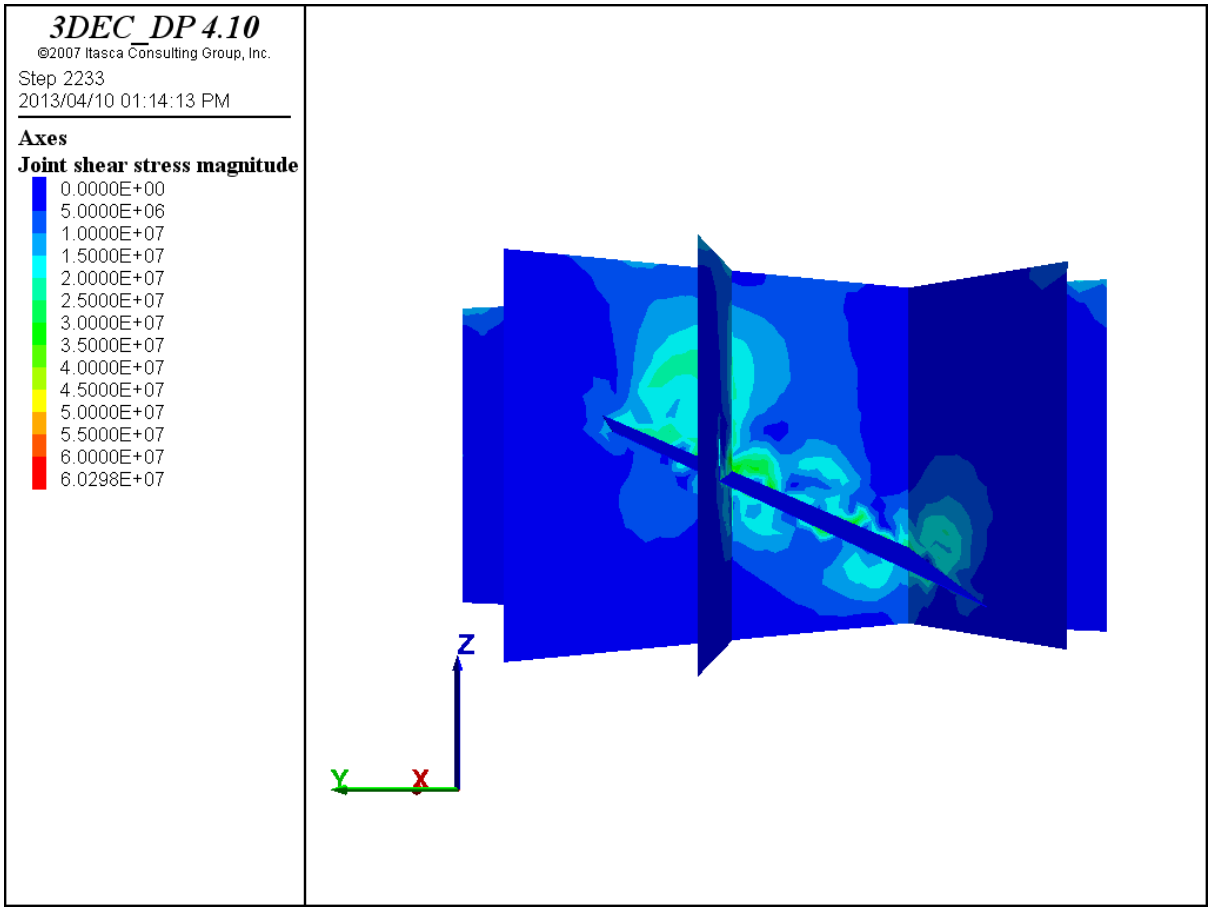

Figure 18 – Joint shear stress magnitude contours that were induced by the formation of the simple void (Stage 3 in the model construction).

The areas that showed major shear displacement (Figure 17) with the formation of the simple void (Stage 3) coincided with the areas that slipped due to the establishment of the water table (Stage 4) in the model. The majority of the deformation occurred in the hanging wall. Remembering that the material is the same for both hanging wall and foot wall around the stope, this artefact in the model is caused by a lower joint normal stress i.e. clamping force, in the shallower parts related to the horizontal stress, which increases with depth in our crustal stress model.

The results from Stage 4 in the model, where the water table is established and the structures experience shear displacement, are presented in the next section. This section deals with the spatial distribution of the structures within the CRB.

© University of Pretoria

UNIVERSITEIT VAN PRETORIA
UNIVERSITY OF PRETORIA
YUNIBESITHI YA PRETORIA

3.4.1. Spatial distribution

Based on the shear displacements that formed on the model discontinuities when the pore pressure was applied, vulnerabilities in each of the models were identified. The distribution of these vulnerable structures within the CRB was plotted on the structural geology map to identify areas that may be at greater risk than others.

Figures 19 to 21 are contour plots of the shear displacement that took place on the joints for each of the different orientations of the dipping, tabular mine void. The models were all at the stage where a water table had been established near the surface and they had been allowed to cycle until equilibrium was reached. The red arrow points in the direction of dip of the mine void.

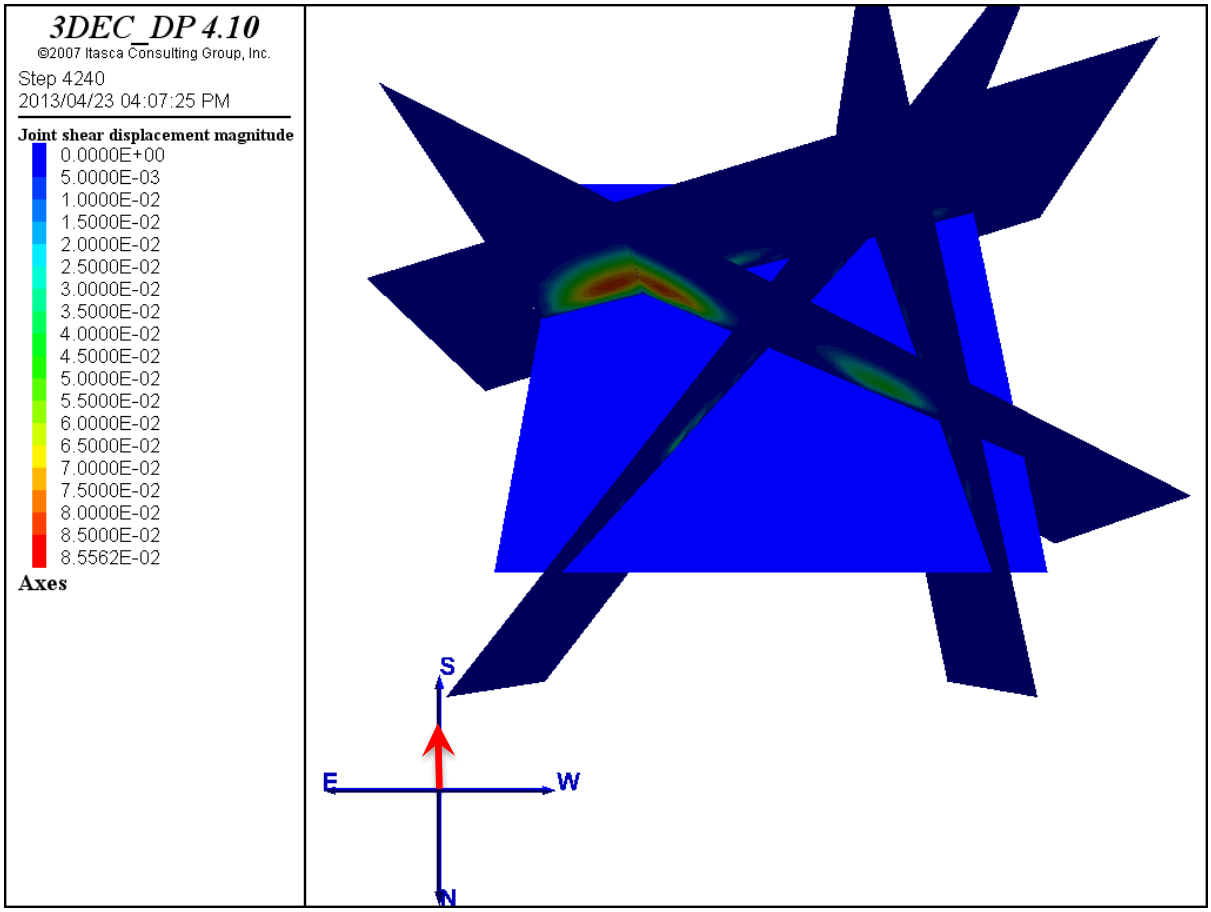

Figure 19 – Shear displacement magnitude contours on features intersecting the southerly dipping (180°) mine, representative of the Robinson Deep to City Deep mines at the centre of the Central Rand Basin.

© University of Pretoria

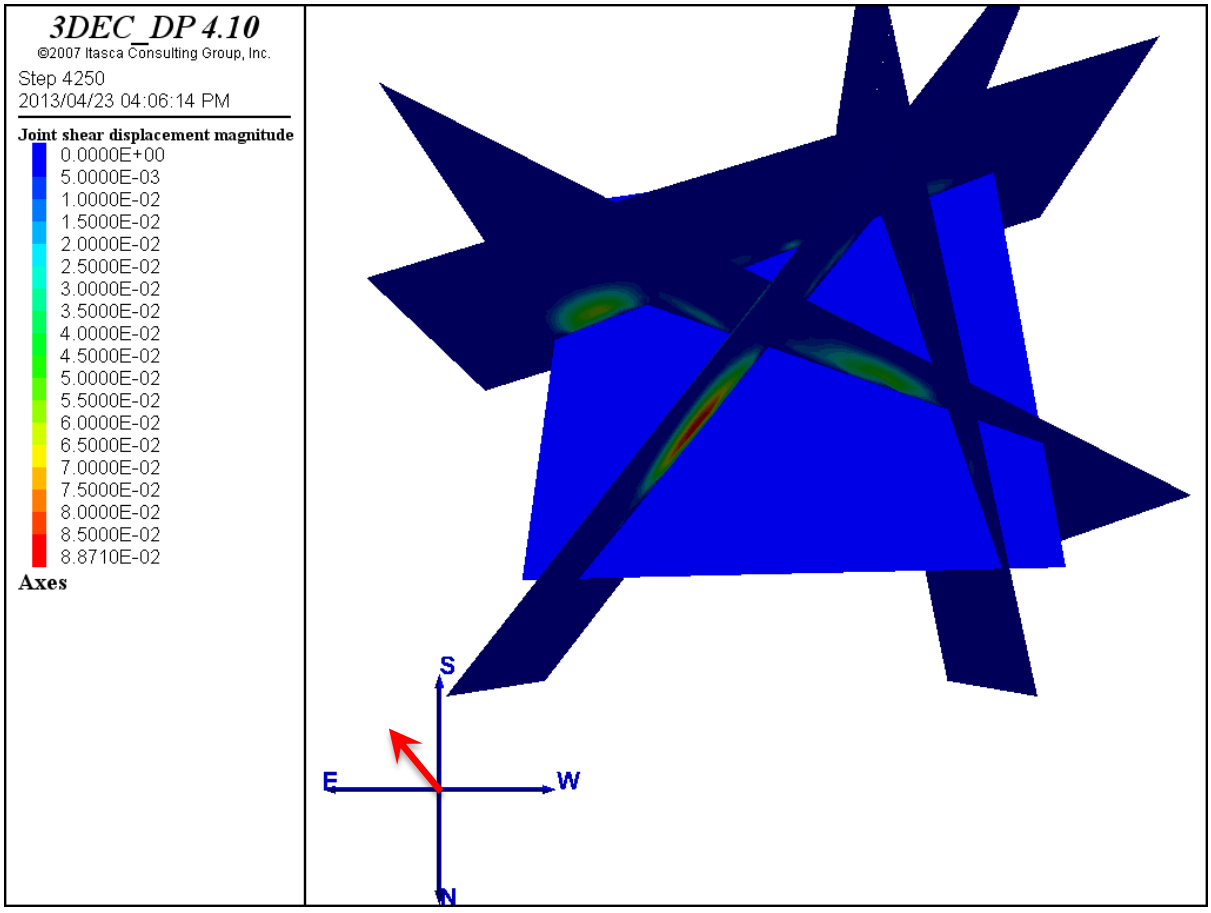

Figure 20 – Shear displacement magnitude contours on features intersecting the south-easterly dipping (142°) mine, representative of the DRD mine in the western section of the Central Rand Basin.

© University of Pretoria

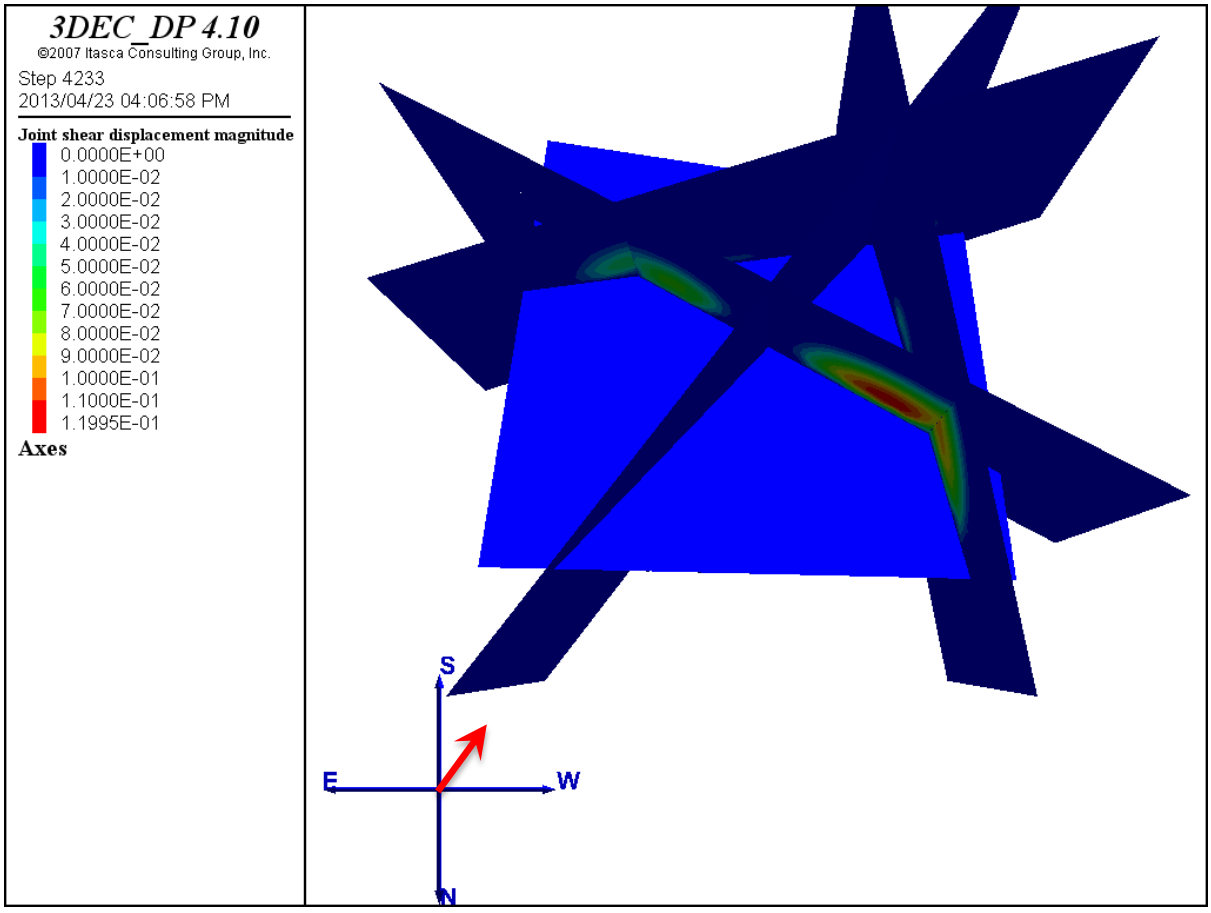

Figure 21 – Shear displacement magnitude contours on features intersecting the south-westerly dipping (218°) mine, representative of ERPM in the eastern section of the Central Rand Basin.

It is clear from Figures 19 to 21 that the features "most perpendicular" to the direction of dip experience most of the shear displacement in the model and those parallel to the mining advance experience very little. In reality, this can be expected since the water would affect a longer length of strike parallel features simultaneously. This illustrates the strong dependence on the geometrical configuration, which is the central theme to this study. The propensity to slip is determined by the relative orientation of the feature with the mining void.

The largest shear displacement magnitude is observed in Figure 21 (modelled after ERPM), where the void is orientated in a south-westerly direction. The maximum amount of shear slip was nearly 12 cm compared to approximately 9 cm in the two previous figures. This can be attributed to the feature being "more parallel" to the dip direction of the mined out reef, e.g. the feature in question is aligned with trend number 3 from Figure 12 (strike ≈ 118°) and the void dips towards a bearing of 218°.

© University of Pretoria

UNIVERSITEIT VAN PRETORIA
UNIVERSITY OF PRETORIA
YUNIBESITHI YA PRETORIA

The results from the models were combined with Figure 11 in an attempt to find areas with a high potential for instability (see Figure 22).

© University of Pretoria

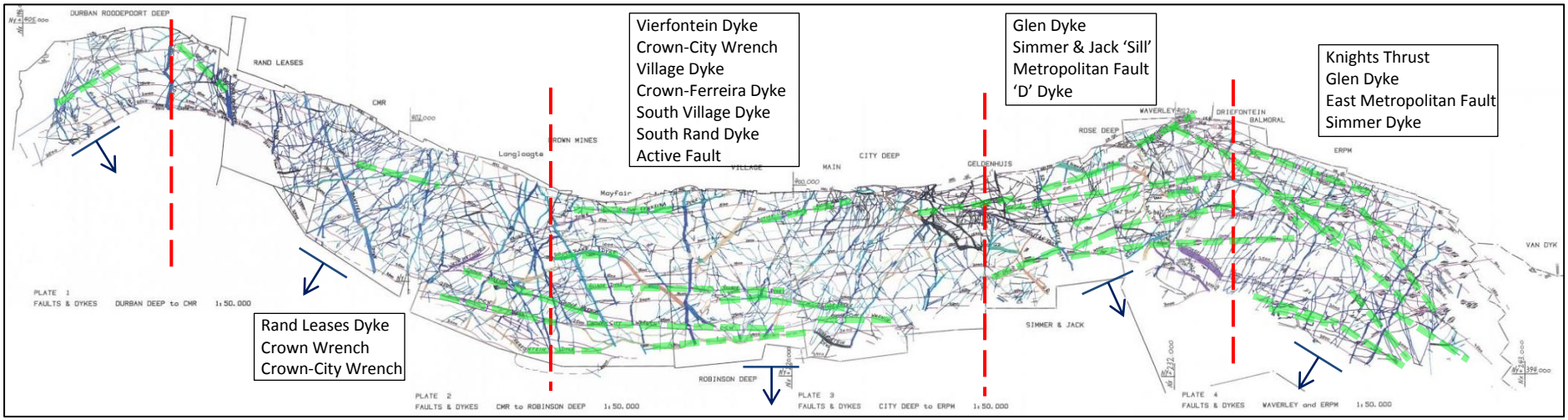

Figure 22 - The structural geology map (Pretorius, circa 1970) was divided (red lines) according to the change in dip direction (blue lines) of the mine void. Features that are likely to slip according to their orientation with respect to the mine void are highlighted (green lines). Some of these were given names during mining and those names are listed in the blocks.

© University of Pretoria

UNIVERSITEIT VAN PRETORIA
UNIVERSITY OF PRETORIA
YUNIBESITHI YA PRETORIA

3.4.2. Maximum observed shear displacements

Using the Hanks and Kanamori (1979) moment magnitude scale and estimation for the seismic moment given by equations 3.1 and 3.2, we were able to estimate the moment magnitude for the largest shear displacements in the three modelled scenarios represented in Figures 19, 20 and 21.

$$M_W = \frac{2}{3}(\log_{10} M_0 - 9.1) \tag{3.1}$$

$$M_0 = \mu A D \tag{3.2}$$

μ = Shear modulus = 30 GPa; A = Area of rupture; D = Average displacement on A.

The areas of rupture and average displacements for the respective Figures 19, 20 and 21 were approximately:

Table 4 – Results from the estimation of the moment magnitude for the maximum observed shear displacement in each of the three models using the Hanks and Kanamori (1979) moment magnitude scale.

Bearing of mining advance	**Area of rupture (km^2)**	**Ave. shear displacement (m)**	**M_W (Eq. 1)**
180°	0.255	0.045	3.62
142°	0.218	0.050	3.61
218°	0.346	0.060	3.80

The maximum moment magnitude from the estimations above was M_W = 3.8 in the model with the mining dipping at a bearing of 218° as in the case of ERPM. This suggests that the earthquakes emanating from the eastern part of the CRB (ERPM) should have a slightly larger magnitude.

© University of Pretoria

UNIVERSITEIT VAN PRETORIA
UNIVERSITY OF PRETORIA
YUNIBESITHI YA PRETORIA

3.5. Comparison with the Seismic Catalogue

A network of 12 seismograph stations has been in operation in the CRB since March 2010, providing valuable seismic data with which to compare results from the analysis of the models.

3.5.1. Spatial distribution

A total of 560 events ranging in magnitude from M_L 0.2 to M_L 3.4 and recorded by this network up to the end of October 2012 were relocated using a double difference program called HypoDD (Waldhauser and Ellsworth, 2000). A detailed list of these events is presented in Appendix C.

The network has a very wide longitudinal coverage (~50 km) as opposed to latitudinal (~15 km) due to the shape of the basin. This has an adverse effect on the latitudinal constraint of the event locations. Additionally, the planar arrangement of a surface network hinders depth determination. A more accurate velocity model is also still to be developed, which may shift locations slightly. Current longitude and latitude location errors are in the range of 500 m. Although 12 stations over such a small area seems dense, depth determination without the use of additional phase identification requires that the nearest station be a distance away from the epicentre that is similar to the depth of the event. Due to the shallow nature of the seismicity (1 – 3 km deep) this rarely happens for the larger events that are observed, making depth determination troublesome.

Nevertheless, some spatial patterns in the relocated seismicity were observed. The first observation is that almost all of the epicentres fall within mine boundaries. This merely indicates that the presence of the abandoned mines is a controlling factor. In other words, the removal of material underground has created instability in the rock mass that is being exploited by the water.

The distribution of seismic events appears to be clustered in Figure 23, in the areas to the west and in the north of ERPM, the southern parts of City Deep and Robinson Deep and tracing across ERPM with a northwest/southeast alignment. This lineament at ERPM is also where the largest events have been observed.

© University of Pretoria

UNIVERSITEIT VAN PRETORIA
UNIVERSITY OF PRETORIA
YUNIBESITHI YA PRETORIA

The overall distribution of seismicity agrees well with the distribution of vulnerable features identified through modelling. Location ambiguities prevent a clear delineation of structural features. This suggests that the shape and orientation of the mine void within the shallow crust as well as the method of mining are indeed controlling factors in the location of features that are most likely to fail and seismicity is being controlled by this rather than tectonic stresses. The fact that this could be demonstrated with a simple model is also an indication of the uniform distribution of crustal stress within the basin.

© University of Pretoria

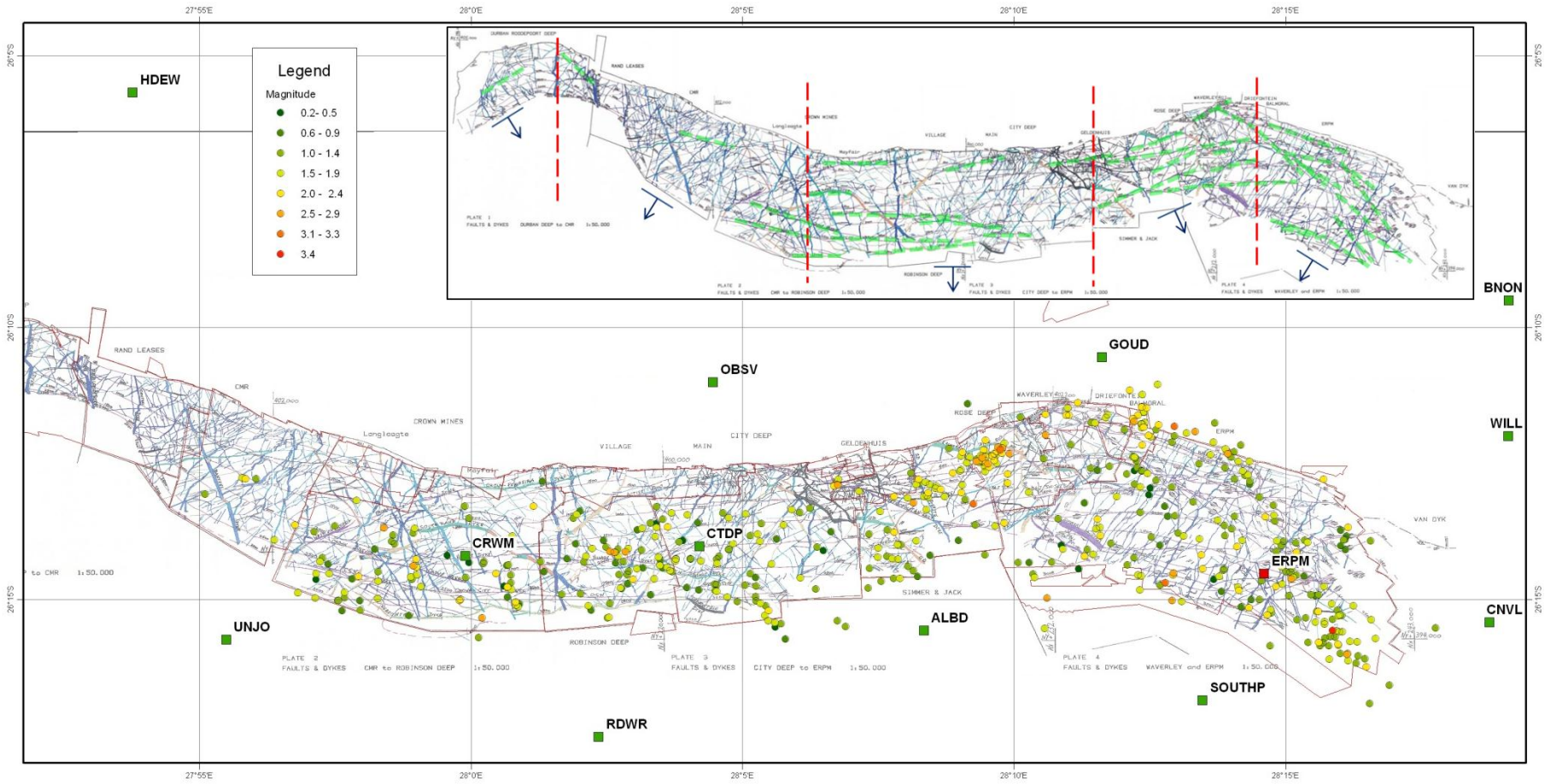

Figure 23 – Structural geology map with the locations of the seismograph stations and relocated seismic events in the Central Rand Basin. Clusters of seismic activity agree well with the clusters of potentially unstable features (insert).

© University of Pretoria

UNIVERSITEIT VAN PRETORIA
UNIVERSITY OF PRETORIA
YUNIBESITHI YA PRETORIA

3.5.2. Maximum magnitude

Maximum expected magnitudes were estimated using statistical and geological approaches by Midzi and Prasad (2011). The statistical approach was largely reliant on the maximum observed earthquake for the region, whereas the geological approach relied on the length of the longest fault that exists in the mines. The two approaches yielded results that differed by almost 1 unit of local magnitude. Both were observational approaches.

The statistical approach is based on a relatively short history of recorded seismicity, from the 1970's to present, during which time almost all of the events were mining induced. This does not address the role played by basin-wide tectonic stresses that may have accumulated or dissipated over millions of years. The presence of long faults, however, is indicative of this tectonic stress regime but whether or not those stresses are still active is difficult to ascertain.

Left-lateral wrenching was only recorded in the vicinity of ERPM, where most of the seismicity is also located. The geomechanical model showed failure along a particular orientation of fault, which intersected the mine void. Although average material and joint properties were used and the material was homogenous, the stress values were in line with measurements and estimates from previous studies. This orientation is, quite possibly, delineated in the relocated seismicity, wherein the maximum magnitude to date has been M_L 3.5. Table 5 lists the different types of maximum magnitudes.

Table 5 – Maximum magnitudes observed and predicted.

Method	Magnitude
Maximum observed	M_L 4.9 (1974)
Maximum observed between 25/03/2010 and 31/10/2012	M_L 3.5
Geological predicted (Midzi and Prasad, 2011)	M_L 5.9
Statistically predicted (Midzi and Prasad, 2011)	M_L 5.13
3DEC model (Hanks and Kanamori, 1979)	M_W 3.80

© University of Pretoria

UNIVERSITEIT VAN PRETORIA
UNIVERSITY OF PRETORIA
YUNIBESITHI YA PRETORIA

Increased pore-pressures acting on critically stressed features is what triggers seismicity, as was demonstrated in the 3DEC model. Such critically stressed features were created through mining which is why the observed seismicity is confined to the mining regions. It is unlikely that large shear stresses exist outside of this on regional features considering that the region is a stable cratonic one.

The 3DEC models can be seen as worst case scenarios due to the simplistic shape of the void, lack of support structures and approach to geological features. Assuming that the pre-mining stress model is a reasonable estimation of the real conditions, the observed shear displacement, which yields a moment magnitude of M_W 3.8, may represent some upper bound to the expected maximum magnitude under the current physical conditions. Although, the maximum observed magnitude of M_L 4.9, which was measured in 1974, cannot be disregarded and provision should be made for an earthquake of at least this size.

© University of Pretoria

UNIVERSITEIT VAN PRETORIA
UNIVERSITY OF PRETORIA
YUNIBESITHI YA PRETORIA

Chapter 4

4. Discussion and Conclusions

4.1. Discussion

The key to any successful seismological investigation is having sufficient data. The temporal variation in the b-value described in Section 2.6 hinted at a possible method of anticipating the larger seismic events but it also identified a common weakness that is present throughout this study. That is, the lack of available data. Continued monitoring with the recently upgraded SWMP Seismograph Network will ensure that more data is available in the future to investigate the effects of water ingress into abandoned mines. Future studies should include accurate depth determination of the seismic events to constrain the volume of rock mass affected by increasing pore pressure.

The question of the current stress state in the rock mass still persists, although an attempt was made at deriving it here. The assumption of equal horizontal crustal stresses limits the results of this study. The discovery of more stress measurement data would contribute to a better understanding of the stress conditions. In the same way, seismic moment tensor calculations on current data would also be of great benefit.

The 3DEC model has treated the rock mass and associated features as homogenous entities that interact entirely mechanically. Future work must address the effects of the alteration of minerals in the fault zone on fault stability especially since oxidised heavy metals are taken into solution by the water, making it acidic. This would accelerate any weathering processes. Simplified material properties present an additional limitation.

The possibility of a seasonal trend should also be investigated as more data becomes available with time. What influence do heavy rains have and what is the delay (if any) before an increase in seismicity is observed? All of the above points aim to address one simple concern and that is; “what level of ground motion can the City of Johannesburg and surrounding areas expect and how often?”

© University of Pretoria

UNIVERSITEIT VAN PRETORIA
UNIVERSITY OF PRETORIA
YUNIBESITHI YA PRETORIA

4.2. Conclusions

4.2.1. Evaluation of the Frequency-Magnitude Distribution

There is danger in any interpretation of this data in that a mixture of earthquake mechanisms exists across the basin. A structural picture of the Central Rand Basin would include dolerite dykes, normal faults and wrench faults, among others. One cannot safely assume that one type of fault and uniform rock mass is responsible for all of the seismic activity or that the entire basin is under the same stress state. This redefines the goal as an investigation into the average state of seismicity in the basin.

The *b*-values before and after the onset of flooding in ERPM are characteristic of *b*-values found for induced seismicity, namely, $b > 1$. The datasets were essentially different in that the magnitude of completeness differed by one order. This was attributed to an improvement in the seismic network coverage in the CRB. The use of the GFT method by Wiemer and Wyss (2000) was beneficial, ensuring that maximum data points were included in the *b*-value estimation by finding the best-fitting M_{min} and that the errors were small enough so as not to hinder possible interpretations.

The *b*-value appears to have decreased when compared for the two time periods, changing from 1.19 ± 0.03 before flooding and during mining, to 1.10 ± 0.01 after mining and pumping had stopped and water ingress was taking place. According to relationships between the *b*-value and physical characteristics of the rock mass described in Section 2.5, it means that stresses are given more time to build up before being released through deformation resulting in a higher proportion of larger events in the frequency-magnitude distribution. The seismicity has, thus, moved from being induced, where stress is released prematurely through a high proportion of smaller events, towards a natural process.

The study of the temporal variation of the *b*-value produced encouraging results. A strong correlation was observed between a decrease in the *b*-value and the occurrence of a relatively large seismic event, $M_L \geq 3.3$. The quality and quantity of early data hinders a fuller evaluation of this pattern. The coverage in the CRB only improved in 2006 with the introduction of one station at ERPM and again in 2010 with the SWMP Network. The *b*-value varied between 0.7 and 1.5, which is normal for mining environments.

© University of Pretoria

UNIVERSITEIT VAN PRETORIA
UNIVERSITY OF PRETORIA
YUNIBESITHI YA PRETORIA

With the high number of seismic events still being recorded in the CRB, this area of the continent can be considered seismically active. The seismicity can no longer be attributed to mining activities but rather the presence of the mine, which allows water to penetrate at great depths. The study of the *b*-value has told us that there remains cause for concern since the system is generating a higher proportion of large events. It remains to be determined how much stress can be accumulated and released naturally i.e. how big the events will become. This will depend on whether or not the main contributor to stress build-up on the geological discontinuities is the presence of residual mining-induced stress (removal of the rock mass) or tectonic stress in the basin.

© University of Pretoria

UNIVERSITEIT VAN PRETORIA
UNIVERSITY OF PRETORIA
YUNIBESITHI YA PRETORIA

4.2.2. A 3-Dimensional Distinct Element Model – Static Solution

Mining of the Central Rand Goldfields had mostly ceased by the close of the 1970's. In By 2002 there was only one mine in operation. It is believed that residual stresses left over from mining are being exploited by the water. Pore pressure changes in the fractured rock mass are causing previously stable features to become unstable. The largest seismic events will most likely occur on the longest pre-existing geological feature, such as a fault or dyke. All of these features were diligently mapped underground by Pretorius (Circa, 1970).

A tectonosedimentary model by Stewart *et al.* (2004) characterizes the structural model of the basin as left-lateral wrenching. Structures associated with this (left-lateral strike-slip faults) are exclusively indicated in the region of ERPM on the structural geology map (Figure 11). This might be the reason for the largest events occurring there, since the area is obviously prone to failure caused by pre-existing tectonic stresses. Another reason might be that ERPM was the last mine to stop pumping and, therefore, has had less time to release residual mining-induced stresses.

Results from the 3D models showed an average shear displacement of approximately 5 cm and a maximum of 12 cm. Joint shear stresses up to 60 MPa were induced by the removal of material to form the void. The model produced stress and strain conditions comparable to those observed underground and demonstrated the strong dependence of an intersecting feature's propensity to slip on its relative orientation with respect to the mine void. Strong assumptions such as; a uniform rock mass and the shape of the mine void and discontinuities, were unavoidable. Despite this, there was good agreement between the spatial distribution of seismicity and the positions of potentially unstable features, which suggests two possibilities:

- Seismicity is mostly being controlled by stresses induced by the shape and orientation of the mined-out reef on intersecting geology rather than by neo-tectonic stresses.
- The shallow crust can be described by a homogenous material and uniform stress model.

Earthquakes are consistently being recorded in the CRB with some reportedly felt by the public. Although, these have not caused any damage yet, the possibility that any of these features may slip over a very large surface area, causing a catastrophic earthquake, still remains.

© University of Pretoria

UNIVERSITEIT VAN PRETORIA
UNIVERSITY OF PRETORIA
YUNIBESITHI YA PRETORIA

References

Aki, K. (1965): Maximum Likelihood estimate of *b* in the formula log *N* = *a*-*bM* and its confidence limits. *Bull. Earthq. Res. Inst. Tokyo Univ.*, Vol. 43, pp. 237-239.

Athavale, R.N. (1975): Induced seepage along a coastal parallel system of faults as a possible cause of the Konya earthquakes. *Bull. Seism. Soc. Am.*, Vol. 65, No. 1, pp. 183-191.

Bell, M. L. and Nur, A. (1978): Strength changes due to reservoir-induced pore pressure and stresses and application to Lake Oroville. *J. Geophys. Res.*, Vol. 83, No. B9, pp. 4469-4483.

Bender, B. (1983): Maximum likelihood estimation of *b*-values for magnitude grouped data. *Bull. Seism. Soc. Am.*, Vol. 73, No. 3, pp. 831-851.

Brandt, M.B.C. (2004): Ground motions for a moderate earthquake for the Katse reservoir, Kingdom of Lesotho. *Africa Geoscience Review*, Vol. 11, No. 1, pp. 31-63.

Brown, E.T. and Hoek, E. (1978): Trends in Relationship between Measured In-Situ Stresses and Depth. *Int. J. Rock Mech. Min. Sci. & Geomech. Abstr.*, Vol 15, pp. 211-215.

Cappa, F. (2009): Modelling fluid transfer and slip in a fault zone when integrating heterogeneous hydromechanical characteristics in its internal structure. *Geophys. J. Int.*, Vol. 178, pp. 1357-1362.

Enescu, B. and Ito, K. (2003): Values of b and p: their variations and relation to physical processes for earthquakes in Japan. *Annals of Disas. Prev. Res. Inst.*, Kyoto Univ., No. 46 B.

Farrell, J., Husen, S. and Smith, R.B. (2009): Earthquake swarm and *b*-value characterization of the Yellowstone volcano-tectonic system. *J. Volcan. Geotherm. Res.*, Vol. 188, pp. 260–276.

Frolich, C. and Davis, S., (1993). Teleseismic *b*-values: or much ado about 1.0. *J. Geophys. Res.*, Vol. 98, pp. 631–644.

Fung, Y.C. (1965): *Foundations of Solid Mechanics.* Prentice-Hall Inc. Englewood Cliffs, New Jersey, pp. 525.

© University of Pretoria

UNIVERSITEIT VAN PRETORIA
UNIVERSITY OF PRETORIA
YUNIBESITHI YA PRETORIA

Gay, N.C. (1975): In situ stress measurements in Southern Africa. *Tectonophysics*, Vol 29, pp. 447-459.

Gay, N.C. (1979): The state of stress in a large dyke on E.R.P.M., Boksburg, South Africa. *Int. J. Rock Mech. Min. Sci. &Geomech.* Abstr.,Vol 16, pp. 179-185.

Gibowicz, S.J. (1973): Variation of the frequency-magnitude relation during earthquake sequences in New Zealand. *Bull. Seism. Soc. Am.*, Vol. 63, No. 2, pp. 517-528.

Gibowicz, S.J. and Kijko, A. (1994): *An Introduction to Mining Seismology.* International Geophysics Series, Vol. 55. Academic Press, Inc. ISBN 0-12-282120-3, pp. 301-305.

Goertz-Allmann, B.P. and Wiemer, S. (2013): Geomechanical modelling of induced seismicity source parameters and implications for seismic hazard assessment. *Geophys.*, Vol. 78, No. 1, pp. KS25-KS39.

Goldbach, O. (2010): What is the Seismic Risk of Mine Flooding? *Science Real and Relevant Conference 2010*, Council for Scientific and Industrial Research, South Africa.

Gupta, A., and C. H. Scholz (1998): Utility of elastic models in predicting fault displacement fields. *J. Geophys. Res.*, Vol. 103, No. B1, pp. 823-834.

Gutneburg, B., and Richter, C.F. (1944): Frequency of earthquakes in California. *Bull. Seism. Soc. Am.*, Vol. 34, pp. 185-188.

Gutneburg, B., and Richter, C.F. (1954): *Seismicity of the Earth and Associated Phenomena*, 2nd ed., Princeton University Press, Princeton, N.J.

Handley, M.F. (2012): Proposed crustal stress model for subsurface excavations in Southern Africa. Based on the Southern African Stress Database in: Stacey, T.R. and Wesseloo, J. (1998): Evaluation and Upgrading of Records of Stress Measurement Data in the Mining Industry. SIMRAC Project GAP511b, Department of Minerals and Energy, Johannesburg, June 1998. Submitted to the *JSAIMM* for publication.

Hanks, T.C. and Kanamori, H. (1979): A moment magnitude scale. *J. Geophys. Res.*, Vol. 84, No. B5, pp. 2348-2350.

Haxby, W.F., and Turcotte, D.L. (1976): Stresses induced by the addition and removal of overburden and associated thermal effects. *Geology*, Vol. 4, pp. 181-184.

© University of Pretoria

UNIVERSITEIT VAN PRETORIA
UNIVERSITY OF PRETORIA
YUNIBESITHI YA PRETORIA

Healy, J.H., Rubey, W.W., Grigs, D.T. and Raleigh, C.B. (1968): The Denver Earthquakes. *Science*, Vol. 161, No. 3848, pp. 1301-1310.

Hoek, E. and Brown, E.T. (1980): *Underground Excavations in Rock.* London: The Institution of Mining and Metallurgy, pp. 527.

Hsieh, P.A. and Bredehoeft, J.D. (1981): A reservoir analysis of the Denver earthquakes: A case of induced seismicity. *J. Geophys. Res.*, Vol. 86, No. B2, pp. 903-920.

Itasca Consulting Group, Inc., (2007): *3DEC 4.1 User's Guide,* 3rd ed., Minneapolis, Minnesota.

Johnston, M.J.S., Borcherdt, R.D., Linde, A.T. and Gladwin, M.T. (2006): Continuous borehole strain and pore pressure in the near field of the 28 September 2006 M 6.0 Parkfield, California, earthquake: Implications for nucleation, fault response, earthquake prediction, and tremor. *Bull. Seism. Soc. Am.*, Vol. 96, No. 4B, pp. S56-S72.

Kanamori, H and Anderson, D.L. (1975): Theoretical basis of some empirical relations in seismology. *Bull. Seism. Soc. Am.*, Vol. 65, No. 5, pp. 1073-1095.

Kijko, A., Drzezla, B. and Stankiewicz, T. (1987): Bimodal character of the distribution of extreme seismic events in Polish mines, *Acta Geophysica Polonica*, Vol. 35, pp. 159-168.

Kijko, A. and Sellevoll, M.A. (1989): Estimation of earthquake hazard parameters from incomplete data files. Part I. Utilization of extreme and incomplete catalogues with different threshold magnitudes. *Bull. Seism. Soc. Am.*, Vol. 79, No. 3, pp. 645-654.

Kijko, A. and Funk, C.W. (1994): The assessment of seismic hazards in mines. *The Journal of the South African Institute of Mining and Metallurgy*, pp. 179-185.

Klose, D. (2007): Mine Water Discharge and Flooding: A Cause of Severe Earthquakes. *Mine Water and the Environment*, Vol. 26, 172-180.

Lightfoot, N. and Goldbach, O.D. (1995): Controlled Fault Slip: Water Injection. *Safety in Mines Research Advisory Committee Project Report GAP030*, Department of Minerals and Energy, Pretoria.

© University of Pretoria

UNIVERSITEIT VAN PRETORIA
UNIVERSITY OF PRETORIA
YUNIBESITHI YA PRETORIA

Love, A.E.H. (1927): *A Treatise on the Mathematical Theory of Elasticity. 4th Edition*, republished in full by Dover Publications, New York, 1944, pp. 643.

Lowrie, W. (2007): *Fundamentals of Geophysics. 2nd Ed.*, Cambridge University Press, pp. 381.

Marzocchi, W. and Sandri, L. (2003): A Review and New Insights on the Estimation of the *b*-Value and its Uncertainty. *Annals of Geophysics*, Vol. 46, N. 6, pp. 1271-1282.

McCarthy, T., and Rubidge, B. (2005): The Story of Earth and Life: A Southern African Perspective on a 4.6-billion-year Journey. Cape Town: *Struik Nature*, pp. 335.

McCutchen, W.R. (1982): Technical Note. Some elements of a theory for in-situ stress. *Int. J. Rock Mech. Min. Sci. & Geomech. Abstr.*, Vol 19, pp. 201-203.

McGarr, A., Spottiswoode, S.M., and Gay, N.C. (1975): Relationship of mine tremors to induced stresses and to rock properties in the focal region. *Bull. Seism. Soc. Am.*, Vol. 65, No. 4, pp. 981-993, August 1975.

McGarr, A. (1976): Dependence of magnitude statistics on strain rate. *Bull. Seism. Soc. Am.*, Vol. 66, No. 1, pp. 33-44.

McGarr, A., and Gay, N.C. (1978): State of stress in the Earth's crust. *Annual Reviews of Earth and Planetary Sciences*, Vol. 6, pp. 404-436.

McGarr, A., Spottiswoode, S.M., Gay, N.C., and Ortlepp, W.D. (1979): Observations relevant to seismic driving stress, stress drop, and seismic efficiency. *J. Geophys. Res.*, Vol. 84, pp. 2251-2261.

McGarr, A. (2006): The effects of pore pressure changes due to mining and mine flooding on seismicity. Appendix 4.5 of *Investigation into the risks to miners, mines and the public associated with large seismic events in gold mining districts*, Vol. 2

Mendecki, A.J., van Aswegen, G. and Mountfort, P. (1999): Chapter 9 of *A Handbook on Rock Engineering Practice for Tabular Hard Rock Mines*, A.J. Jager and J.A. Ryder (eds.). Safety In Mines Research Advisory Committee (SIMRAC) to the Department of Minerals and Energy, South Africa.

© University of Pretoria

UNIVERSITEIT VAN PRETORIA
UNIVERSITY OF PRETORIA
YUNIBESITHI YA PRETORIA

Midzi, V. and Prasad, K. (2011): *Mine-Flooding Induced Seismicity in the Central and East Rand Goldfield: Maximum Expected Magnitude.* Unpublished internal document, Council for Geoscience.

Nuannin, P., Kulhanek, O., Persson, L., and Askemur, T. (2005): Inverse Correlation between Induced Seismicity and *b*-Value, Observed in the Zingruvan Mine, Sweden. *Acta Geodyn. Geomater.*, Vol.2, No.4, pp. 5-13.

Pallister, G.F. (1969): The Measurement of Virgin Rock Stress. MSc. Dissertation, University of the Witwatersrand, Johannesburg, 1969.

Pretorius, D.A. (circa 1970): Hand-drawn structural map of the Central Rand Basin, replotted by Pen Plotter. Economic Geology Research Unit, University of the Witwatersrand.

Price, N.J. (1966): *Fault and Joint Development in Brittle and Semi-brittle Rock.* Oxford: Pergamon Press, pp. 176.

Richardson, E. and Jordan, T.H. (2002): Seismicity in deep gold mines of South Africa: Implications for tectonic earthquakes. *Bull. Seism. Soc. Am.*, Vol. 92, No. 5, pp. 1766-1782.

Roeloffs, E.A. (1988): Fault stability changes induced beneath a reservoir with cyclic variations in water level. *Journal of Geophysical Research*, Vol. 93, No. B3, pp. 2107-2124.

Saar, M.O. and Manga, M. (2003): Seismicity induced by seasonal groundwater recharge at Mt. Hood, Oregon. *Earth and Planetary Science Letters*, Vol. 214, pp. 605-618.

Saunders, I., Brandt, M., Steyn, J., Roblin, D. and Kijko, A. (2008): The South African National Seismograph Network. *Seismological Research Letters*, Vol. 79, No. 2, pp. 203-210.

Saunders, I., Brandt, M., Molea, T., Akromah, L. and Sutherland, B. (2010): Seismicity of Southern Africa during 2006 with special reference to the M_W 7 Mechaze earthquake. *South African Journal of Geology*, Vol. 113.4, pp. 369-380.

Scholz, C.H. (1968): The Frequency-Magnitude Relation of Microfracturing in Rock and its Relation to Earthquakes. *Bull. Seism. Soc. Am.*, Vol. 58, No. 1, pp. 399-415.

© University of Pretoria

UNIVERSITEIT VAN PRETORIA
UNIVERSITY OF PRETORIA
YUNIBESITHI YA PRETORIA

Schweitzer, J.K. and Johnson, R.A. (1997): Geotechnical Classification of Deep and Ultra-Deep Witwatersrand Mining Areas, South Africa. *Mineralium Deposita*, Vol. 32, pp. 335-348.

Shi, Y. and Bolt, B.A. (1982): The standard error of the magnitude-frequency *b* value. *Bull. Seism. Soc. Am.*, Vol. 72, No. 5, pp. 1677-1687.

Sheorey, P.R. (1994): A theory for In Situ stresses in isotropic and transversely isotropic rock. *Int. J. Rock Mech. Min. Sci. & Geomech. Abstr.*, Vol 31, pp. 23-34.

Simpson, D.W. (1976): Seismicity changes associated with reservoir loading. *Engineering Geology*, Vol. 10, pp. 123-150.

Singh, C., Bhattacharya, P.M. and Chadha, R.K. (2008): Seismicity in the Koyna–Warna Reservoir Site in Western India: Fractal and *b*-Value Mapping. *Bull. Seism. Soc. Am.*, Vol. 98, No. 1, pp. 476–482.

Stacey, T.R., and Wesseloo, J. (1998a): Evaluation and Upgrading of Records of Stress Measurement Data in the Mining Industry. *Safety In Mines Research Advisory Committee Project Report GAP511*, Department of Mineral Resources, Johannesburg, South Africa.

Stewart, R.A., Riemold, W.U., and Charlesworth, E.G. (2004): Tectonosedimentary model for the Central Rand Goldfield, Witwatersrand Basin, South Africa. *South African Journal of Geology*, Vol. 107, pp. 603-618.

Terzaghi, K., and Richart, F.E. (1952): Stresses in rock about cavities. *Géotechnique*, Vol. 3, Issue 2, pp. 57-90.

Tsukakoshi, Y. and Shimazaki, K. (2008): Decreased *b*-value prior to the M 6.2 Northern Miyagi, Japan, earthquake of 26 July 2003. *Earth Planets Space*, Vol. 60, pp. 915-924.

Utsu, T. (1965): A method for determining the value of *b* on the formula log *n* = *a-bM* showing the magnitude-frequency relation for earthquakes. *Geophys. Bull., Hokkaido Univ.*, Vol. 13, pp. 99-103 (in Japanese; English abstract).

Utsu, T. (1966): A statistical significance test of the difference in *b*-value between two earthquake groups. *J. Phys. Earth*, Vol. 14, pp. 37-40.

© University of Pretoria

UNIVERSITEIT VAN PRETORIA
UNIVERSITY OF PRETORIA
YUNIBESITHI YA PRETORIA

Van der Pluijm, B.A., and Marshak, S. (2004): *Earth Structure 2nd Edition: An Introduction to Structural Geology and Tectonic*s, W. W. Norton & Company, Inc. ISBN 0-393-92467-X, pp. 48.

Voight, B. (1966): Beziehung zwischen grossen horizontalen spannungen im gebirge und der tektonik und der abtragung. *1st Congress of the International Society of Rock Mechanics*, Lisbon, 1966, Vol. 2, pp. 51-56.

Waldhauser, F. and Ellsworth, W.L. (2000): A double-difference earthquake location algorithm: Method and application to the northern Hayward fault. *Bull. Seism. Soc. Am.*, Vol. 90, pp. 1353-1368.

Warren, N.W. and Latham, G.V. (1970): An experimental study of thermally induced microfracturing and its relation to volcanic seismicity. *J. Geophys. Res.,* Vol. 75, pp. 4455-4464.

Wiemer, S. and Wyss, M. (2000): Minimum magnitude of completeness in earthquake catalogs: Examples from Alaska, the Western United States, and Japan. *Bull. Seism. Soc. Am.*, Vol. 90, No. 4, pp. 859-869.

Woessner, J. and Wiemer, S. (2005): Assessing the quality of earthquake catalogues: Estimating the magnitude of completeness and its uncertainty. *Bull. Seism. Soc. Am.*, Vol. 95, No. 2, pp. 684-698.

Wolf, L.W., Rowe, C.A. and Horner, R.B. (1997): Periodic seismicity near Mt. Ogden on the Alaska-British Columbia border: A case for hydrologically triggered earthquakes? *Bull. Seism. Soc. Am.*, Vol. 87, No. 6, pp. 1473-1483.

Zhang, J.Z. and Song, L.Y. (1981): On the method of estimating *b*-value and its standard error. *Acta Seism. Sin.*, Vol. 3, pp. 292-301, 1981.

© University of Pretoria

UNIVERSITEIT VAN PRETORIA
UNIVERSITY OF PRETORIA
YUNIBESITHI YA PRETORIA

Appendix A

This is an expansion of a Gibowicz and Kijko (1994) demonstration of the procedure to evaluate the Aki-Utsu maximum-likelihood estimate for b that was introduced by Aki (1965) and Utsu (1965). The expansion starts from the maximum-likelihood condition expressed in equation 2.5.

$$L(\beta|M_1,\dots,M_N) = const \prod_{i=1}^{N} f(M_i|\beta) = max \tag{2.5}$$

The procedure for finding the maximum to the likelihood function is to find the value, in this case $\hat{\beta}$, which equates the first derivative of the log-likelihood to zero.

$$\frac{\partial \ln L(\beta|M_1,\dots,M_N)}{\partial \beta} = \frac{\partial}{\partial \beta}[\ln const + \ln f(M_1|\beta) + \cdots + \ln f(M_N|\beta)] = 0 \tag{A1}$$

Equation A1 can be written in a condensed form:

$$\sum_{i=1}^{N} \frac{\partial}{\partial \beta} \ln f(M_i|\beta) = 0 \tag{2.6}$$

Taking the logarithm and calculating its derivative:

$$\sum_{i=1}^{N} \frac{\partial}{\partial \beta} \ln \beta \exp[-\beta(M_i - M_{min})] = \sum_{i=1}^{N} \frac{\partial}{\partial \beta}[\ln \beta - \beta(M_i - M_{min})] \tag{A2}$$

$$\therefore \sum_{i=1}^{N} \left[\frac{1}{\beta} - (M_i - M_{min})\right] = 0 \tag{A3}$$

Taking the summation inside gives:

$$\frac{N}{\beta} - \left(\sum_{i=1}^{N} M_i - NM_{min}\right) = 0 \tag{2.7}$$

Dividing through by *N* and rearranging the equation:

$$\frac{1}{\beta} - \left(\frac{\sum_{i=1}^{N} M_i}{N} - M_{min}\right) = 0 \tag{A4}$$

$$\beta = \frac{1}{\left(\frac{\sum_{i=1}^{N} M_i}{N} - M_{min}\right)} \tag{A5}$$

The sample mean magnitude is defined as:

$$\bar{M} = \sum_{i=1}^{N} M_i / N \tag{A6}$$

© University of Pretoria

UNIVERSITEIT VAN PRETORIA
UNIVERSITY OF PRETORIA
YUNIBESITHI YA PRETORIA

The value $\hat{\beta}$ is then the Aki-Utsu maximum-likelihood estimate of β for which the maximum likelihood function is maximised, therefore:

$$\hat{\beta} = \frac{1}{\bar{M} - M_{min}} \tag{2.8}$$

Written out explicitly, the estimate for b is (Aki, 1965 and Utsu, 1965):

$$b = \frac{1}{\ln 10(\bar{M} - M_{min})} \tag{2.9}$$

© University of Pretoria

Appendix B

Scripts written in MATLAB to calculate the b-Value.

```
function [b,sigma_b,numM,b_temp,b_sigma_temp,time,date] = bvalue(invoke)

eval = 0;

% Exract data from S-files

[mag,date,latlon] = sfile_extract;

while eval == 0
    % Determine the temporal variation of b

    if exist('invoke','var') == 1
        [b_temp,b_sigma_temp,time] = b_temporal_var(mag,date);
    end

    % Evaluate different levels of completeness

    if exist('invoke','var') == 0
        qq = input('perform threshold magnitude test? 1 = yes 0 = no: ');
        if qq == 1
            [b_compare] = Mmin_test(mag,date)
            break
        end
    end


    % Calculate and plot number of events recorded per month

    if exist('invoke','var') == 0
        [events_bimonthly,edges] = activity(date);
        figure; bar(edges,events_bimonthly);
        datetick('x',12);
        title('Number of events bi-monthly');
        xlabel('Date'); ylabel('Number of Events');
    end

    % Compile data into a cumulative distribution

    bin_size = 0.1; % for instrumentally recorded data % also set in minM
    bins = min(mag):bin_size:max(mag);
    [n_events,bin_loc] = hist(mag,bins);
    h = figure;
    bar(bin_loc,log10(n_events));
    hold on;
    flip = fliplr(n_events);
    cum = cumsum(flip);
    cum = sort(cum,'descend');
    plot(bin_loc,log10(cum),'or','LineWidth',2,'MarkerSize',6); hold on;

    % Calculate the minimum magnitude
```


© University of Pretoria

UNIVERSITEIT VAN PRETORIA
UNIVERSITY OF PRETORIA
YUNIBESITHI YA PRETORIA

```
    [minM,kk] = Mmin(cum,bins,bin_loc,n_events,mag);
    if isempty(minM)
        [minM,kk] = Mmin(cum,bins,bin_loc,n_events,mag);
    end

    % Max magnitude is just the maximum observed magnitude

    maxM = max(mag);

    % Calculate the sampling average of the allowed magnitudes

    x = [];
    for i = 1:length(mag)
        if mag(i,1) >= minM
            x = [x;mag(i,1)];
        else
            x = x;
        end
    end

    aveM = mean(x);
    for i =1:length(bins)
        if bin_loc(i) >= aveM && aveM >= (bin_loc(i)-bin_size/2)
            jj = i;
            break;
        elseif bin_loc(i) >= aveM && aveM <= (bin_loc(i)-bin_size/2)
            jj = i-1;
            break
        end
    end

    % Calculate the number of events used for the b-value estimation i.e. >= Mmin

    numM = sum(n_events(1,kk:end));

    % Max Likelihood estimation of b

    [b,sigma_b] = LM_b(bin_size,aveM,minM,kk,bin_loc,numM,cum,jj,h);

    hold off;
    if exist('invoke','var') == 0
        eval = input('keep result after inspection? 1 = yes 0 = no: ');
    else
        eval = 1;
    end

end

function [mag,date,latlon] = sfile_extract

[FileName,PathName] = uigetfile('*.*','Select the Nordic input file');
inpFile= fullfile(PathName,FileName);
fid = fopen(inpFile);
mag = [];
date = [];
latlon = [];
```


© University of Pretoria

UNIVERSITEIT VAN PRETORIA
UNIVERSITY OF PRETORIA
YUNIBESITHI YA PRETORIA

```
% reading file info from 1st line, header

while feof(fid)==0
    aux             = fscanf(fid,' %9c',1);
    YmD             = sscanf(aux,'%d');
    yr_mnth_day     = transpose(YmD);
    if length(yr_mnth_day) == 2
        mnth        = yr_mnth_day(1,2);
        yr_mnth_day(1,2) = floor(mnth/100);
        yr_mnth_day(1,3) = mnth - yr_mnth_day(1,2)*100;
    end
    aux1            = fscanf(fid,'%f',1);
    hour            = floor(aux1/100);
    minute          = aux1-hour*100;
    second          = fscanf(fid,'%f',1);
    location_type   = fscanf(fid,'%s',1);
    latitude       = fscanf(fid,'%f',1);
    longitude       = fscanf(fid,'%f',1);
    depth           = fscanf(fid,'%s',1);

    if ~isempty(strfind(depth,'FF')) && length(depth)>2
        %disp('depth is fixed');
        hypo_agency    = depth(1,6:8);
        depth      = str2num(depth(1,1:3));
    elseif ismember('F',depth) && length(depth)>1
        %disp('depth and location are fixed');
        depth      = str2num(depth(1,1:3));
        hypo_agency    = fscanf(fid,'%s',1);
    else
        hypo_agency = fscanf(fid,'%s',1);
    end

    num_stat_used  = fscanf(fid,'%f',1);
    tres_rms       = fscanf(fid,'%f',1);
    magnitude      = fscanf(fid,'%f',1);
    event_type     = fscanf(fid,'%1s',1);
    rest           = fgetl(fid);

    while sum(isspace(fscanf(fid,'%c',5)))<5 && feof(fid)==0
        line = fgetl(fid);
    end

    date_vector = [yr_mnth_day,hour,minute,second];
    date_num = datenum(date_vector);


    if magnitude >= 0
        mag = [mag;magnitude];
        date = [date;date_num];
        latlon = [latlon;latitude,longitude];
    else
        mag = mag;
        date = date;
    end

end
```


© University of Pretoria

UNIVERSITEIT VAN PRETORIA
UNIVERSITY OF PRETORIA
YUNIBESITHI YA PRETORIA

```
function [b_temp,b_sigma_temp,time] = b_temporal_var(mag,date)

int = 100; % number of events (M>=Mmin) used to calculate b-value for each window
wind = floor(length(mag)/int); % window index - number of windows
b_temp = [];
b_sigma_temp = [];
time = [];

for i = 1:wind
    if i == wind
        mag_int = mag((1+(i-1)*int):end,1);
        [b,sigma_b] = b_bin(mag_int);
        time = [time;date(end,1)];
    else
        mag_int = mag((1+(i-1)*int):i*int,1);
        [b,sigma_b] = b_bin(mag_int);
        time = [time;date((i*int),1)];
    end
    b_temp = [b_temp;b];
    b_sigma_temp = [b_sigma_temp;sigma_b];
end

function [events_bimonthly,edges] = activity(date)

% plot number of events recorded bi-monthly

strt = datevec(date(1,1)); stp = datevec(date(end,1));
ti = stp-strt; nMonth = 12*ti(1,1)+ti(1,2)+1;
if mod(strt(1,2),2)==0
    if mod(nMonth+strt(1,2),2)==0
        Month = strt(1,2):2:nMonth+strt(1,2);
        edges = datenum(strt(1,1),Month,1);
    else
        Month = strt(1,2):2:nMonth+strt(1,2)+1;
        edges = datenum(strt(1,1),Month,1);
    end
else
    Month = strt(1,2):2:nMonth+strt(1,2)+1;
    edges = datenum(strt(1,1),Month,1);
end
[events_bimonthly] = histc(date,edges);

function [b,sigma_b] = LM_b(bin_size,aveM,minM,kk,bin_loc,numM,cum,jj,h)

% calculate b from Aki 1965 with Utsu 1966 modification for binning

deltaM = bin_size;  %the width of the bins
b = log10(exp(1))/(aveM-minM+deltaM/2);

% sigma_b calculated from Shi and Bolt 1982

for i = kk:length(bin_loc)
    zz = bin_loc(i)-aveM;
end
sigma_b = 2.30*b^2*sqrt((sum(zz)^2)/(numM*(numM-1)));
```


© University of Pretoria

UNIVERSITEIT VAN PRETORIA
UNIVERSITY OF PRETORIA
YUNIBESITHI YA PRETORIA

```
% Plot Log(N) = a - bM; for events M >= minM

% calculate "a"
a = log10(cum(kk))+b*(minM); %use minM,kk or aveM,jj??


ilogN = []; iM = [];
logN = []; M = [];
for j = kk:length(cum)
    ilogN = [ilogN;(-b*bin_loc(j)+a)];
    iM = [iM;bin_loc(j)];
end

% remove negative values from linear plot
for c = 1:length(ilogN)
    if ilogN(c,1) > 0
        logN = [logN;ilogN(c,1)];
        M = [M;iM(c,1)];
    end
end

figure(h);
plot(M,logN,'-b',bin_loc,log10(cum),'or','LineWidth',2,'MarkerSize',6)
title('Cumulative Magnitude Distribution'); xlabel('Magnitude ML'); ylabel('Log10(N)');
text(2.7,0.98*max(log10(cum)),['b = ',num2str(b,'%3.2f'),' +-',...
    num2str(sigma_b,'%3.2f'),'     a = ',num2str(a,'%3.2f')]);
text(2.7,0.92*max(log10(cum)),['events = ',num2str(numM,'%4.0f')]);
```

Published with MATLAB® R2012b

© University of Pretoria

UNIVERSITEIT VAN PRETORIA
UNIVERSITY OF PRETORIA
YUNIBESITHI YA PRETORIA

Appendix C

Catalogue of seismic events recorded in the Central Rand Basin between 25.03.2010 and 31.10.2012, and relocated using a double difference program called HypoDD (Waldhauser and Ellsworth, 2000) plotted in Figure 23.

YYYY	MM	DAY	HR	MIN	SEC	Longitude South (deg)	Latitude East (deg)	Error Long (m)	Error Lat (m)	M_L
2010	3	26	3	5	17.11	27.796395	-26.234124	506.6	806.7	1.6
2010	3	26	6	47	10.06	27.779147	-26.232199	571.8	829.8	1.7
2010	3	27	23	27	46.88	28.176408	-26.193495	256.5	323.6	2.1
2010	3	28	3	15	35.23	28.109759	-26.273253	761.9	1437.3	0.6
2010	3	28	6	16	24.08	28.079235	-26.234961	10.9	22.6	1
2010	3	28	6	16	24.08	28.079235	-26.234961	10.8	22.6	1
2010	3	28	14	29	58.13	28.234439	-26.213137	340	367.2	1.2
2010	3	30	20	4	23.09	28.228016	-26.244097	445.1	592	0.5
2010	3	30	23	24	28.52	27.980958	-26.255074	429.5	691.2	0.7
2010	4	3	6	17	36.02	28.233501	-26.228603	392.3	541.5	1.3
2010	4	6	11	1	19.64	28.181709	-26.234735	248.4	285.5	1.6
2010	4	9	5	15	19.36	28.193169	-26.228137	283.1	288.2	1.9
2010	4	11	23	10	24.68	28.259214	-26.257141	350.7	369.3	1.7
2010	5	1	17	12	47.35	28.248706	-26.23373	295.1	294.3	1.2
2010	5	6	19	4	53.2	28.228414	-26.196025	280.6	350.9	1.1
2010	5	22	23	34	36.99	28.088013	-26.230218	305	335.7	1.9
2010	6	4	19	45	3.25	28.236294	-26.20294	267.8	293.2	1.4
2010	6	4	23	43	44.64	28.149752	-26.232156	227.2	276.3	0.8
2010	6	8	11	14	45.02	27.802963	-26.244343	554.6	653	1.8
2010	6	10	11	20	36.88	27.772053	-26.153432	406.5	729.6	1.7
2010	6	10	11	20	36.88	27.772053	-26.153432	406.5	729.6	1.7
2010	6	10	20	41	10.19	28.135895	-26.22057	231.8	329.9	2.5
2010	6	11	14	39	8.22	28.137418	-26.21475	190.6	204.2	1.3
2010	6	12	19	3	11.53	28.181282	-26.233515	269.1	324	0.5
2010	6	13	11	6	30.44	28.135105	-26.211443	310.7	339.4	1.1
2010	6	16	17	23	39.02	28.058924	-26.240561	269.1	264.2	0.8
2010	6	18	20	33	17.99	28.141033	-26.236685	259.1	312.9	0.7
2010	6	19	17	7	18.28	28.046287	-26.246782	265.1	260.5	0.7
2010	6	19	22	46	35.33	28.093468	-26.258646	269.4	281.6	0.5
2010	6	20	10	11	27.15	27.981649	-26.243347	261.4	347.7	1.9
2010	6	22	23	16	51.19	28.096641	-26.262384	250.9	269.9	0.7
2010	6	27	11	36	23.52	28.154302	-26.220946	288.3	393	3.3
2010	6	29	12	13	3.06	28.045488	-26.242611	248.8	253.1	1
2010	6	29	15	28	7.24	28.033623	-26.223051	223.7	255.8	0.7
2010	6	29	18	55	31.54	28.011868	-26.234084	261.2	293.3	1.7

© University of Pretoria

UNIVERSITEIT VAN PRETORIA
UNIVERSITY OF PRETORIA
YUNIBESITHI YA PRETORIA

YYYY	MM	DAY	HR	MIN	SEC	Longitude South (deg)	Latitude East (deg)	Error Long (m)	Error Lat (m)	M_L
2010	6	30	17	46	46.79	28.076232	-26.236914	248.3	245	1
2010	7	2	12	22	10.4	28.367566	-26.229476	531.3	535.8	1.8
2010	7	2	14	27	19.73	28.142746	-26.21542	219.1	248.2	1.9
2010	7	3	13	34	31.73	27.813246	-26.215408	369.2	670.2	1.4
2010	7	4	5	28	18.36	28.075494	-26.245632	305.4	459.7	1.3
2010	7	6	22	1	17.18	28.032536	-26.224077	234.6	266	1.6
2010	7	8	15	23	42.27	28.231453	-26.209788	319.2	476	1.2
2010	7	9	23	10	32.73	27.981956	-26.244049	268.1	350.9	1
2010	7	10	12	8	32.84	28.256819	-26.232674	352.9	356.7	1.6
2010	7	12	9	59	29.6	28.144313	-26.216398	210.9	313	2
2010	7	15	10	44	56.24	28.257872	-26.248766	321.3	317.2	1.4
2010	7	16	20	25	25.76	28.21965	-26.199202	288.5	344	1.7
2010	7	16	23	21	28.99	28.215979	-26.197155	271.1	340.5	3.3
2010	7	17	13	40	46.9	27.790951	-26.221356	402.6	706.2	1.7
2010	7	17	19	23	20.66	28.004004	-26.238584	272.7	301.4	1.3
2010	7	18	5	24	40.33	28.029574	-26.237753	210.9	250	0.8
2010	7	21	17	7	30.16	27.965885	-26.250596	270.4	388.9	0.9
2010	7	22	15	26	14.58	28.236054	-26.183578	496.6	810	1
2010	7	24	12	26	2.91	28.238968	-26.207931	318.2	478.4	1.7
2010	7	28	12	5	4.46	28.384121	-26.226467	495.3	582.1	1.9
2010	7	29	22	40	13.23	28.062781	-26.238409	270.5	240.4	1.6
2010	7	30	22	8	47.07	27.992878	-26.236689	275.3	315.9	0.4
2010	7	31	5	15	13.97	27.982347	-26.229886	281.5	351.5	1.2
2010	7	31	12	15	58.15	27.788211	-26.232928	366.2	711.1	1.5
2010	8	1	17	55	38.34	28.223438	-26.208569	268.5	328.5	1.3
2010	8	7	7	56	56.96	28.17835	-26.238806	288.6	299.9	1
2010	8	8	21	56	53.78	28.262237	-26.2621	344.4	333.4	1
2010	8	9	7	24	22.64	28.077428	-26.223741	250.8	219.7	1.2
2010	8	9	14	0	27.89	28.055076	-26.226769	268.9	245.3	1
2010	8	9	17	18	6.12	28.087478	-26.243431	238.2	237.6	0.6
2010	8	9	21	8	18	28.239654	-26.250248	315.2	294.1	0.9
2010	8	14	17	55	18.32	28.211492	-26.233608	287.7	275.7	0.7
2010	8	15	6	4	24.63	28.208543	-26.215979	271	283.6	0.4
2010	8	15	14	16	37.14	28.056935	-26.22696	261.2	233.5	0.5
2010	8	15	16	33	49.01	28.108264	-26.235149	235.6	256.2	0.5
2010	8	15	22	47	54.08	28.256077	-26.238995	310.2	284	0.5
2010	8	16	4	57	24.15	27.970482	-26.234722	261.8	366.7	0.8
2010	8	18	6	26	14.03	27.959259	-26.25059	270.2	414.2	1
2010	8	18	6	52	25.9	27.960482	-26.253709	260.8	399.3	0.8
2010	8	18	17	14	39.89	28.052433	-26.235053	268.2	248.3	1
2010	8	19	12	48	21.77	28.151728	-26.219485	251.4	303.9	1
2010	8	20	16	58	29.34	27.952577	-26.242302	276.1	412.9	1.7

© University of Pretoria

UNIVERSITEIT VAN PRETORIA
UNIVERSITY OF PRETORIA
YUNIBESITHI YA PRETORIA

YYYY	MM	DAY	HR	MIN	SEC	Longitude South (deg)	Latitude East (deg)	Error Long (m)	Error Lat (m)	M_L
2010	8	20	17	12	2.99	27.952572	-26.244018	271.5	398.1	0.5
2010	8	22	2	39	12.01	28.065066	-26.232085	270.8	256.5	0.2
2010	8	26	4	13	9.88	28.445173	-26.24581	579.2	790.5	1.6
2010	8	26	19	4	56.19	27.973352	-26.228328	278.4	367.1	2.6
2010	8	29	10	41	0.87	28.059014	-26.22563	267	255.5	1
2010	8	31	20	26	42.33	28.203733	-26.210715	286.1	296.3	0.5
2010	9	4	10	57	21.6	27.769091	-26.237332	381.3	766.3	1.9
2010	9	4	18	6	28.21	28.01133	-26.249509	263.4	291.2	0.8
2010	9	5	3	29	23.09	28.186662	-26.240775	283.5	342.2	0.5
2010	9	7	9	1	11.68	27.956259	-26.239358	276.4	401.1	0.8
2010	9	9	5	1	46.02	27.783876	-26.287154	456.8	844.3	1.3
2010	9	13	18	42	46.97	28.215278	-26.201959	279.3	306	1.1
2010	9	16	21	12	5.46	28.010251	-26.246064	256.2	282.1	0.5
2010	9	17	7	39	45.31	28.037001	-26.253535	278.1	269.2	0.8
2010	9	18	9	18	37.65	28.111539	-26.215365	230.6	292	2.1
2010	9	19	6	4	44.72	28.112617	-26.215174	241.8	214.7	2.9
2010	9	19	6	7	4.01	28.112367	-26.215037	270.5	241.7	1.9
2010	9	21	8	9	13.91	28.052623	-26.228476	262.9	272.5	1.7
2010	9	24	13	16	8.33	28.215532	-26.242699	288	286.3	2.3
2010	9	25	21	34	10.85	28.256281	-26.255826	360.6	440.5	1.1
2010	9	27	9	17	57.85	27.769478	-26.233787	378.4	770.9	1.5
2010	9	28	20	13	20.66	28.247383	-26.232182	307.9	304.5	1.5
2010	9	29	22	57	27.46	28.21601	-26.200091	287.4	373.2	1
2010	10	1	20	17	27.75	28.040835	-26.232092	233.2	248.4	0.6
2010	10	8	23	4	20.09	28.23435	-26.204876	271.9	305	1.4
2010	10	12	4	23	12.4	28.063981	-26.23253	280.7	264.1	1.3
2010	10	13	17	0	19.66	28.188352	-26.22062	275.7	363.2	0.7
2010	10	14	10	30	0.4	27.990728	-26.3142	496.8	630.7	1.1
2010	10	14	12	39	16.18	28.140802	-26.215015	224.3	239.1	1.6
2010	10	17	10	47	25.04	28.066249	-26.246485	343.8	279.9	0.8
2010	10	20	12	49	16.25	28.394588	-26.213498	528.6	615.4	1.9
2010	10	21	23	36	31.29	28.058184	-26.2381	273.9	241.5	0.6
2010	10	23	14	19	10.76	28.204557	-26.209777	256	254.3	1.1
2010	10	26	16	53	58.19	28.239225	-26.214873	292	329.9	0.9
2010	10	28	17	34	26.39	28.112798	-26.213305	232.4	224.5	1.8
2010	10	31	4	29	28.81	28.190427	-26.195963	253.6	313.8	1.4
2010	11	5	21	59	13.77	27.999391	-26.238856	282.7	308.5	0.4
2010	11	6	13	57	57.18	28.137423	-26.213334	183.7	205.2	2.1
2010	11	17	11	36	34.2	28.398072	-26.234382	710.4	676	2.4
2010	11	17	22	6	16.91	28.136757	-26.214922	191.1	217.5	1.5
2010	11	18	13	12	4.94	28.139886	-26.222659	326.2	414.8	1.6
2010	11	27	18	33	28.38	28.081795	-26.250906	257.5	258.9	1.3

© University of Pretoria

UNIVERSITEIT VAN PRETORIA
UNIVERSITY OF PRETORIA
YUNIBESITHI YA PRETORIA

YYYY	MM	DAY	HR	MIN	SEC	Longitude South (deg)	Latitude East (deg)	Error Long (m)	Error Lat (m)	M_L
2010	11	30	12	6	52.58	28.399907	-26.26172	722.9	732.8	2.1
2010	11	30	21	23	6.3	27.781876	-26.26954	314.1	718.8	1.9
2010	12	2	19	25	25.03	28.227886	-26.202052	268.1	341.7	1.7
2010	12	7	13	13	34.7	27.961295	-26.248027	269.8	421.6	1.7
2010	12	12	23	24	21.94	28.084292	-26.223958	264.8	302.6	1.5
2010	12	16	13	40	56.2	28.191987	-26.22856	271	311.2	1.6
2010	12	16	23	32	35.95	28.443712	-26.282333	611.8	845	3.1
2010	12	22	8	14	38.47	28.147928	-26.211418	209.1	227.2	2
2010	12	22	17	30	44.86	28.235406	-26.246369	313.8	322.2	1.8
2010	12	22	23	3	59.5	28.150948	-26.215115	222.3	254.7	1.6
2010	12	24	13	13	17.29	28.003814	-26.239207	281.3	306.6	1.2
2010	12	26	10	14	27.58	28.206074	-26.187341	271.5	393.4	1.7
2010	12	28	12	13	12.6	28.075544	-26.247784	274.9	267.1	1.7
2010	12	31	15	48	20.08	28.250234	-26.241761	358.5	325.4	1.4
2010	12	31	22	13	19.26	27.783494	-26.246708	481.9	810.5	1.9
2011	1	1	9	35	59.65	28.202211	-26.186039	240.4	314.2	2.3
2011	1	2	14	11	30.62	28.227082	-26.205805	270.4	358.2	1.9
2011	1	4	18	9	42.54	27.983412	-26.240294	272.9	348.2	2.4
2011	1	4	18	48	0.51	27.982406	-26.239969	262.9	340.1	2.6
2011	1	4	19	51	19.72	28.204278	-26.20767	286.2	282	1
2011	1	10	9	29	5.8	28.019267	-26.221579	558.2	779	2.1
2011	1	11	11	54	39.92	28.206004	-26.191214	259.6	341.2	2.2
2011	1	11	22	26	19.3	27.98329	-26.237893	627.2	479.7	2
2011	1	12	4	46	31.21	28.21571	-26.242169	336.3	441.4	2.5
2011	1	14	16	59	2.38	28.222258	-26.198674	271.3	410.9	2.9
2011	1	15	13	8	25.37	28.247089	-26.246269	325.2	299.6	2.3
2011	1	15	22	54	57.24	28.206478	-26.19735	282.1	339.4	2.4
2011	1	19	9	3	5.44	28.205919	-26.191056	269.5	335.1	1.9
2011	1	21	4	53	34.95	27.956534	-26.242241	260.3	385.6	1.9
2011	1	22	18	31	42.65	28.207947	-26.199932	285	339.9	2.1
2011	1	25	9	1	25.74	28.206657	-26.192813	249.4	304.6	1.5
2011	1	25	9	2	50.86	28.210888	-26.184269	302	419.2	1.9
2011	1	25	17	57	0.39	28.142692	-26.216124	207.7	226	1.6
2011	1	25	20	29	2.27	28.093892	-26.231675	323.7	266.2	0.9
2011	1	26	23	5	19.32	28.210367	-26.19817	324.6	323.3	1.4
2011	1	26	23	50	30.73	28.033679	-26.248542	275.1	280.9	1.3
2011	1	27	22	16	11.24	28.05286	-26.240549	261.3	241.8	0.8
2011	1	28	13	28	30.49	28.195463	-26.19352	323.7	356.6	1.5
2011	1	29	7	59	27.35	28.203516	-26.195599	258.6	317.3	2.8
2011	1	29	11	7	59.56	27.801793	-26.187948	462.2	808.8	1.6
2011	1	30	2	19	2.87	27.965577	-26.243231	248.5	375.6	2.1
2011	1	30	3	56	52.09	27.982788	-26.228383	280.7	347.7	1.6

© University of Pretoria

UNIVERSITEIT VAN PRETORIA
UNIVERSITY OF PRETORIA
YUNIBESITHI YA PRETORIA

YYYY	MM	DAY	HR	MIN	SEC	Longitude South (deg)	Latitude East (deg)	Error Long (m)	Error Lat (m)	M_L
2011	2	2	15	27	54.1	28.260659	-26.264356	348.6	333.8	1.4
2011	2	3	1	23	47.04	28.013757	-26.251059	257	277.1	2
2011	2	4	17	57	6.94	28.012396	-26.247165	310	278.5	1.5
2011	2	4	23	25	10.72	28.014984	-26.251545	366.8	285.7	0.9
2011	2	9	4	49	6.51	28.263554	-26.268501	354.8	333.8	1.7
2011	2	9	4	50	38.9	28.260332	-26.263435	353.8	330.8	2
2011	2	9	9	57	52.4	28.218859	-26.230763	398	330.8	1.7
2011	2	13	21	56	55.41	28.041481	-26.234159	244	251.3	1
2011	2	19	9	15	56.36	28.249053	-26.245525	641.7	850.5	1.7
2011	2	20	5	50	57.61	28.216076	-26.224554	287.5	248.6	1.3
2011	2	20	22	41	19.16	28.205978	-26.196402	262.7	323.3	1.6
2011	2	20	23	45	58.75	28.203258	-26.194825	291.5	303.3	2.3
2011	2	24	0	27	36.4	28.002437	-26.26197	291.5	305.7	1
2011	2	25	11	18	16.89	28.091231	-26.256704	312.1	380.5	1.7
2011	3	2	6	36	48.23	28.129899	-26.218608	220.7	268.3	2.1
2011	3	7	16	55	57.41	28.060321	-26.240425	281.7	248.1	1.9
2011	3	7	22	8	19.9	28.186306	-26.189893	272.2	349.6	2.1
2011	3	7	23	49	56.92	28.205823	-26.196388	293	334.5	1.6
2011	3	9	12	4	28.76	28.206396	-26.192904	272.3	326.2	1.6
2011	3	12	15	33	37.4	27.790038	-26.255832	572	736	1.9
2011	3	16	0	16	44.92	28.175802	-26.206933	226	250.8	1.4
2011	3	17	22	39	12.44	28.196043	-26.209319	253.7	272.3	1.4
2011	3	18	23	35	17.53	28.04598	-26.246703	257.3	258.8	1.9
2011	3	19	3	13	20.19	27.788586	-26.262164	395.9	685.8	1.7
2011	3	19	9	49	19.05	28.184322	-26.20278	274.4	293.5	1.4
2011	3	20	22	32	23.5	28.26632	-26.264342	373.9	379.3	1.7
2011	3	21	17	15	12.82	27.966135	-26.253469	240.8	388	1.1
2011	3	22	23	37	38.12	28.011167	-26.239763	262	288.7	0.9
2011	3	23	3	28	26.33	27.813297	-26.260375	397.1	697.9	1.2
2011	3	23	14	22	21.89	28.091366	-26.253692	234.6	247.7	2.1
2011	3	25	20	55	46.08	27.752907	-26.272717	338.7	706.9	1.7
2011	3	27	7	6	1.48	28.183653	-26.193655	269.1	343.8	2
2011	3	28	2	44	28.9	28.193217	-26.230632	297.7	396.8	2.3
2011	3	28	15	46	39.13	28.191561	-26.196124	360.9	401.6	1.6
2011	3	29	13	21	37.88	28.235177	-26.23406	298.1	258	2.2
2011	3	30	1	50	36.83	28.17143	-26.238843	346.3	347.2	0.7
2011	3	30	6	41	59.7	28.05092	-26.240781	262.7	257	1.5
2011	4	1	4	48	20.47	28.032242	-26.233119	203.9	245.8	0.9
2011	4	1	11	53	46.37	28.049766	-26.244009	254.3	251.7	2.3
2011	4	3	2	1	16.44	28.069699	-26.2267	358.9	256	0.9
2011	4	3	3	6	13.09	28.06157	-26.223726	264.3	232	1.8
2011	4	3	23	50	59.3	28.206394	-26.196956	240.3	287.6	1.4

© University of Pretoria

UNIVERSITEIT VAN PRETORIA
UNIVERSITY OF PRETORIA
YUNIBESITHI YA PRETORIA

YYYY	MM	DAY	HR	MIN	SEC	Longitude South (deg)	Latitude East (deg)	Error Long (m)	Error Lat (m)	M_L
2011	4	4	2	38	13.01	28.01236	-26.245014	262.6	283.5	1.4
2011	4	4	19	27	48.87	27.781249	-26.262812	332.7	702.1	1.8
2011	4	5	1	31	49.57	27.769502	-26.260072	326.8	696	1.8
2011	4	6	17	0	40.44	28.011548	-26.239586	262.1	286.6	1.1
2011	4	8	10	20	41.56	28.206154	-26.20286	293	338.1	2
2011	4	8	12	48	8.7	28.204791	-26.193743	278.7	353.3	2
2011	4	10	19	52	28.51	28.159681	-26.205957	232.6	239.4	1.4
2011	4	15	19	36	25.57	28.23158	-26.204008	294.2	424	1.8
2011	4	15	20	26	11.38	28.156108	-26.207578	199	235.1	2
2011	4	21	11	21	18.14	28.207488	-26.191439	278.8	318.8	2.4
2011	4	22	23	17	20.28	28.232406	-26.20548	348.8	333.9	2.8
2011	4	23	16	51	5.76	27.971541	-26.241665	255.9	366.5	1.4
2011	4	24	10	19	36.38	28.205993	-26.197511	256.9	329.6	1.6
2011	4	25	14	26	23.56	28.014519	-26.25252	260.1	286.6	1.7
2011	4	25	14	52	26.01	28.013954	-26.25198	257.3	284.5	1.8
2011	4	25	15	44	32.09	28.136756	-26.232168	210.6	264.3	1.7
2011	4	26	0	29	39.1	28.022553	-26.241713	259.7	278.5	0.9
2011	4	26	5	8	49.31	28.042649	-26.23554	237.8	245.3	2.5
2011	4	26	21	5	27.98	28.160609	-26.206959	216.3	246.4	1.8
2011	4	28	1	23	52.81	28.20685	-26.195925	252.4	259.5	1.7
2011	4	29	8	53	28	28.062992	-26.237857	258.5	235.3	1.8
2011	4	30	14	59	8	28.044053	-26.235793	239.2	242.2	2.7
2011	4	30	20	43	51.75	27.93082	-26.213238	299.4	365.3	2
2011	5	1	2	2	3.71	28.215216	-26.25051	327.2	331.1	2.6
2011	5	3	17	55	37.95	27.798767	-26.252178	338.7	670.1	1.8
2011	5	5	1	54	27.32	28.2013	-26.211681	249.2	286.5	1.4
2011	5	5	4	4	50.4	28.189265	-26.234896	286.3	309.3	1.1
2011	5	6	19	18	58.41	28.213065	-26.221645	274	282.6	0.6
2011	5	7	8	59	27.83	27.951918	-26.229507	256.6	377.5	1.4
2011	5	8	2	10	40.12	28.037182	-26.234565	221.6	242.8	1.6
2011	5	9	16	4	10.67	28.119217	-26.217014	228.1	243.5	1.6
2011	5	11	19	50	0.71	27.934098	-26.213259	347.2	403.2	1.3
2011	5	12	18	34	28.69	28.230495	-26.247806	433.6	541	0.7
2011	5	16	5	16	19.71	28.264521	-26.259726	352.4	334.8	3.4
2011	5	18	0	10	36.33	28.231508	-26.230647	290.7	227.5	1.2
2011	5	18	18	47	11.15	28.255931	-26.232045	371.6	355.9	1.1
2011	5	20	2	7	13.89	28.188401	-26.236937	267.3	270.6	2.4
2011	5	23	0	15	14.81	28.245441	-26.253359	325.1	293.6	1.7
2011	5	26	14	21	30.22	27.971545	-26.244676	316.6	376	1.6
2011	5	26	20	14	29.75	28.157152	-26.207976	202.4	240.3	1.7
2011	5	27	22	53	56.35	28.192335	-26.210616	246	232.5	0.7
2011	5	29	8	12	44.3	28.124846	-26.237261	234.6	265.2	1.7

© University of Pretoria

UNIVERSITEIT VAN PRETORIA
UNIVERSITY OF PRETORIA
YUNIBESITHI YA PRETORIA

YYYY	MM	DAY	HR	MIN	SEC	Longitude South (deg)	Latitude East (deg)	Error Long (m)	Error Lat (m)	M_L
2011	5	30	3	41	5.03	28.253328	-26.232838	312.7	291.8	1.3
2011	6	6	1	53	58.89	28.211518	-26.245816	317.3	273.2	1.4
2011	6	17	4	18	9.28	27.971428	-26.249963	287.2	369.8	1.6
2011	6	17	8	50	24.37	28.090531	-26.25214	264	262.5	1.4
2011	6	23	23	34	57.4	27.790498	-26.263496	307	685.1	1.9
2011	6	26	1	56	55.06	28.08583	-26.242323	243.3	242.1	1.1
2011	6	27	19	20	58.79	28.047365	-26.235706	249.5	242.7	2.6
2011	6	29	8	4	43.96	27.983306	-26.242788	260	333.7	1.8
2011	6	29	17	36	55.29	28.125638	-26.22325	220.1	220.8	1.5
2011	7	1	11	2	23.81	28.242039	-26.250287	319.1	286.3	1.3
2011	7	3	14	37	25.85	28.287856	-26.302519	759.4	1009.7	1.1
2011	7	5	17	18	59.77	28.045155	-26.234765	273	259.5	1.4
2011	7	6	23	7	27.08	27.963534	-26.243957	266.7	371.5	0.9
2011	7	6	23	11	31.2	28.134082	-26.219115	208.6	218.4	1.5
2011	7	8	20	26	34.42	28.104126	-26.222154	243.4	224.9	1.2
2011	7	9	0	35	15.08	28.265954	-26.253497	333.2	339.8	1
2011	7	11	10	43	50.84	28.122231	-26.230118	235.6	290.5	1.4
2011	7	12	20	22	18.39	28.208771	-26.20041	259	323.1	1.5
2011	7	12	20	47	51.68	28.14004	-26.218335	189.7	219.1	1.8
2011	7	13	6	58	43.03	28.269322	-26.268993	352.7	339	1.7
2011	7	14	6	51	3.93	28.158023	-26.206468	199.6	237.8	2.2
2011	7	18	19	0	59.52	28.089184	-26.226913	277.2	259.3	1.4
2011	7	21	1	23	18.35	27.78761	-26.24897	338.3	661.7	1.4
2011	7	22	19	49	31.78	28.203735	-26.206606	253.1	249.7	1.7
2011	7	22	23	8	52.92	28.203832	-26.20689	250.1	267.9	1.3
2011	7	23	14	16	54.01	28.048005	-26.242565	240.3	239.6	1.4
2011	7	23	20	29	9.78	27.817453	-26.253413	517.7	738	1.7
2011	7	24	0	29	34.68	28.231159	-26.24076	297.1	262.7	1.1
2011	7	24	20	45	58.7	28.088784	-26.232429	237.9	239.9	1.7
2011	7	24	21	31	3.34	28.249415	-26.232399	295.5	284.4	1
2011	7	25	19	27	55.36	28.067316	-26.237756	239.3	248.1	1.2
2011	7	28	10	48	7.69	28.160002	-26.206277	227.1	262.4	2.1
2011	7	29	5	10	58.22	28.101078	-26.223483	282.9	249.7	1.3
2011	7	29	13	53	11.67	28.204819	-26.242687	295.4	261.4	1.5
2011	7	29	20	57	7.75	28.056984	-26.221769	428.3	515.4	1.2
2011	7	30	19	17	9.72	28.263853	-26.261592	357.1	335.8	1.2
2011	8	1	7	51	42.86	28.087629	-26.250748	251.2	255.5	1.3
2011	8	2	1	23	14.65	28.203257	-26.206372	255.8	319.2	1.2
2011	8	3	10	1	9.3	28.057582	-26.237222	262.1	235.1	1.8
2011	8	4	3	31	39.43	28.048425	-26.241478	290.3	280.6	1.1
2011	8	9	0	50	40.94	28.206009	-26.21064	244.2	249.4	1.4
2011	8	9	0	51	7.29	28.205919	-26.210882	252.9	288.5	1.4

© University of Pretoria

UNIVERSITEIT VAN PRETORIA
UNIVERSITY OF PRETORIA
YUNIBESITHI YA PRETORIA

YYYY	MM	DAY	HR	MIN	SEC	Longitude South (deg)	Latitude East (deg)	Error Long (m)	Error Lat (m)	M_L
2011	8	13	1	28	15.98	28.23134	-26.227587	335.2	357.3	1.3
2011	8	13	1	59	3.88	28.075406	-26.237915	263.7	236.7	1
2011	8	13	2	11	28.51	28.239193	-26.214007	287.3	260.1	1.1
2011	8	13	11	38	20.89	27.964928	-26.21986	303.6	382.5	1.6
2011	8	14	7	57	31.66	28.061097	-26.241337	256.2	238.7	1.7
2011	8	15	23	54	47.05	28.034763	-26.23879	238.4	255.1	1.3
2011	8	16	17	15	49.84	28.140447	-26.21742	206.5	259.2	2
2011	8	21	0	35	37.85	28.282006	-26.276504	384.8	392.9	1.4
2011	8	21	7	6	10.36	28.160689	-26.207621	206.2	227.4	2.1
2011	8	21	13	24	51.21	28.08421	-26.24579	281.8	265.6	1
2011	8	22	6	23	51.15	28.160904	-26.227659	229.3	268.9	1.8
2011	8	25	12	14	38.18	28.156975	-26.206787	202.6	268.3	2.8
2011	8	25	13	23	29.57	27.817261	-26.210514	452.9	766.3	1.5
2011	8	25	13	25	55.55	27.808105	-26.21582	469.3	752.9	1.2
2011	8	30	18	38	48.92	28.087499	-26.249333	260.3	255.8	1.4
2011	8	31	17	29	9	27.918453	-26.2179	330.4	409.2	1.4
2011	9	1	3	59	51.25	28.168753	-26.194318	241.5	295.7	1.3
2011	9	4	6	11	25.06	28.161078	-26.206171	248.8	332.2	1.9
2011	9	6	12	4	40.45	28.021465	-26.238532	251	278.9	1.3
2011	9	6	18	11	31.19	28.24658	-26.224449	306.1	332.6	1.7
2011	9	7	21	19	36.78	28.009318	-26.232847	268.8	293.6	2.1
2011	9	8	0	15	22.86	28.266862	-26.266763	355.8	318.3	1
2011	9	8	1	28	45.33	28.01134	-26.246459	257.4	282.9	2.1
2011	9	9	23	25	34.2	28.012345	-26.242653	264.9	279.9	1.2
2011	9	10	19	24	12.25	28.122384	-26.240602	222.5	280.1	1.2
2011	9	11	5	33	58.5	27.976099	-26.230449	315.2	357	1.2
2011	9	11	15	10	44.62	28.051113	-26.228776	265.6	239.1	0.8
2011	9	12	20	35	32.76	28.06041	-26.227974	269.7	269.9	2
2011	9	13	11	47	4.61	28.045201	-26.236903	248.9	245.4	1.6
2011	9	14	21	52	59.96	28.161359	-26.204939	238.7	319	2.1
2011	9	15	2	37	3.45	28.242105	-26.218805	295.6	290.2	1.3
2011	9	15	3	4	35.3	28.152463	-26.190188	362.2	757.4	0.9
2011	9	15	10	47	45.37	28.205575	-26.223552	302	353.6	1.1
2011	9	17	20	23	2.33	28.246876	-26.226194	295	266	1.2
2011	9	18	18	40	24.18	28.20058	-26.198219	250	315.9	1.2
2011	9	20	23	18	18.54	28.221759	-26.220328	269	257	1.4
2011	9	21	0	24	51.52	28.012811	-26.230826	262.3	294.8	1.5
2011	9	21	0	49	29.8	28.203521	-26.237376	297.9	282.2	1.4
2011	9	21	13	22	37.21	28.070011	-26.247301	368.3	277.3	0.8
2011	9	21	22	36	38.09	28.061713	-26.241727	297.1	280.6	1.3
2011	9	22	1	31	42.12	28.157759	-26.204425	201.6	273.3	1.7
2011	9	22	9	23	1.99	28.215267	-26.215779	276	255.3	1.3

© University of Pretoria

UNIVERSITEIT VAN PRETORIA
UNIVERSITY OF PRETORIA
YUNIBESITHI YA PRETORIA

YYYY	MM	DAY	HR	MIN	SEC	Longitude South (deg)	Latitude East (deg)	Error Long (m)	Error Lat (m)	M_L
2011	9	24	2	51	11.81	28.237722	-26.212176	293.2	301.6	1.1
2011	9	24	2	57	3.15	28.233379	-26.206574	282.7	317	1.2
2011	9	24	3	20	34.87	28.236967	-26.210886	291	277.8	1.5
2011	9	24	4	47	59.59	28.101144	-26.243648	235.4	264	1.7
2011	9	24	5	2	17.78	28.238539	-26.211961	299.8	308.8	1.7
2011	9	24	5	52	42.98	28.163665	-26.202299	290.9	380.5	1.5
2011	9	24	6	59	32.54	28.235607	-26.207826	298.3	389.5	1.6
2011	9	25	11	59	11.49	28.056339	-26.243902	257.5	238.7	1.6
2011	9	26	9	55	9.57	28.190329	-26.209886	270.3	399.7	1
2011	9	26	22	19	56.21	28.271827	-26.269732	354.4	330.8	1.2
2011	9	27	6	53	11.83	28.156034	-26.20823	200.4	257.9	1.8
2011	9	30	2	7	59.06	28.145502	-26.218687	209.7	272.6	1.8
2011	9	30	19	46	33.5	28.042348	-26.25569	250.2	259.5	1.7
2011	10	1	6	34	20.58	28.041937	-26.255821	433.2	347.9	1.2
2011	10	1	20	39	14.25	27.952155	-26.249803	299.6	392.2	1.6
2011	10	2	1	23	8.81	28.022037	-26.214004	296.6	283.4	0.8
2011	10	2	2	12	37.2	28.067523	-26.237838	318.6	252.8	1.1
2011	10	2	22	42	32.17	28.157879	-26.207519	213.4	287.3	2.1
2011	10	3	1	59	11.45	28.070616	-26.238367	278.3	247.9	1.9
2011	10	3	5	7	47.57	28.229298	-26.225967	606.6	903.7	1.6
2011	10	3	9	4	41.54	28.194828	-26.194467	260.5	335.1	1.7
2011	10	3	10	30	41.74	28.157101	-26.20626	221.1	305.7	2.3
2011	10	4	7	4	27.76	28.252429	-26.243407	327.2	362.1	1.8
2011	10	9	19	2	57.75	28.229768	-26.243212	312	371.5	1.5
2011	10	12	20	12	52.95	27.996487	-26.250521	269.4	319.5	2.1
2011	10	13	10	36	39.32	28.224629	-26.240822	299.7	246.3	2.3
2011	10	16	18	6	43.99	28.272327	-26.26754	367.2	381.5	1
2011	10	20	1	49	17.88	27.764076	-26.26185	293.7	713.9	1.9
2011	10	20	23	50	14.53	28.158674	-26.208645	183.6	213.9	2.7
2011	10	21	0	28	51.58	28.156763	-26.207769	202.8	232.2	1.8
2011	10	22	5	19	59.98	28.265738	-26.259896	354.3	364.4	1.7
2011	10	22	8	26	22.7	28.160638	-26.205526	225.3	260.6	2
2011	10	26	0	10	38.58	28.044264	-26.235798	244.1	244.8	1.7
2011	10	26	22	24	19.16	28.150139	-26.210792	224.4	252.2	1.6
2011	10	29	15	7	50.21	28.090287	-26.25515	233.7	245.9	1.9
2011	10	30	0	16	48.31	28.253612	-26.256489	346.7	359.9	1.3
2011	10	31	3	32	39.17	28.26157	-26.263585	352.1	356.2	1.1
2011	11	1	5	39	3.67	27.975699	-26.232351	305	351.4	1.4
2011	11	2	0	29	1.22	28.19656	-26.232984	318	332.4	1.2
2011	11	2	8	26	38.81	28.150384	-26.210331	233.6	234.3	1.7
2011	11	2	14	23	38.56	28.261983	-26.257746	349.9	327.9	1.6
2011	11	2	18	44	13.77	28.140436	-26.218894	209.9	224.5	1.7

© University of Pretoria

UNIVERSITEIT VAN PRETORIA
UNIVERSITY OF PRETORIA
YUNIBESITHI YA PRETORIA

YYYY	MM	DAY	HR	MIN	SEC	Longitude South (deg)	Latitude East (deg)	Error Long (m)	Error Lat (m)	M_L
2011	11	3	21	32	36.02	28.156513	-26.206109	210.3	234.7	1.9
2011	11	5	0	1	54.88	27.976578	-26.233151	286.5	360	1.1
2011	11	6	1	27	43.84	28.242645	-26.244533	315.8	283.1	1.4
2011	11	8	21	16	50.6	28.055309	-26.248727	265.5	249.1	0.9
2011	11	9	6	16	19.93	27.999487	-26.225278	295	323.7	1.4
2011	11	9	17	31	10.71	28.098529	-26.222671	238.4	225.4	1.6
2011	11	10	19	32	12.38	28.20883	-26.231073	285.4	260.7	1.3
2011	11	12	3	58	26.2	27.929834	-26.212868	305.6	374.9	1.7
2011	11	13	8	4	18.22	28.183284	-26.191554	340.7	363.8	1.8
2011	11	13	16	37	28.46	28.182733	-26.193767	313	380.9	2.1
2011	11	20	1	42	25.44	28.044513	-26.238977	249	254.6	0.8
2011	11	25	11	47	1.23	27.797064	-26.251904	505.8	760.7	2.5
2011	11	30	0	36	18.96	28.048158	-26.24531	270.5	255.3	0.8
2011	12	1	23	55	25.59	28.268984	-26.267095	346.8	334.8	2.9
2011	12	2	16	11	2.99	27.96127	-26.249716	289	386.6	1.3
2011	12	2	20	36	27.39	27.939729	-26.231922	295	386.2	1.6
2011	12	3	9	2	7.68	27.945997	-26.227422	288.5	389.3	2
2011	12	3	18	55	32.02	28.218221	-26.250866	308.8	378.2	1.5
2011	12	4	11	15	55.36	28.110619	-26.229407	214.4	229.4	0.7
2011	12	6	8	8	22.67	28.075046	-26.247445	267.8	247.6	1.2
2011	12	8	0	9	20.64	27.998175	-26.221681	285.4	328.1	1.4
2011	12	12	11	40	51.01	28.066479	-26.224209	258.3	220.9	1.8
2011	12	15	4	7	24.38	28.157835	-26.236566	223.7	265.5	1.2
2011	12	16	16	19	57.03	28.074834	-26.245467	259.1	248.3	1.4
2011	12	23	2	21	59.1	28.260227	-26.248783	342.1	384.6	1.1
2011	12	23	4	37	24.53	28.046908	-26.238535	271.4	242.4	1.4
2011	12	24	10	51	48.44	28.139579	-26.214234	249.9	251	1.7
2011	12	25	3	21	9.03	28.15219	-26.208262	231.4	293.5	1.5
2011	12	25	22	50	51.47	28.085746	-26.230689	254.1	238.4	1.3
2011	12	25	23	28	15.86	28.134225	-26.240121	259.7	277.9	1.4
2011	12	26	1	54	48.8	28.062894	-26.237672	256.3	234.6	1.2
2011	12	26	4	50	58.61	28.180318	-26.225509	314.9	401	1
2011	12	26	21	12	59.98	28.112491	-26.256783	340.7	367.9	1.1
2011	12	28	21	15	29.1	28.139065	-26.218728	209.8	237.4	1.7
2012	1	12	20	37	0.25	28.207675	-26.211586	572.2	429.6	1.8
2012	1	22	21	38	42.75	28.150422	-26.206321	305.9	310	1.7
2012	1	28	22	16	26.51	28.168049	-26.23883	387.1	332.9	1.2
2012	2	1	12	59	50.27	27.99843	-26.24349	278.2	317.6	1.3
2012	2	2	21	28	55.72	28.027985	-26.248599	287.2	261.6	1.2
2012	2	2	23	31	10.71	28.10631	-26.234225	224.4	293.6	1.4
2012	2	3	9	2	31.91	28.244543	-26.254934	341.9	404.6	2
2012	2	4	8	59	48.25	28.274945	-26.270869	426.3	466.9	2.3

© University of Pretoria

UNIVERSITEIT VAN PRETORIA
UNIVERSITY OF PRETORIA
YUNIBESITHI YA PRETORIA

YYYY	MM	DAY	HR	MIN	SEC	Longitude South (deg)	Latitude East (deg)	Error Long (m)	Error Lat (m)	M_L
2012	2	4	22	38	9.2	27.996746	-26.250207	276	322.3	2.1
2012	2	5	3	24	4.57	28.092276	-26.239338	229.4	261.2	1.8
2012	2	5	6	23	6.78	28.088963	-26.251496	243.9	266.5	1.9
2012	2	5	18	0	45.32	28.26649	-26.26012	502.8	563.9	1.9
2012	2	6	4	27	39.09	28.176825	-26.249853	427.5	581	2.7
2012	2	8	1	4	56.65	27.959179	-26.250596	253.7	400.4	0.8
2012	2	12	5	11	27.19	28.048387	-26.234572	252	255.2	1.9
2012	2	12	22	47	20.16	28.157948	-26.201464	223.3	325.9	2
2012	2	16	0	51	22.21	28.165296	-26.205571	254.4	353.4	2.8
2012	2	21	0	51	53.9	28.224267	-26.236512	358.8	464.7	2
2012	2	24	22	21	50.05	28.164826	-26.214513	250.3	340.1	2.1
2012	2	26	17	47	25.7	28.19233	-26.225566	292.6	358.4	2.1
2012	2	28	18	23	17.14	28.176398	-26.19972	324.4	348.9	2.7
2012	3	1	19	20	38.22	27.958215	-26.227726	276	385.9	1.1
2012	3	2	22	13	4.38	28.253455	-26.235802	512.9	602.9	2
2012	3	3	7	13	28.27	28.036112	-26.252222	256.8	257.8	1.5
2012	3	5	19	3	58.99	28.031443	-26.225244	242.7	286.8	1.1
2012	3	8	3	8	40.11	28.079135	-26.225134	253.2	273.9	1.9
2012	3	9	2	29	33.08	28.164723	-26.211698	243.8	345.3	2.2
2012	3	9	19	52	11.2	28.078684	-26.249458	246.3	261.1	1.6
2012	3	9	22	45	31.04	28.007689	-26.242295	269.1	299.4	2.1
2012	3	11	12	29	28.45	28.269791	-26.263016	382.2	385.6	1.9
2012	3	12	0	27	2.98	28.171333	-26.217362	291.9	343.7	1.5
2012	3	16	22	24	36.22	28.271997	-26.263166	412	500.9	1.9
2012	3	17	6	26	57.88	28.213149	-26.245113	291.7	373.9	3.1
2012	3	18	21	33	26.39	28.266231	-26.263987	375.7	406.2	2.2
2012	3	19	3	21	27.34	28.277748	-26.262228	404	463.1	1.6
2012	3	19	9	23	33.7	27.984639	-26.246262	276.1	350.1	1.5
2012	3	19	20	14	34.04	28.095932	-26.227305	237.2	285.6	1.8
2012	3	20	23	17	2.37	28.276362	-26.256472	407.9	439.5	1.9
2012	3	20	23	39	59.7	28.266704	-26.254921	384.3	398.3	1.5
2012	4	13	16	28	37.95	28.201576	-26.239608	280.4	318.1	1.4
2012	4	27	10	8	40.84	28.211153	-26.196679	353.8	473.2	2.4
2012	5	4	23	26	14.13	28.057058	-26.228063	282.1	251.4	1.7
2012	5	10	22	15	53.02	28.26905	-26.266751	416	471.6	2
2012	5	11	13	35	5.51	28.162517	-26.204364	205	287.5	3.1
2012	5	14	1	5	10.09	28.163021	-26.205401	231.4	329.5	2.1
2012	5	20	0	35	55.52	28.213967	-26.224743	424.3	513.7	0.9
2012	5	20	1	14	5.75	28.157636	-26.209422	216.4	286.4	1.7
2012	5	23	19	40	53.34	28.087528	-26.246096	252.9	248.5	1.1
2012	5	27	2	11	39.77	28.161414	-26.208543	254.2	383.7	1.6
2012	5	27	16	41	50.53	28.251043	-26.249138	391.1	444.4	1.3

© University of Pretoria

UNIVERSITEIT VAN PRETORIA
UNIVERSITY OF PRETORIA
YUNIBESITHI YA PRETORIA

YYYY	MM	DAY	HR	MIN	SEC	Longitude South (deg)	Latitude East (deg)	Error Long (m)	Error Lat (m)	M_L
2012	5	29	0	12	43.58	28.157877	-26.210982	218.5	332.6	1.9
2012	5	31	9	23	43.63	28.27594	-26.28206	655.2	930.1	1.3
2012	6	4	8	38	31.26	28.163794	-26.226766	230.8	350.9	2.1
2012	6	8	1	3	17.02	28.16321	-26.203688	198.2	290	2.6
2012	6	10	0	34	50.47	28.274464	-26.268386	393.6	449.2	1.1
2012	6	10	12	15	42.27	27.954422	-26.237473	278	396	1.3
2012	6	11	12	25	19.42	28.257084	-26.263335	366.4	366.6	1.1
2012	6	11	20	58	44.05	27.769612	-26.273321	352	691.3	1.5
2012	6	15	20	10	40.95	28.093377	-26.257331	289.1	478.3	1.7
2012	6	16	20	35	43.75	28.203671	-26.214833	276.6	356.2	1.2
2012	6	17	21	51	48.7	28.150646	-26.217551	218.1	333.8	2.2
2012	6	19	11	17	49	28.03529	-26.236919	255.9	265.1	1.6
2012	6	20	4	4	3.99	28.16185	-26.203436	227.3	293.3	2.7
2012	6	22	19	59	36.5	28.265298	-26.261709	368.4	367.7	1
2012	6	23	2	4	1.84	28.205288	-26.247303	311.8	464.5	1.5
2012	6	24	21	45	23.22	28.095285	-26.25767	300	284.8	1
2012	6	26	0	19	27.51	28.125904	-26.244575	268.7	327.3	1.2
2012	6	26	8	55	35.36	28.131697	-26.24376	279.3	341.6	1.5
2012	6	26	13	50	23.66	28.231063	-26.241197	317.3	396.7	1.4
2012	6	26	18	49	27.75	27.820191	-26.230243	395.5	658.5	2
2012	6	30	19	37	33.74	28.252013	-26.240811	343.3	364.1	1.2
2012	7	3	1	7	37.71	28.259207	-26.248995	434.4	506.5	0.9
2012	7	4	6	44	13.08	28.080451	-26.233111	267.3	243.4	1.8
2012	7	5	9	48	20.69	28.270928	-26.252192	374.6	407.4	1.5
2012	7	6	1	59	5.2	28.146788	-26.203918	207.3	291.9	1.4
2012	7	6	2	36	14.61	28.217104	-26.229906	297.8	345.2	1.1
2012	7	12	5	15	58.86	27.848226	-26.233118	516.5	721.1	2
2012	7	15	2	13	8.11	28.042745	-26.251428	289.9	274.3	1.3
2012	7	15	12	53	59.25	28.23886	-26.252685	317.3	323.5	2.2
2012	7	15	18	51	40.79	28.23574	-26.247405	310.2	313.6	2
2012	7	15	20	25	47.5	28.245322	-26.264392	330.8	334.7	1.2
2012	7	23	21	20	49.54	28.266363	-26.255281	357.6	374.2	1.5
2012	7	25	6	27	46.02	28.262092	-26.257098	436.4	506.2	1.7
2012	7	26	15	39	9.11	27.946988	-26.248184	340.2	476.5	1.7
2012	7	27	15	27	53.26	28.155152	-26.207818	184.1	252.4	2.6
2012	7	27	15	30	39.6	28.159129	-26.209604	230	282.1	2
2012	7	27	15	59	20.9	28.13094	-26.233367	233.6	294.1	1.9
2012	7	28	6	49	53.88	28.267538	-26.26021	370.9	393.3	1.9
2012	7	28	7	12	50.61	28.129925	-26.22956	230.3	292.8	2
2012	7	29	7	22	7.62	28.157357	-26.204275	198.2	284.3	2.3
2012	8	3	16	37	51.14	28.075628	-26.239222	295.1	278.5	1.8
2012	8	3	19	59	11.02	28.248933	-26.240173	348	359.3	1.7

© University of Pretoria

UNIVERSITEIT VAN PRETORIA
UNIVERSITY OF PRETORIA
YUNIBESITHI YA PRETORIA

YYYY	MM	DAY	HR	MIN	SEC	Longitude South (deg)	Latitude East (deg)	Error Long (m)	Error Lat (m)	M_L
2012	8	4	4	24	21.22	28.247232	-26.235514	342.2	339.7	1.4
2012	8	4	13	19	49.1	28.127858	-26.228909	364.2	504	1.2
2012	8	4	13	24	53.61	28.154841	-26.227444	316.1	418.3	1.4
2012	8	4	13	35	16.37	28.129797	-26.243781	317.8	404	1.4
2012	8	4	13	56	19.38	28.127675	-26.236908	438.1	535.1	1
2012	8	5	0	46	27.62	28.155342	-26.207097	230.4	295.2	1.4
2012	8	5	0	47	22.63	28.250381	-26.23795	322.3	344.9	2
2012	8	5	7	28	58.03	28.251539	-26.241796	355.7	386.6	1.2
2012	8	5	17	22	30.31	28.137153	-26.243204	227.5	305.1	0.7
2012	8	5	20	36	48.19	28.263292	-26.264484	370.9	375.3	1.3
2012	8	6	13	44	31.08	28.248641	-26.239495	347.8	366	1.7
2012	8	9	11	12	47	28.210392	-26.213694	370.2	382.3	1.2
2012	8	9	18	59	26.52	28.249725	-26.239013	321.9	356	1.5
2012	8	10	9	5	4.55	28.243851	-26.224838	320.9	355.8	2
2012	8	11	3	55	6.96	28.251799	-26.243947	326.7	322.9	2.6
2012	8	11	20	26	17.44	28.135899	-26.241378	224.5	285.2	1
2012	8	13	22	45	1.82	28.259613	-26.25392	356	363.1	1
2012	8	14	19	21	38.39	28.245653	-26.254422	352.6	369.2	1.4
2012	8	19	17	31	3.42	28.172621	-26.242374	346	384.9	1
2012	8	20	21	59	35.93	28.176103	-26.259133	461.1	1055.3	1.6
2012	8	23	5	26	27.65	28.223681	-26.231684	300	365.5	1.9
2012	8	24	12	28	23.68	28.172962	-26.243505	281	425.5	1.7
2012	8	25	1	44	40.66	28.236563	-26.252455	348.3	384.3	0.9
2012	8	28	0	54	14.74	28.003397	-26.255893	261.9	312.8	2.5
2012	8	30	23	22	43.32	28.153035	-26.206512	240.1	297.3	1.8
2012	9	1	14	43	19.05	28.114992	-26.25846	319	383.3	1.4
2012	9	2	16	54	36.96	28.125084	-26.234386	240.1	277.6	1.7
2012	9	8	3	33	8.64	28.264493	-26.256364	387.4	478.5	1.3
2012	9	10	23	16	9.29	28.260119	-26.253959	391.4	488	2.4
2012	9	19	3	47	43.94	28.253528	-26.242708	321.8	313.7	1.3
2012	9	19	7	49	29.51	27.953668	-26.238657	380.4	448.2	1.5
2012	9	21	19	14	6.7	28.261921	-26.246323	382.6	455.7	1.5
2012	9	23	3	16	50.76	28.24635	-26.221301	344.4	388.1	1.2
2012	9	23	14	25	39.46	28.129295	-26.237727	224.6	288	1.7
2012	9	24	1	12	45.44	28.276131	-26.232301	372.3	441.5	1.4
2012	9	24	1	52	26.72	28.268754	-26.230787	363.5	373.7	0.7
2012	9	24	4	8	15.38	28.2693	-26.228177	399.8	440.5	2.3
2012	9	24	4	17	59.6	28.26709	-26.228959	361.8	366.1	0.8
2012	9	24	5	33	40.36	28.267079	-26.233662	381.3	392	0.8
2012	9	24	21	9	37.27	28.268312	-26.231827	365.1	374.4	0.8
2012	9	25	22	54	46.33	28.267978	-26.231998	372.2	379.6	1
2012	9	25	23	19	39.04	28.268563	-26.234878	363.8	375.5	0.9

© University of Pretoria

UNIVERSITEIT VAN PRETORIA
UNIVERSITY OF PRETORIA
YUNIBESITHI YA PRETORIA

YYYY	MM	DAY	HR	MIN	SEC	Longitude South (deg)	Latitude East (deg)	Error Long (m)	Error Lat (m)	M_L
2012	9	26	20	35	58.58	28.296078	-26.258916	472	537	1.1
2012	9	27	1	47	58.48	28.261774	-26.21335	344.9	359.5	2
2012	9	27	14	10	31.34	28.131055	-26.237836	343.8	552.6	1.9
2012	9	28	0	17	0.91	28.255843	-26.243053	363.1	371.9	0.9
2012	9	29	19	46	42.25	28.191014	-26.236329	293.2	452.2	1.8
2012	9	30	22	25	4.85	28.208214	-26.218118	335.6	413.1	0.5
2012	10	2	21	10	28.52	28.20576	-26.242953	312.2	427.6	1.5
2012	10	7	6	11	12.42	28.122024	-26.246695	466.5	663.5	1.2
2012	10	11	13	57	48.85	28.205494	-26.21572	299.4	404.6	1.8
2012	10	12	0	56	51.72	28.056565	-26.230891	267.5	256.1	1.8
2012	10	12	1	59	56.55	28.267337	-26.255138	387.5	453.8	1.2
2012	10	15	18	39	57.31	28.264231	-26.251633	407.6	506.7	1.8
2012	10	22	0	17	27.72	28.058114	-26.239823	260.7	237.8	1.7
2012	10	23	4	49	3.24	28.236745	-26.232097	315.2	342	1.8
2012	10	25	15	18	36.91	28.132034	-26.233488	218.8	280.1	1.2
2012	10	27	19	4	7.93	28.198244	-26.218604	329	459.6	1.9
2012	10	28	1	30	59.57	28.234469	-26.224747	330.1	351.9	1.4
2012	10	30	18	9	54.31	28.105803	-26.247073	231	265.8	1.3
2012	10	31	10	33	20.54	28.150925	-26.205126	249.9	311	2.1
2010	6	3	21	22	53	27.766855	-26.254127	3955.5	6899.4	1.4
2010	6	6	10	2	27	27.760155	-26.28903	4086.8	5398.3	1.3

© University of Pretoria